Construction of an electron spin resonance spectrometer and the measurement of the hyperfine solution spectrum of copper salicylaldimine

A thesis presented in canditure for

the degree of

Master of Science

by

Allan Marriage

B.Sc.(Hons.) London

Department of Physics

University of Adelaide

July 1964

ACKNOWLEDGEMENTS

This work was carried out at the R.G. Menzies Laboratory and is presented by permission of Philips Electrical Industries Pty. Ltd.

The author would like to thank his supervisors Dr. A.F. Nicholson and Dr. H. Medlin and also Dr. S. Tomlin for help and encouragement. He would also like to thank all his colleagues at the R.G. Menzies Laboratory, in particular Mr. M.J. Kay for advice with electronic problems, Mr. J. Beretka for preparing the chemical samples, Mrs. C.P. Taylor for typing and Mr. R.S. Taylor for graph drawing.

A.J.M.

CONTENTS

CONTENTS

PART 2

This work, except where otherwise stated is, according to the author's knowledge and belief, entirely original and contains no material which has been previously presented in any University either by the author himself or by any other person.

July 1964

SUMMARY

Part 1

A description of the operation and principles of an electron spin resonance spectrometer is given together with a comparison of the various types in common use. The advantages of using a resonant cavity as a sample holder and the necessity for klystron frequency locking are shown together with a description of the various types of magnetic field modulation that can be employed. The construction of a 3 cm electron spin resonance spectrometer using 100 kc magnetic field modulation is described in detail together with the design of magnetic field stabilising and sweeping circuits. Details are given of the construction of a proton resonance magnetometer for precise field measurement. Finally the method for determining the spectrometer sensitivity is described.

Part 2

Studies of the hyperfine spectrum of copper salicylaldimine in solution have been experimentally made. The spin Hamiltonian for a tumbling paramagnetic complex is described and the linebroadening is shown to depend on the rotational speed of the complex. Solvents of differing viscosities were used and also the effective planar area of the microcrystal was altered by the addition of aliphatic chains to the basic chelate. The linewidths of the four line spectrum obtained were analysed by fitting four equal area Lorentzian curves by means of an iterative process. The necessity for using eight parameters in the curve fitting required the writing of the curve fitting procedure in FORTRAN and the use of a computer.

PART I

1. INTRODUCTION

Radio frequency spectroscopy is a comparatively new form of absorption spectroscopy involving a range of frequencies from the limits of the far infrared region to the very low radio frequency region. The general term covers nuclear magnetic resonance, paramagnetic resonance, microwave and direct quadrupole spectroscopy. Radio frequency spectroscopy can be divided into two main branches, the first measuring molecular resonance frequencies in the absence of any large perturbing fields and the second in which the energy level system is considerably altered by the application of a large magnetic field and resonant absorption is obtained from transitions between the new levels.

Paramagnetic resonance absorption spectroscopy or electron spin resonance lies in the second class and is a technique for detecting the unpaired electrons in a substance and studying the interaction of these electrons with their environment.

In a simple model of a free radical in which the unpaired electron is not coupled to any nuclei or other electrons the free electron has a spin S of ½ and can exist in two states with equal energy. This degeneracy can be removed by the application of an external magnetic field which will produce two separate levels with spin quantum numbers $-\frac{1}{2}$ and $+\frac{1}{2}$. The lower energy level corresponds to the parallel alignment of the electron spin with the magnetic field and the upper level corresponds to an antiparallel alignment. The separation between the levels is equal to $g\beta H$ where g is a constant splitting factor equal to 2.0023 for a free electron, β is the Bohr magneton and H is the applied field in oersteds. The application of the appropriate radio frequency ν that satisfies the equation

$$h\nu = g\beta H \qquad \ldots\ldots\ldots(1)$$

will cause transitions to occur between the two energy states. In normal thermal equilibrium the population of the lower energy state is greater than that of the upper energy state and there is a net absorption of radio frequency energy. For low radio frequency power levels saturation of the upper energy level does not usually

occur as energy is lost from the upper level by spin-spin or spin lattice interaction. A constant proportion of the incident power is absorbed providing the relaxation time, defined as the time taken for the spin system energy to decrease to e^{-1} of its initial value, is small or the incident RF energy is maintained at a low level.

In a real substance considerable modifications occur to the single free electron spectrum case described above. The local field actually seen by the unpaired electron is modified from the applied field by the magnetic field generated by the relative motion of the electron with respect to neighbouring electric charges and also the direct magnetic action of other electron and nuclear magnetic moments. These various influences alter the g value and the width of the absorption line and also split the energy levels to produce fine and hyperfine structure.

In most organic free radicals the unpaired electron is not rigidly attached to a particular atom but occupies an orbit embracing several atoms. The interaction of the magnetic moment of the unpaired electron and the magnetic moment of the nuclei which are embraced by the molecular orbit of the electron will produce a hyperfine structure of the ESR spectrum. In a simple case if the electron interacts with one hydrogen atom the effective field is either $H + \Delta H$ or $H - \Delta H$, the ΔH term coming from the proton whose moment may be oriented either parallel or antiparallel to the main field. A two line spectrum with equal intensity lines will be produced to satisfy the equation

$$h\nu = g\beta(H \pm \Delta H) \qquad \ldots\ldots\ldots(2)$$

Interaction with a second proton will cause a second splitting, the unpaired electron being in one of four possible magnetic fields with the proton orientations being as follows $\uparrow\uparrow, \downarrow\uparrow, \uparrow\downarrow, \downarrow\downarrow$. As can easily be seen this will produce a three line spectrum with the centre line of double intensity. In the general case in which the orbit of the unpaired electron embraces n equivalent protons a spectrum of n + 1 hyperfine lines is produced whose relative intensities are proportional to the coefficients of the binomial

expansion of order n. This type of spectrum is very important in organic free radical work.

Substances suitable for study by ESR techniques are found in the following groups:

1. Crystals containing bonded atoms of the transition elements.
2. Crystals having broken bonds or defects such as F centres where free electrons occupy atomic sites.
3. Semiconductors containing electron donor impurities.
4. Metals and semiconductors in which conduction band electrons provide resonance absorption.
5. Free radicals.
6. Ferromagnetic materials.

In addition to structure determination ESR has been used to investigate a variety of effects such as the polymerisation of materials, x-ray and neutron damage, photosynthesis and even by inference the possible carcinogenic effect of cigarette smoke.

2. PRINCIPLES OF SPECTROMETER DESIGN

The following is based on Refs. 1 - 6.

An electron spin resonance spectrometer can be built in a variety of ways depending on the inclination of the constructor and the availability of components. There are two main types of spectrometer in common use, one employing high frequency magnetic modulation and the other using superheterodyne detection of the microwave signal. Both types of system have advantages in different situations. High frequency magnetic modulation, commonly at 100 kc, is more generally useful because the electronic circuitry is simpler, easier to operate and with modern detection diodes that have a low noise spectrum at 100 kc there is very little loss in sensitivity compared to a superheterodyne system. Superheterodyne detection becomes necessary if experiments are being performed at liquid helium temperatures or if materials with long relaxation times are studied when the line broadening produced by high frequency modulation would be undesirable.

All spectrometers, however, require the basic components listed below:

1. A source of radio frequency energy.
2. A magnet system capable of supplying a sufficiently uniform field of suitable intensity.
3. A sample holder of suitable shape such that the specimen is in a region of radio frequency magnetic field orthogonal to the DC magnetic field.
4. A system to detect and display the resonant absorption of energy of the sample.

For a free electron the absorption condition $h\nu = g\beta H$ can be written in practical units as

$$\text{Frequency in Mc} = 2.802.(\text{Field in oersted}) \qquad \ldots\ldots\ldots(3)$$

ESR absorption can be observed at any frequency providing the applied DC magnetic field satisfies the above equation. The distribution of electrons in the two energy levels in the absence of the RF field is given by the Boltzmann distribution expression

$$\frac{n_1}{n_2} = e^{\frac{-\Delta E}{kT}} \qquad \ldots\ldots\ldots(4)$$

where

n_1 is the number of electrons in the upper state,

n_2 is the number of electrons in the lower state,

k is Boltzmann's constant,

T is absolute temperature,

ΔE is the energy separation between the levels,

and so greater sensitivity is obtained by working with small T or large ΔE. For most general purpose spectrometers a frequency of 10,000 Mc and a field of about 3500 oe are used. This frequency is easily obtained with current techniques and a variety of components are commercially obtainable. The magnetic field requirements can be satisfied with an electromagnet using a soft iron yoke without any risk of saturating the material. Although increasing the value of ΔE should increase the sensitivity, in practice this advantage is to some extent nullified by the low output powers of short

microwave klystrons and the decrease in sensitivity of the detectors. If a resonant cavity is used as a sample holder the small size permits the examination of only small samples without excessive cavity loading.

The power absorbed by the spin system can be shown to be (Ref.6)

$$P(\nu) = N(\pi g\beta)^2 \nu H_1^2 \nu_o G(\nu)/8kT \qquad \ldots\ldots\ldots(5)$$

where

ν is the applied frequency,

N is the number of unpaired spins,

ν_o is the resonant frequency determined by the DC applied field,

H_1 is the RF field strength,

$G(\nu)$ is the observed absorption line shape normalised so that

$$\int_o^\infty G(\nu)\, d\nu = 1.$$

It can be seen that the power absorbed is proportional to H_1^2 and it is usual to increase the effective RF field strength seen by the sample by placing it in a resonant cavity. The effect of the sample resonance on the cavity properties is simply shown below.

A microwave resonant cavity with the sample in the position of maximum RF magnetic field can be represented by a tuned circuit, as shown in Fig.1, with the sample inserted in the coil. The impedance across the circuit is

$$Z_s = R + j(\omega L - \frac{1}{\omega C}) \qquad \ldots\ldots\ldots(6)$$

At paramagnetic resonance let the change in complex susceptibility be

$$\chi = \chi' - j\chi''$$

then since the permeability $\mu = 1 + 4\pi\chi$ the new value of inductance is

$$L(1+4\pi\eta\chi)$$

where η is the filling factor $0 < \eta < 1$.

FIG.1

MICROWAVE CAVITY EQUIVALENT CIRCUIT

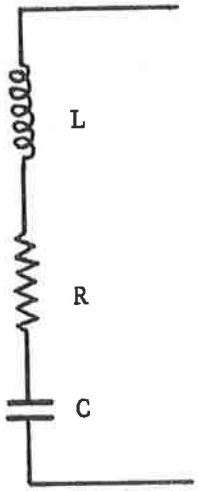

FIG.2

SIMPLE MICROWAVE SPECTROMETER

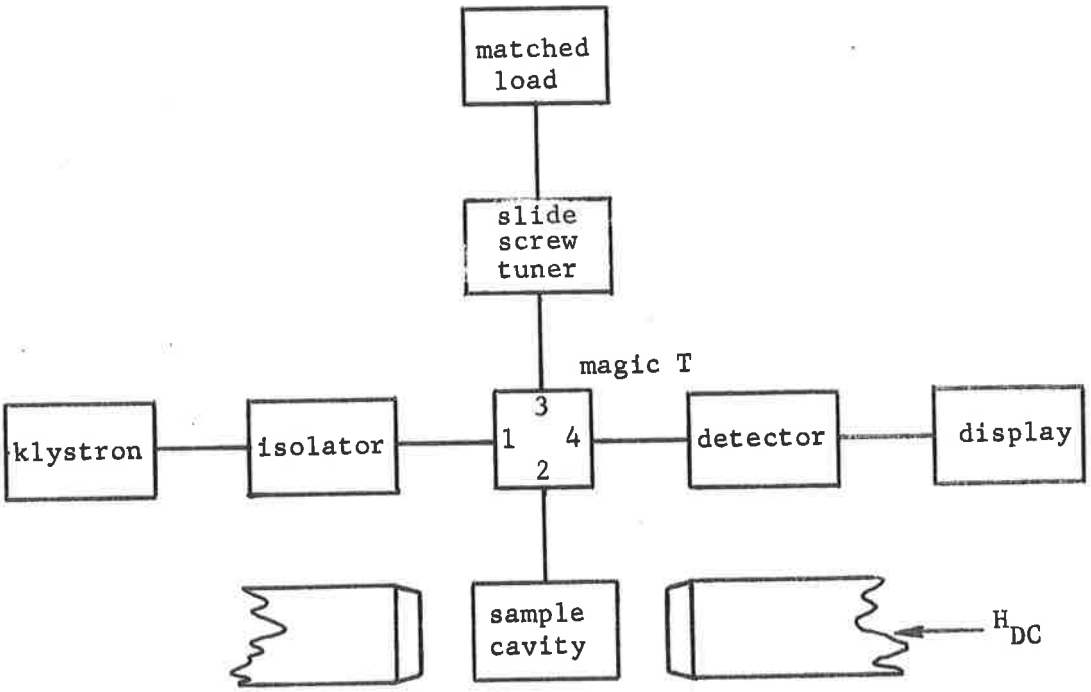

The circuit impedance now becomes

$$Z_s = R + j(\omega L\ (1 + 4\pi\eta\chi) - \frac{1}{\omega C}) \qquad \ldots\ldots\ldots(7)$$

$$= R + 4\pi\eta\ \ \omega L\chi'' + j(\omega L + 4\pi\ \chi'\omega L - \frac{1}{\omega C}). \qquad \ldots\ldots\ldots(8)$$

At resonance the sample has increased the circuit loss by

$$4\pi\eta\chi''\omega L$$

and the inductance by

$$4\pi\eta\chi' L.$$

$$\text{Since } Q = \frac{\omega L}{R}\ , \qquad \ldots\ldots\ldots(9)$$

$$dQ = \frac{\omega}{R}\ \delta\ L - \frac{\omega L}{R^2}\delta R$$

$$= \frac{\omega}{R}\ 4\pi\eta\chi' L - \frac{\omega L}{R^2}\ 4\pi\eta\chi''\omega L$$

$$= Q4\pi\eta\chi' - Q^2 4\pi\eta\chi''$$

Experimentally the change in L is found to be small so

$$dQ = -Q^2 4\pi\eta\chi'' \qquad \ldots\ldots\ldots(10)$$

Similarly the change in resonant frequency can be found

$$\omega_r = \frac{1}{\sqrt{LC}}\ , \qquad \ldots\ldots\ldots(11)$$

$$d\omega_r = -\frac{1}{\sqrt{C}}\ .\tfrac{1}{2}L^{-\frac{3}{2}}\ dL$$

$$= -2\pi\eta\ \omega_r\chi' \qquad \ldots\ldots\ldots(12)$$

ESR spectroscopy can either detect the absorption susceptibility component χ'' or the dispersive component χ'. The former is detected as the change in Q of the tuned circuit and the latter by the change in the resonant frequency. Practical considerations make it easier to work at a fixed frequency and to vary the magnetic field to obtain the required spectrum. The klystron frequency is usually locked to the resonant cavity eliminating the dispersive component and leaving only the absorption component.

A simple type of microwave reflection spectrometer is shown in Fig.2. Radio frequency power, supplied by a klystron which is isolated from reflections in the circuit by a ferrite isolator, is fed into a Magic T where it is equally split between arms 2 and 3. Arm 2 terminates in a resonant cavity containing the sample material. Arm 3 terminates in a matched load preceded by a slide screw tuner, a device to produce a reflected signal that is independently variable in phase and amplitude. The slide screw tuner is normally adjusted to nearly balance the reflected signal from the cavity so that only a small signal emerges from arm 4 into the detector. The resonant absorption of energy by the sample will produce a change in the cavity reflection coefficient which produces a variation in the bridge balance that can be detected in arm 4 and displayed either on an oscilloscope or a pen recorder.

A method for determining the optimum cavity coupling has been described by Feher (Ref.7). The reflection cavity can be represented by the equivalent circuit shown in Fig.3. The input power is divided by two due to the power split at the Magic T. By considering the change in reflected power when absorption occurs and optimising this change of power by differentiating with respect to the coupling parameter n it can be shown that for a square law detector the cavity should be undercoupled so as to produce a VSWR of 3.74 at resonance.

The detection of the microwave signal can be done by using a bolometer or a silicon crystal detector. The change in power level at the detector is obscured by the noise generated in the waveguide run, the crystal detector and its following amplifier.

The noise power at the detector output is (Ref.7)

$$P_{noise} = (GN_K + F_A + t_D - 1) \quad (kT\Delta\nu) \qquad .....(13)$$

where

G is the conversion gain of the detector,

N_K is the noise figure at the input to the detector,

F_A is the noise figure of the amplifier,

FIG.3

COUPLED REFLECTION CAVITY

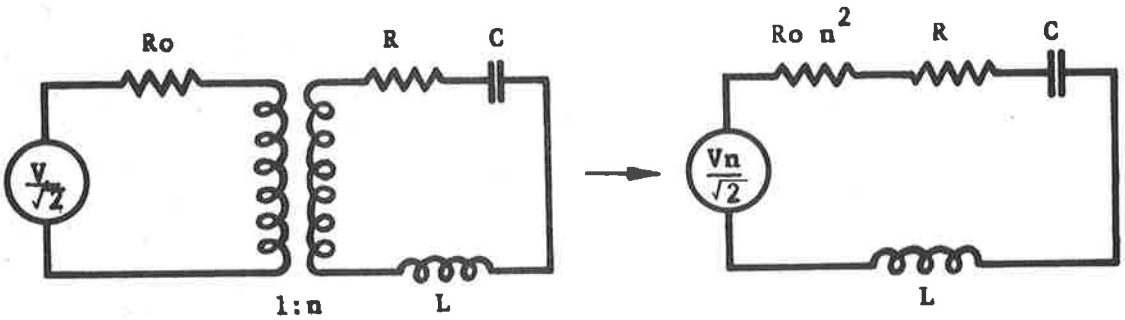

FIG.4

SMALL MAGNETIC MODULATION

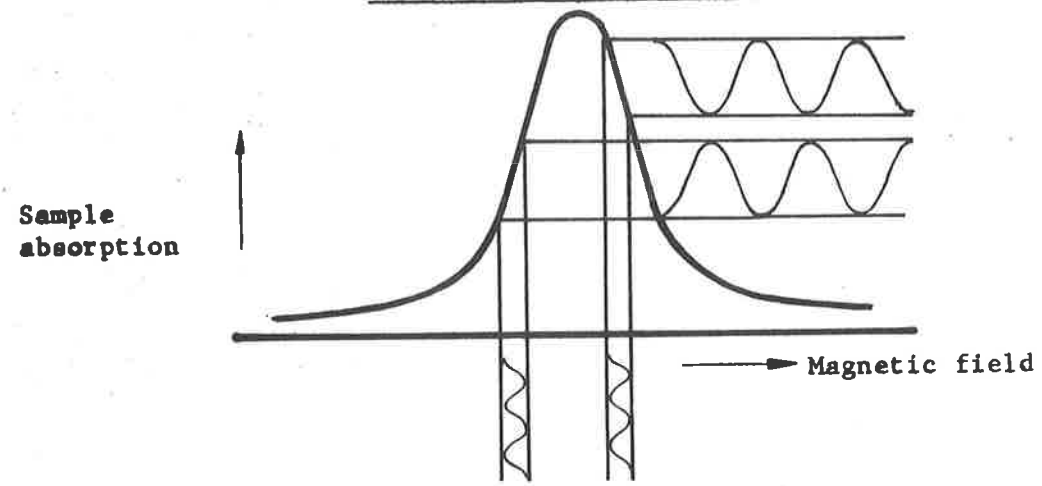

FIG.5

LARGE MAGNETIC MODULATION

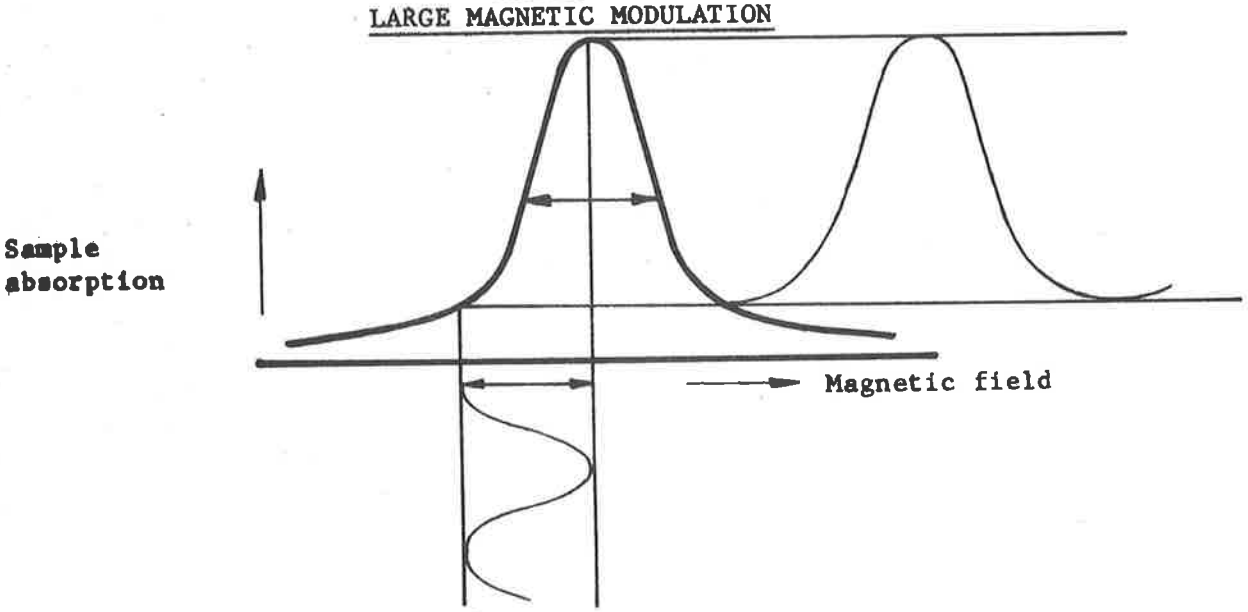

t_D is the noise temperature of the detector,

k is Boltzmann's constant,

T is the temperature,

$\Delta \nu$ is the bandwidth of the system.

Using this value of detector noise the minimum detectable χ'' for a signal to noise ratio of 1 is (Ref.7)

$$\chi'' = \frac{1}{Q_o \eta \pi} \left\{ \frac{(GN_K + F_A + t_D - 1)\, kT\Delta\nu}{2GP_o} \right\}^{\frac{1}{2}} \qquad \ldots\ldots\ldots(14)$$

where

Q_o is the unloaded cavity Q,

η is the filling factor,

P_o is the incident power.

From this expression it can be seen that the maximum sensitivity will be obtained when the product $Q_o \eta$ is a maximum and the numerator is a minimum. The quantity determined by the detector is

$$\left\{ \frac{GN_K + F_A + t_D - 1}{G} \right\}^{\frac{1}{2}}$$

and for optimum sensitivity this quantity has to be minimised.

Two types of detectors are available for microwave use, bolometer and crystal, but as bolometer detectors have high conversion losses at low powers, crystal detectors are usually employed in spectrometers. The excess noise generated in a crystal detector is inversely proportional to frequency and increases with increasing power. The crystal characteristic changes with increasing incident power and for normal silicon crystal detectors the characteristic can be divided into two parts: a square law region in which the rectified current is proportional to the incident power, which in this region is less than 10^{-5} watts, and a linear region extending into milliwatts where the rectified current is proportional to the square root of the incident power. In the first region the conversion loss of the crystal is inversely proportional to the incident power and in the second region the conversion loss is constant. From the above it will be seen that there is an

optimum value of input power to the crystal detector. Power levels below this result in high conversion losses and power levels above this produce excessive crystal noise. Although the optimum detector power range is small (Ref.7) it is easily achieved in practice and, in the spectrometer described above can be done by adjusting the slide screw tuner to suitably unbalance the bridge.

The excess crystal noise that is inversely proportional to frequency can be minimised by employing either superheterodyne detection or high frequency magnetic field modulation. The most sensitive spectrometers employ superheterodyne detection but the complexities of this system can be avoided, with some loss of sensitivity, by employing high frequency magnetic field modulation. The disadvantages of this method are not only the practical one of producing the required magnetic sweep but also the fact that the absorption lines are broadened by approximately the frequency of the modulation (Ref.8). A modulating frequency of 100 kc will produce a line broadening of 0.036 oe but unless the specimen spectrum contains narrow hyperfine lines that are being studied which would require a magnet producing a very uniform field over the specimen, this broadening is usually unimportant. A loss of sensitivity of less than 3, compared to a superheterodyne system, is obtained together with a considerable decrease in constructional and operating complexity.

From equation (11) it can be seen that the noise power at the output of the detector is proportional to the detector bandwidth. Although the simplest resonant absorption display system uses an oscilloscope in conjunction with a magnetic field modulation large compared to the linewidth of the specimen, a large detector bandwidth is required to preserve the shape of the absorption line. The bandwidth can be reduced to a few cps, with consequent noise reduction, if a magnetic sweep amplitude small compared to the linewidth is used in conjunction with a slowly varying DC magnetic field. This is shown in Fig.4. The output signal in this case is proportional to the slope of the absorption line and the phase is dependent on the sign of the slope so that by using a phase sensitive detector the derivative of the absorption line can be

FIG.6

BLOCK DIAGRAM OF ESR SPECTROMETER

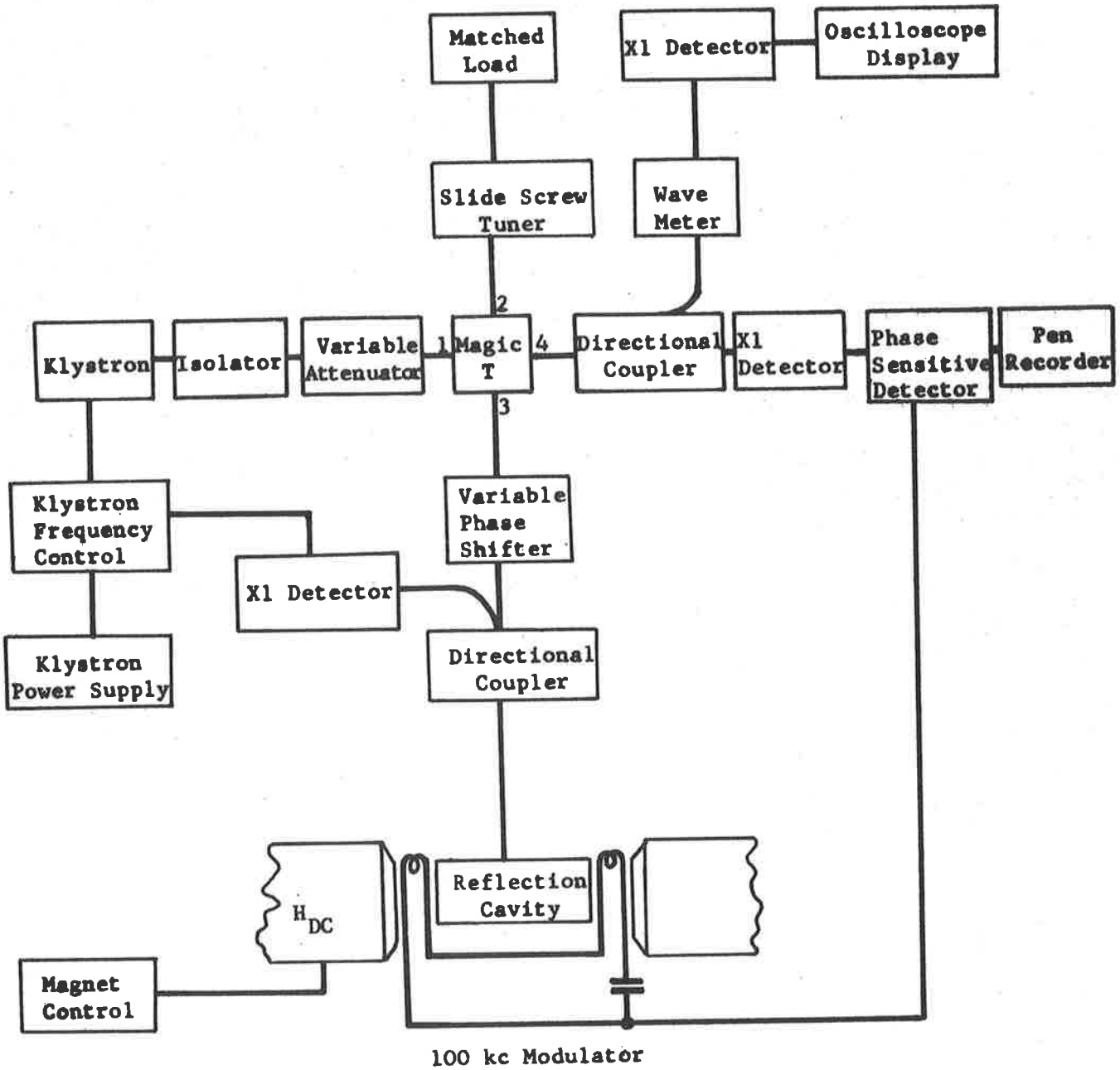

displayed. The DC magnetic field is usually varied very slowly and the derivative signal is plotted on a pen recorder for later analysis. If the magnetic field modulation is equal to the line-width as shown in Fig.5, the sample output signal is larger but the derivative curve is considerably distorted. Where only the g value is required, the large modulating signal produces no error with a symmetrical curve since the zero output signal field value corresponds to the true absorption maximum.

3. KLYSTRON FREQUENCY STABILISER

3.1 Necessity for klystron frequency locking

Using the above design principles a 3 cm spectrometer was constructed to the block diagram shown in Fig.6. The design and construction of the various components are described below.

The conventional ESR spectrometer employs a sample-holding cavity to increase the sensitivity of the system. The spectrometer sensitivity is limited by short term frequency fluctuation and long term frequency drift of the klystron away from the cavity frequency. The required order of stability can be found by comparing the change in cavity reflection coefficients produced by change of incident frequency and sample absorption.

Consider a resonant cavity terminating a waveguide, shown in Fig.7, where R_g is the generator impedance assumed to be matched to the waveguide, and R_c represents the cavity loss. The voltage reflection coefficient Γ is defined by

$$\Gamma = \frac{V_r}{V_i} \qquad \ldots\ldots\ldots(15)$$

where

V_r is the reflected signal voltage from the cavity,

V_i is the incident signal voltage on the cavity,

the reflected power being $P_r = |\Gamma|^2 P_i$. $\ldots\ldots\ldots(16)$

For the two conductor transmission line shown

$$\Gamma = \frac{Z - Z_o}{Z + Z_o} \qquad \ldots\ldots\ldots(17)$$

FIG.7

EQUIVALENT CIRCUIT OF COUPLED CIRCUIT

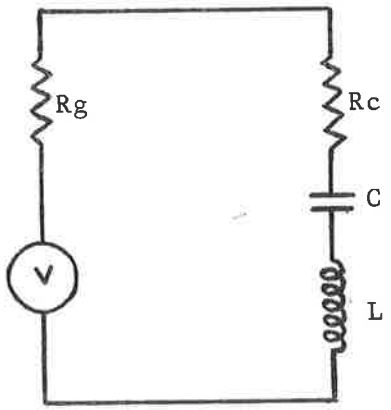

FIG.8

BLOCK DIAGRAM OF POUND CONTROL CIRCUIT

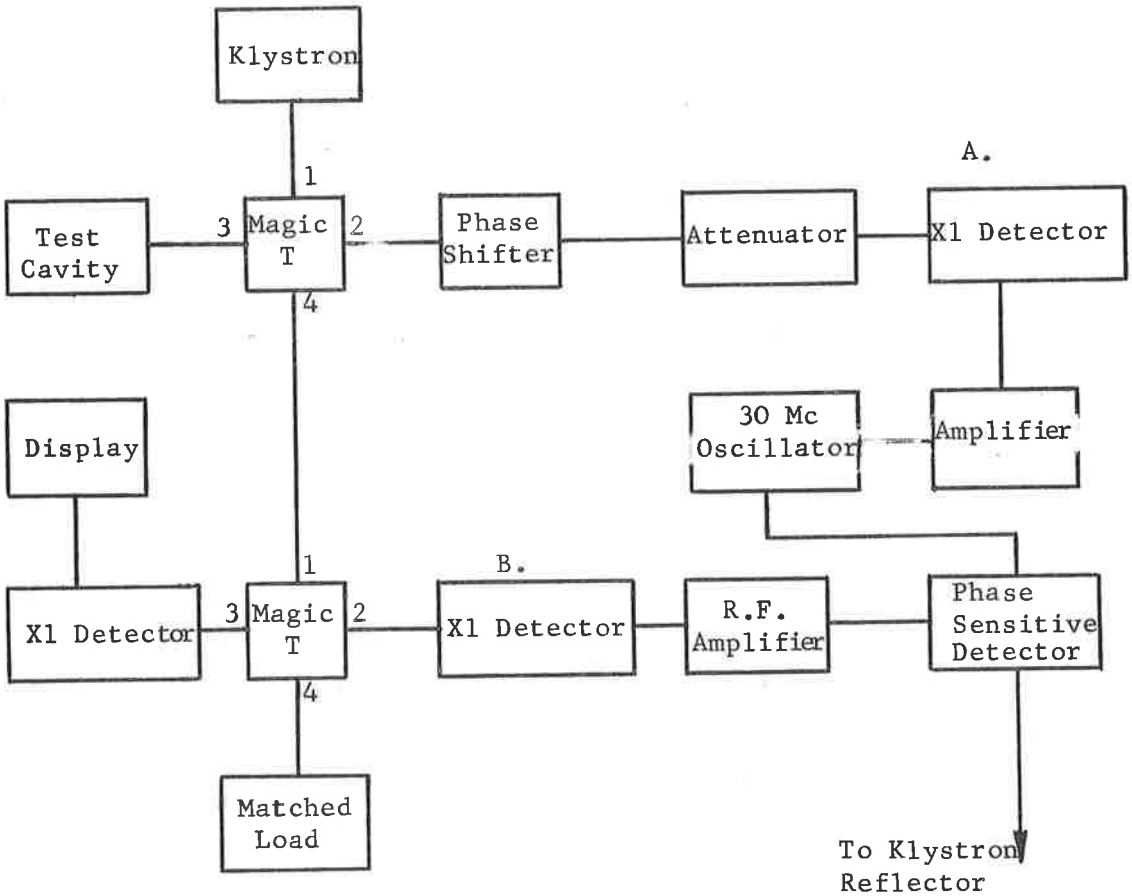

where

Z_o is the characteristic impedance of the line,

Z is the impedance of the terminating load.

The voltage reflection coefficient for the cavity is

$$\Gamma = \frac{R_c + j\left(\omega L - \frac{1}{\omega C}\right) - R_g}{R_c + j\left(\omega L - \frac{1}{\omega C}\right) + R_g} \quad . \qquad \ldots\ldots\ldots(18)$$

If unloaded Q of the cavity is

$$Q_u = \frac{\omega_o L}{R_c} \quad ,$$

where ω_o is the resonant frequency

$$\omega_o = \frac{1}{2\pi\sqrt{LC}} \quad ,$$

and if the radiation Q is defined as

$$Q_R = \frac{\omega_o L}{R_g}$$

then

$$\Gamma = \frac{\frac{\omega_o L}{Q_u} - \frac{\omega_o L}{Q_R} + j\left(\omega L - \frac{1}{\omega C}\right)}{\frac{\omega_o L}{Q_R} + \frac{\omega_o L}{Q_u} + j\left(\omega L - \frac{1}{\omega C}\right)} \qquad \ldots\ldots\ldots(19)$$

$$= \frac{\frac{1}{Q_u} - \frac{1}{Q_R} + j\left(\frac{\omega}{\omega_o} - \frac{\omega_o}{\omega}\right)}{\frac{1}{Q_R} + \frac{1}{Q_u} + j\left(\frac{\omega}{\omega_o} - \frac{\omega_o}{\omega}\right)} \quad . \qquad \ldots\ldots\ldots(20)$$

At resonance when $\omega = \omega_o$

$$\Gamma_{res} = \frac{Q_R - Q_u}{Q_R + Q_u} \quad . \qquad \ldots\ldots\ldots(21)$$

The loaded Q of the circuit is

$$Q_L = \frac{\omega_o L}{R_g + R_c} = \frac{Q_u Q_R}{Q_u + Q_R} \quad . \qquad \ldots\ldots\ldots(22)$$

Equation (20) can be rewritten as

$$\Gamma = \frac{\Gamma_{res} + j Q_L \left(\frac{\omega}{\omega_o} - \frac{\omega_o}{\omega}\right)}{1 + j Q_L \left(\frac{\omega}{\omega_o} - \frac{\omega_o}{\omega}\right)} \quad . \qquad \ldots\ldots\ldots(23)$$

When magnetic resonance occurs in the sample the values of L and R_c change. The resistance changes to a new value

$$R' = R_c + \Delta R \qquad \text{.....(24)}$$

and a new value of unloaded Q is obtained:

$$\frac{1}{Q_{um}} = \frac{1}{Q_u} + \frac{\eta}{Q_m} \qquad \text{.....(25)}$$

where

$$\frac{\eta}{Q_m} = \frac{\Delta R}{\omega_{om} L} \qquad \text{.....(26)}$$

and the change in L is small.

The magnetic Q, Q_m is a figure of merit which determines the ratio of energy stored in the cavity to the energy lost per cycle by magnetic absorption; and η, the filling factor, is the ratio of the magnetic field density effective in causing absorption to the total magnetic field density in the cavity. Using the expressions derived on page 7 the change in Q and frequency can be found

$$\frac{1}{Q_m} = \frac{\Delta R}{\eta \omega_{om} L} = \frac{4\pi\eta\omega_{om} L \chi''}{\eta \omega_{om} L} = 4\pi\chi''. \qquad \text{.....(27)}$$

The inductance also changes to a new value

$$L = L + \Delta L \qquad \text{.....(28)}$$

which changes the frequency from ω_o to ω_{om}, where

$$\omega_{om} = \frac{\omega_o}{\sqrt{1 + 4\pi\eta\chi'}} \approx \omega_o (1 - 2\pi\eta\chi'). \qquad \text{.....(29)}$$

Changing the value of the unloaded Q changes equation (23) to

$$\Gamma_m = \frac{\Gamma_{res} + \eta\frac{Q_L}{Q_m} + jQ_L\left\{\frac{\omega}{\omega_{om}} - \frac{\omega_{om}}{\omega}\right\}}{1 + \eta\frac{Q_L}{Q_m} + jQ_L\left\{\frac{\omega}{\omega_{om}} - \frac{\omega_{om}}{\omega}\right\}} \qquad \text{.....(30)}$$

Let

$$r = \eta \frac{Q_L}{Q_m} \qquad \ldots\ldots\ldots(31)$$

and

$$x = Q_L \left\{ \frac{\omega}{\omega_{om}} - \frac{\omega_{om}}{\omega} \right\} \qquad \ldots\ldots\ldots(32)$$

then

$$\Gamma_m = \frac{\Gamma_{res} + r + jx}{1 + r + jx} . \qquad \ldots\ldots\ldots(33)$$

For small frequency changes

$$x = Q_L \left\{ \frac{\omega}{\omega_{om}} - \frac{\omega_{om}}{\omega} \right\} \approx 2Q_L \left\{ \frac{\omega - \omega_{om}}{\omega_{om}} \right\} . \qquad \ldots\ldots\ldots(34)$$

If the klystron frequency is held fixed the dependence of x on dispersion is

$$x = 2Q_L \left\{ \frac{\omega - \omega_{om}}{\omega_{om}} \right\} = 2Q_L \frac{\omega - \omega(1 - 2\pi\eta\chi')}{\omega(1 - 2\pi\eta\chi')} \qquad \ldots\ldots\ldots(35)$$

$$\approx 4Q_L \pi \eta \chi' .$$

Similarly if the klystron fluctuates about ω_{om} by $\delta\omega$,

$$x = \frac{2Q_L \delta\omega}{\omega_{om}} . \qquad \ldots\ldots\ldots(36)$$

Expanding equation (33),

$$\Gamma_m = (\Gamma_{res} + r + jx)(1 + r + jx)^{-1},$$

and taking the real parts

$$Rl\,\Gamma_m = \Gamma_{res} + (r - r^2 + x^2)(1 - \Gamma_{res}) . \qquad \ldots\ldots\ldots(37)$$

If the bridge is balanced to be sensitive to the real part of the reflection coefficient, frequency variations will produce a signal output of magnitude equal to the absorption signal if

$$r(1 - r) = -x^2 \qquad \ldots\ldots\ldots(38)$$

If $r \ll 1$, then using (27), (31) and (36) this condition becomes

$$\frac{\delta\omega}{\omega_{om}} = \frac{\delta\nu}{\nu_{om}} = \sqrt{\frac{\pi\chi''\eta}{Q_L}}. \qquad \ldots\ldots(39)$$

Some typical figures for a high sensitivity spectrometer are

$4\pi\eta\chi'' \sim 10^{-10}$ for 6×10^{12} spins hydrazyl

$Q_L \sim 2 \times 10^3$

making $\frac{\delta\nu}{\nu_m} \sim 1 \times 10^{-7}$

For a 723A/B klystron in a normal working mode tuned by the reflector voltage, $\frac{\Delta\nu}{V_{ref}} = 2$ Mc/volt and so, if the working frequency is 10,000 Mc, $\delta\nu = 1$ kc and the klystron reflector voltage is required to have a short term stability of about 0.5 mV.

3.2 Methods of klystron achieving frequency locking

By using a klystron locked onto the sample cavity the klystron will follow any changes in the cavity frequency due to cavity vibrations or change of shape due to thermal effects in addition to removing the dispersion signal due to the change in χ'. Frequency locking circuits commonly control by using the dependence of klystron frequency on reflector voltage. A system is used which produces a voltage whose sign is dependent upon and amplitude proportional to, the imaginary part of the cavity reflection coefficient. This voltage is algebraically added to the normal reflector supply voltage to produce frequency control.

An initial attempt to control the klystron frequency was made by using a Pound type RF frequency control system. The block diagram is shown in Fig.8 and the circuitry used was derived from Ref.5.

Signal from the klystron enters arm 1 of the Magic T and is equally split into arms 2 and 3. The crystal detector A is matched to the waveguide in the absence of an RF signal being applied to it, so that in operation the signal reflected from crystal A contains only the upper and lower sidebands and none of the carrier. These sidebands, together with the signal reflected

from the cavity, are eventually incident on crystal B where detection takes place. If the cavity is matched to the waveguide at resonance there is no output at crystal B at the modulating frequency. Away from resonance a signal is reflected from the cavity with amplitude dependent on the frequency deviation and phase dependent on the direction of the deviation. The mixed output of these signals is amplified and used in a phase sensitive detector to control the klystron frequency.

A Pound system was constructed based on a 33 Mc crystal oscillator but considerable difficulty was experienced in use. For ESR work the cavity should have a VSWR of about 3.7 at resonance and so even with the cavity on frequency there was a large RF signal output from crystal B which made the system more difficult to set up and less sensitive than one in which the cavity is matched to the line at resonance. Another difficulty was that the variable μ valves used in the RF amplifier strip to control the gain produced a variable phase shift with varying gain resulting in changing discriminator characteristics. In the microwave part of the system spurious reflections from discontinuities in the waveguide run produced signals that the klystron would lock on to. The adjustment of the phase shifter and attenuator in the crystal A arm were found to be sensitive and changing the cavity resonant frequency, by inserting a sample, required readjustment of these controls and the matching screws of the crystal modulator to obtain a match at the new frequency. The system also required to be re-set if components were added that changed the bridge arm lengths. These difficulties, although not insuperable, made the use of the stabiliser time consuming and tedious and so it was decided to change the locking system to a different type.

The three main conditions required of the new system were:

1. To be insensitive to bridge arm lengths and spurious reflections from improperly matched components.
2. Zero RF control signal from the detector when the klystron frequency equalled the cavity resonant frequency.

FIG.9

AMPLITUDE MODULATION PRODUCED BY FREQUENCY MODULATION

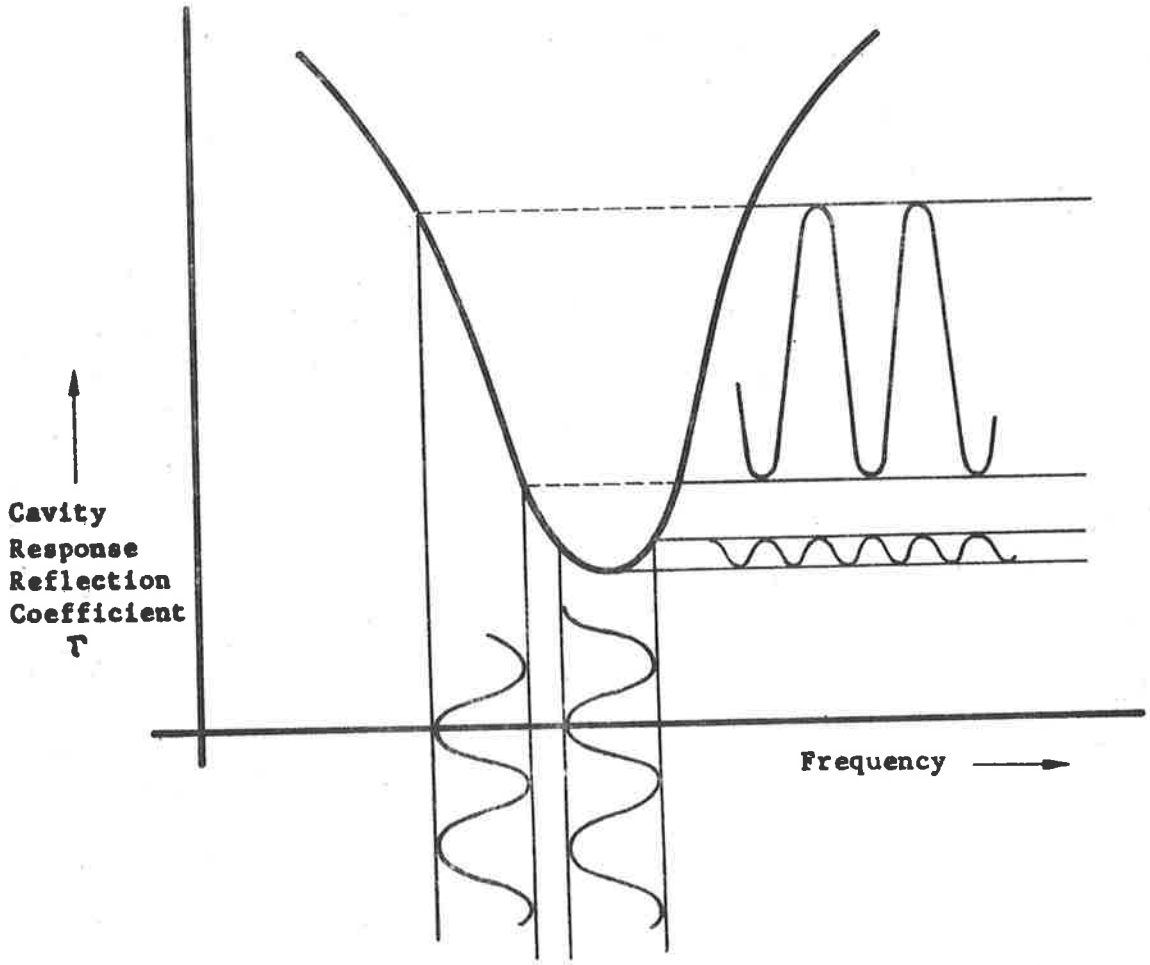

3. Zero output from the phase sensitive detector when the above frequency condition is met. The previous system had used a 6AS6 as a phase sensitive detector and the output of this had varied about a fixed non zero potential.

The above conditions can be satisfied by using a system employing frequency modulation of the klystron by impressing an RF signal on the DC reflector potential. This system can cause modulation broadening of the ESR absorption lines but providing the amplitude of the modulating signal is small the broadening is insignificant unless very narrow lines are being studied. The principle of the system is shown in Fig.9. If the cavity and klystron are exactly on tune no amplitude modulation of the reflected microwave signal occurs at the modulating frequency. If the klystron deviates from the cavity frequency a sign sensitive amplitude modulation occurs which can be detected and used to return the klystron frequency to the cavity frequency.

3.3 Circuit construction and operation

A klystron frequency stabiliser was designed as shown in Fig.10. This unit operates in conjunction with a PRD Type 809A klystron power supply. The operating frequency of the stabiliser is 455 kc, a frequency chosen because of the ready availability of domestic radio IF transformers.

The circuit was designed to be operated in two different ways controlled by a function switch. The first switch position used a sweeping mode for testing with the second position used for frequency locking. The -150V reflector line from the klystron power supply was connected to the circuit at point 4, shown in Fig.10, and leaves to the klystron reflector from point 5. In the sweeping position of the function switch no correction voltage was applied to this signal. A 455 kc signal was generated by the oscillator V8 and applied to point 5 via an attenuator, cathode follower and DC blocking condenser. Under normal operating conditions a signal of about 3 mV peak to peak was applied to the klystron reflector. The 723A/B klystron used has a frequency change

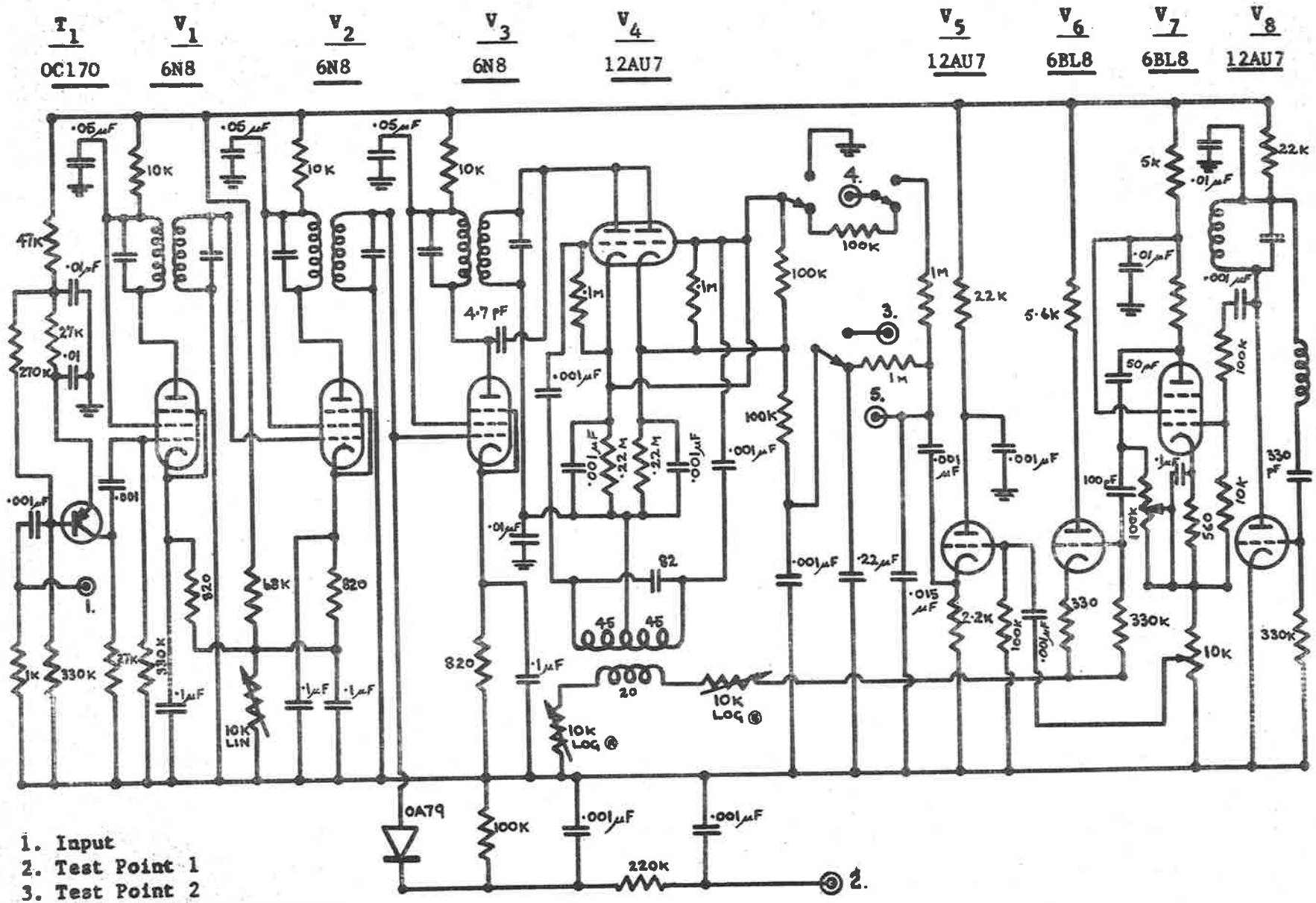

FIG.10
KLYSTRON FREQUENCY STABILISER

of 2 Mc per volt and so a modulation of about $\pm$ 3 kc is produced. This will produce a modulation line broadening of about 0.002 oe.

The amplitude modulated signal reflected from the cavity was detected in a crystal detector and fed to point 1. A three valve amplifier strip was used with 6N8 valves, remote cutoff RF pentodes, and the amplifier gain was controlled by varying the effective grid bias to two of them. After construction it was found that the correction voltage for small frequency deviations was insufficient and so a single OC170 untuned transistor amplifier was added before the main amplifier. The output from V3 was tightly coupled to the phase sensitive detector V4 by means of an RF transformer and a 4.7 pf condenser. Several experiments were made using diodes in a balanced circuit as a phase detector but a steeper discriminator curve resulted when the double triode circuit shown was used. The 455 kc oscillator was used in conjunction with a phase shifting circuit and cathode follower to supply a reference signal of about 5V peak to peak to the triode grids. The out of balance voltage developed between the cathode resistors appears across a 100K resistor in the klystron reflector supply circuit.

The circuit was initially adjusted with the assistance of two test points. A sawtooth wave was applied to the klystron reflector to sweep the klystron frequency through the cavity resonance with the first test point showing a rectified output of the RF signal existing at the grid of V3. The second test point was used to show the output of the phase sensitive detector. Figs. 11, 12, 13 and 14 show a typical set of waveforms obtained during the initial adjustment of the stabilising circuit.

The upper trace in Fig.11 shows the sawtooth applied to the klystron reflector. The sawtooth is rounded by the condensers fixed in the reflector line to stop high frequency oscillations when the circuit operates in the locked position. The lower trace shows the detected microwave signal reflected from the cavity. The first dip is due to the cavity being swept during the sawtooth flyback.

Fig.11: Testing Oscillogram

Upper trace: Klystron reflector sawtooth 5 volts/cm sensitivity

Lower trace: Reflected cavity signal 0.2 volts/cm sensitivity

1 cm graticule

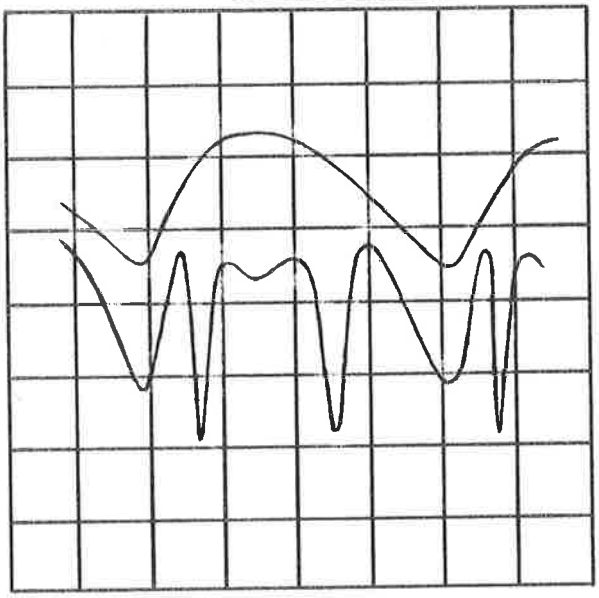

Fig.12: Testing Oscillogram

Upper trace: Signal at test point 2 0.5 volts/cm sensitivity

Lower trace: Reflected cavity signal 0.2 volts/cm sensitivity

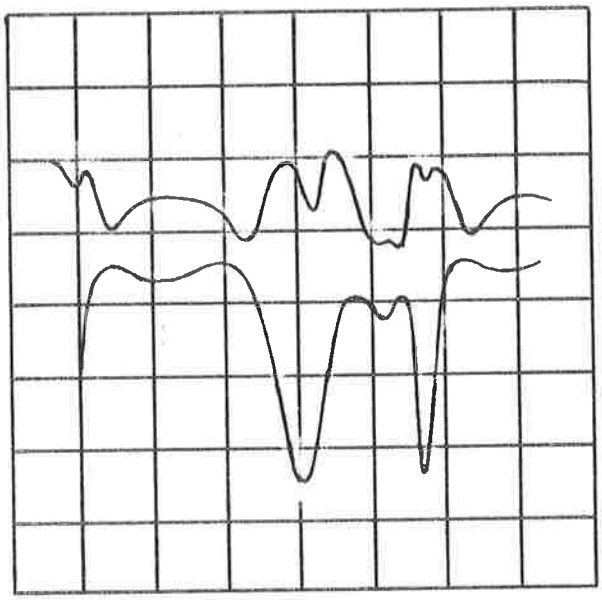

The lower trace in Fig.12 is the cavity reflection signal as in Fig.11 but the upper trace is taken at test point 2, the grid of V3. Two effects are noticed in this trace: the signal does not go to zero at the cavity resonant frequency due to the sweeping speed of the klystron and the phase shift of the RF response compared to the cavity response. Both of these effects only occurred during testing and are unimportant at the normal frequency correction rates required due to drift etc.

Fig.13 shows the waveform at test point 2 on the upper trace and the phase sensitive detector output, test point 3, on the lower trace.

The upper trace of Fig.14 shows the klystron reflector sawtooth and the lower trace shows the correction signal from the phase sensitive detector displayed at 1/5 of the upper trace sensitivity.

After the initial circuit adjustments had been made the locking circuit was used with the function switch in the second position and the amplifier gain set to minimum. The klystron reflector voltage was adjusted by hand to set the klystron on the cavity resonance and then the amplifier gain was increased to its maximum value to lock the klystron frequency to the cavity.

4. MAGNETIC MODULATION AND DISPLAY CIRCUITS

Electron spin resonance spectrometers usually employ a magnetic field sweep to trace out the absorption line. The simplest spectrometers use a manually adjusted field and a point by point plotting technique, but this method is limited to concentrated paramagnetic materials. A considerable improvement is obtained by using a low frequency cyclic variation of the magnetic field obtained by applying a sinusoidal voltage to separate coils wound close to the magnet gap. The magnetic field modulation is adjusted to be several times larger than the linewidth of the absorption line and by applying the modulation voltage to the X axis of an oscilloscope and the detector signal to the Y axis the resonance line can be displayed. The use of this large amplitude magnetic

Fig.13: Testing Oscillogram

Upper trace: Signal at test point 2 0.5 volts/cm sensitivity

Lower trace: Phase sensitive detector output, test point 3

10 volts/cm sensitivity

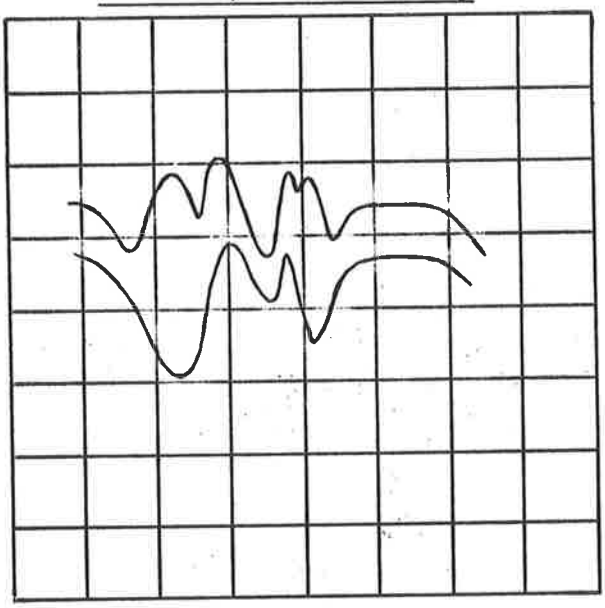

Fig.14: Testing Oscillogram

Upper trace: Klystron reflector sawtooth 2 volts/cm sensitivity

Lower trace: Phase sensitive detector output 10 volts/cm sensitivity

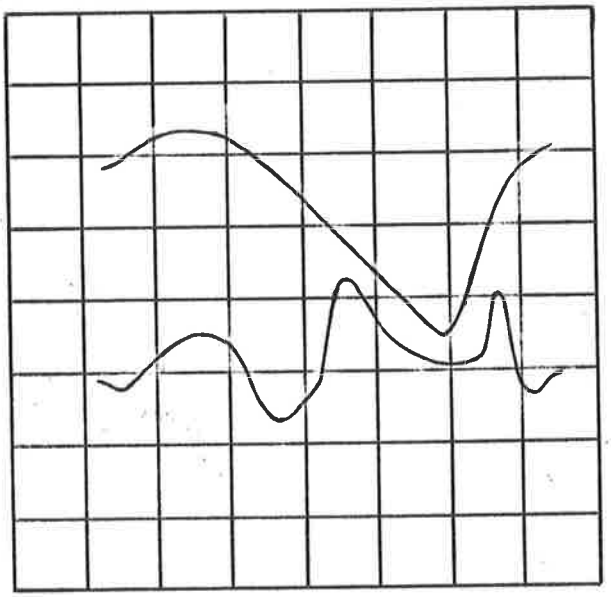

modulation produces a detector signal that not only contains frequency terms at the fundamental but also higher frequencies, the exact frequency spectrum being determined by the line shape. To avoid distorting the line, a bandwidth of at least ten times the modulating frequency is required, which results in a poor signal to noise ratio.

Large amplitude magnetic field modulation is only practicable for use with absorption lines of width less than about 30 oersteds. The large alternating magnetic fields required for lines wider than this produce undesirable vibrations in the magnet and waveguide system due to eddy current and magnetic field interaction.

A considerable increase in sensitivity can be obtained by using a field modulation amplitude small compared to the absorption line. In this system the derivative of the line is generated and after amplification can be displayed on a pen recorder. When modulation is applied the output at the detector is dependent on the line shape function $G(B)$ and can be found from a series expansion of $G(B)$ about the steady field value B^{o}.

$$
\begin{aligned}
G(B) &= G(B^{o} + B_{m}\cos\omega_{m}t) \\
&= G(B^{o}) + G'(B^{o})\, B_{m}\cos\omega_{m}t + \tfrac{1}{2}G''(B^{o})\,(B_{m}\cos\omega_{m}t)^{2} \\
&\quad + \tfrac{1}{6}G'''(B^{o})\,(B_{m}\cos\omega_{m}t)^{3}\ldots\ldots \\
&= G(B^{o}) + (B_{m}G'(B^{o}) + \tfrac{1}{8}B_{m}^{3}\,G'''(B^{o}) + \ldots\ldots)\cos\omega_{m}t \\
&\quad + \text{terms at } 2\omega_{m},\ 3\omega_{m},\ \ldots\ldots\ldots
\end{aligned}
$$

For small amplitude modulation the time varying part is proportional to the first derivative of the absorption line at the field value B^{o}, assuming a narrow band amplifier tuned to ω_{m} is used to suppress the terms at $2\omega_{m}$ etc. By using a slow magnetic field sweep the derivative of the absorption line can be obtained with a greatly increased signal to noise ratio compared to the large amplitude field modulation system. Large values of B_{m} will change the amplifier signal from the derivative of the absorption line and result in an apparent increase in the linewidth. Fig.15, taken from Ref.9 shows the detected signal amplitude and apparent

FIG.15

VARIATION OF LINEWIDTH AND DERIVATIVE SIGNAL AMPLITUDE WITH MAGNETIC MODULATION

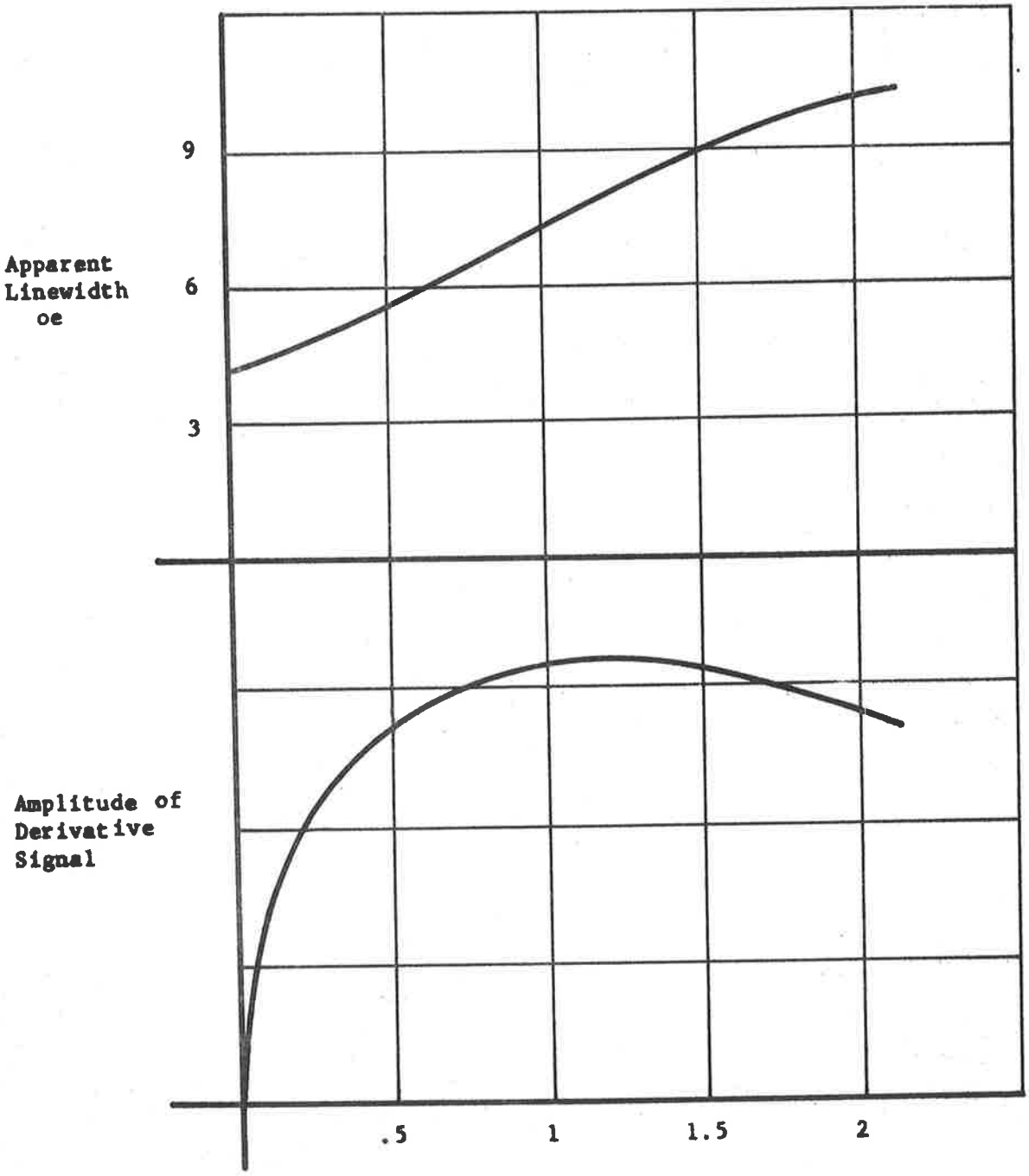

Magnetic field sweep normalised to the true linewidth

linewidth for a Lorentz curve plotted against normalised magnetic field modulation amplitude. It will be seen that the maximum detectable signal is obtained when the magnetic field sweep equals the absorption linewidth but then considerable distortion occurs. An analysis of the distortion produced by large modulation is given in Ref.10. For line shape studies the field modulation should be of the order of one tenth of the absorption linewidth. Using small magnetic field modulation produces maximum signal at the position of maximum slope and not at the true half height position. The correction factors that have to be applied for Gaussian and Lorentzian line shapes are given in Ref.2, page 128.

4.1 Practical circuit construction

A practical device to obtain and display absorption line derivatives is required to have the following parts:

1. A stable oscillator.
2. A power amplifier working at the oscillator frequency to supply the magnetic field sweep.
3. A high sensitivity low noise amplifier to detect the derivative signal.
4. A phase sensitive detector to compare the phase of the received signal with the master oscillator.
5. A display system such as a pen recorder.

4.2 Crystal oscillator, power amplifier and reference signal

A frequency of 95 kc was chosen for the master oscillator. This frequency is a compromise between the high frequency required to reduce the 1/f noise in the crystal detector and the low frequency required to minimise the line broadening produced by the magnetic field modulation. The oscillator, power amplifier and reference signal circuits are shown in Fig.16.

A crystal oscillator was used for the master oscillator with a 95 kc X cut bar series resonant in a Butler circuit, the valve anode being run from a 150V stabilised supply. Two outputs are taken from the oscillator, one to the power amplifier and the other to the phase shifting circuit for a reference signal.

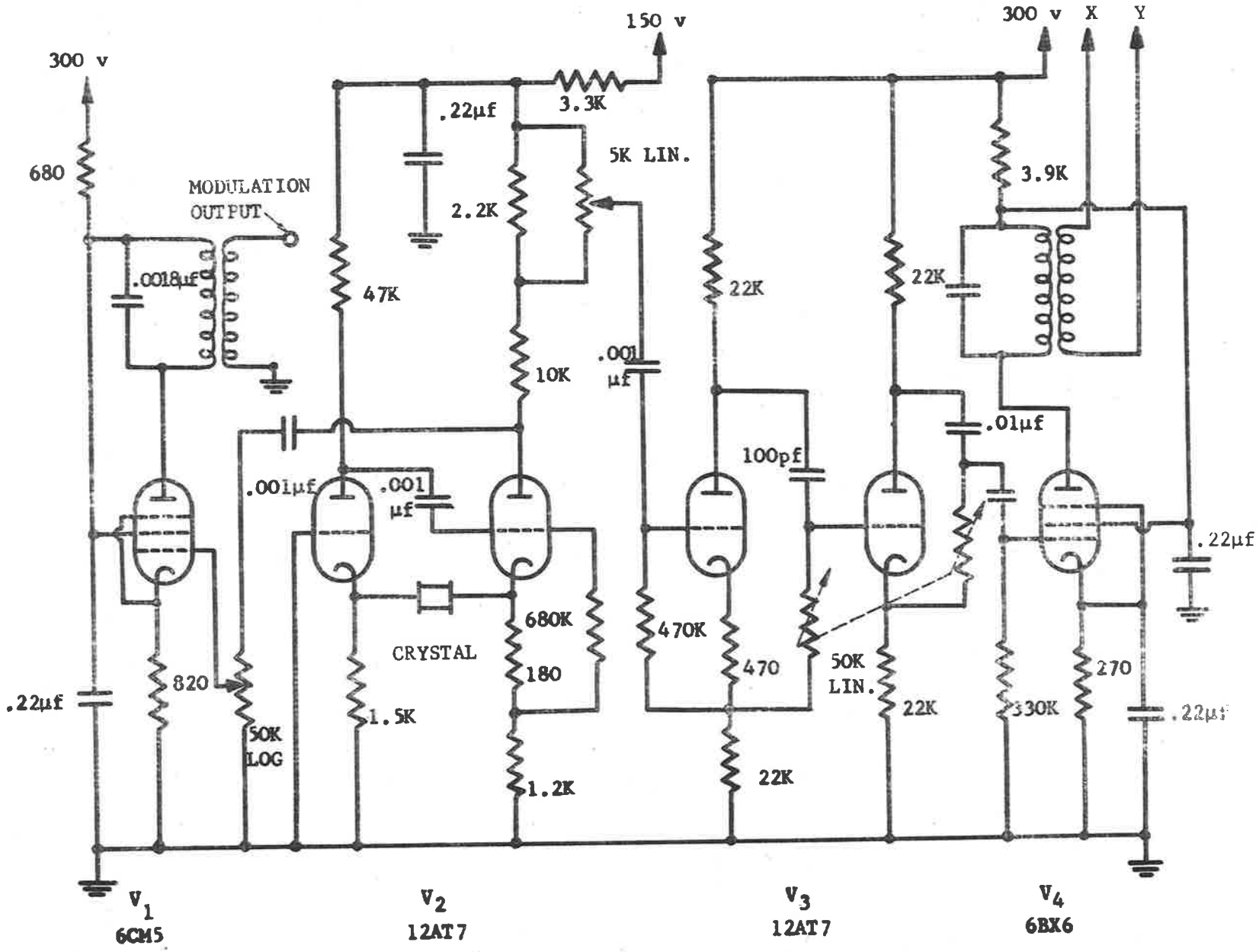

FIG.16

CRYSTAL OSCILLATOR, POWER AMPLIFIER & REFERENCE SIGNAL

The power amplifier used a 6CM5 valve and control of the magnetic sweep amplitude was obtained by a potentiometer controlling the input signal to the valve. The anode load was a tuned transformer wound on a Ferroxcube U core Type KS.450 71 with a 10:1 turns ratio to provide a low impedance output. Because of the high signal levels existing in this part of the circuit, considerable care was taken in shielding to prevent stray radiation being picked up in the main amplifier.

A signal was also taken from the crystal oscillator and, after passing through a phase shifting network, applied to a reference voltage amplifier V_4. The variable phase shift of the reference signal was obtained by using the double triode V_3, the phase shift being obtained by splitting the signal into two antiphase parts and applying it to an RC network with variable R. The reference signal amplifier anode load was a tuned transformer wound on a 1½ in. ferrite pot core with the reference output tightly coupled. The reference output level was set to approximately 10V peak to peak.

4.3 Preamplifier

The effect of stray signal pick-up in the main amplifier was minimised by using a separate preamplifier in a shielded box. The circuit for this preamplifier, shown in Fig.17, is a modification of a low noise amplifier described in Ref.2. The amplifier used a 6ES8 frame grid low noise twin triode in a cascode circuit. The input signal from the crystal detector was developed across a load resistor and inductance and then fed via a DC blocking condenser to a series tuned circuit. The anode load of V_5 was a tuned secondary RF transformer wound on a ferrite pot core with a step up ratio of two to one. A cathode follower V_6 was used to provide a low impedance output. A stabilised HT line was used to supply the amplifier and heater chokes were included to prevent unwanted signal transfer.

FIG.17

PREAMPLIFIER

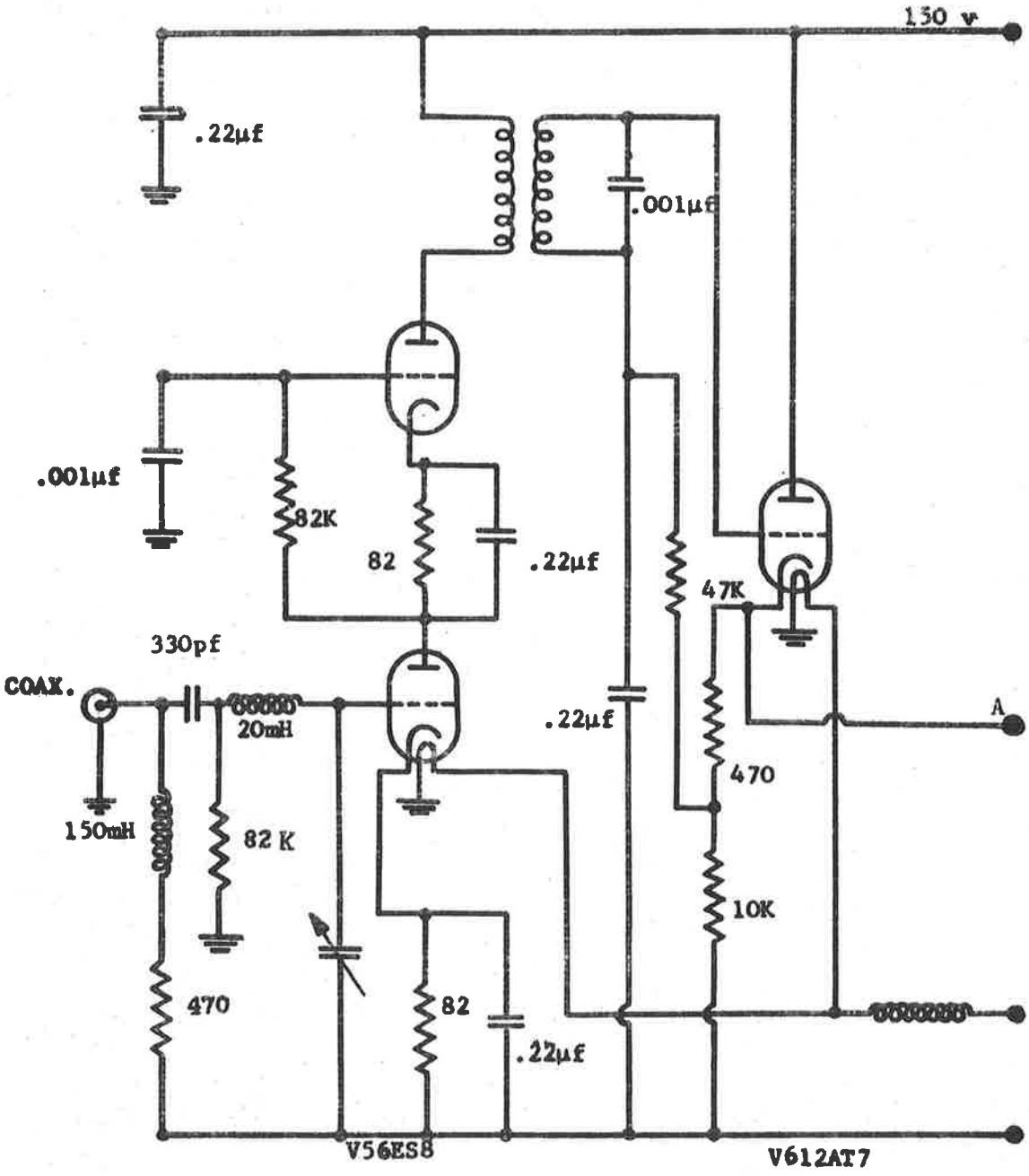

4.4 Main amplifier and phase detector

The main amplifier of the system, shown in Fig.18, was comprised of valves V_7, V_8 and V_9. The first two are connected as an untuned amplifier using 6BY7 valves. These valves are remote cut off pentodes and gain control of the amplifier was obtained by varying the effective grid bias to these valves. Despite attempts to shield the power amplifier stage completely from the amplifying circuits, a small amount of signal was induced in the main amplifier from this source. The amplitude of the unwanted signal was directly related to the amplitude of the magnetic modulation output and some of this signal was used for cancellation of the unwanted pick-up.

The bucking circuit is shown on the left of Fig.18. An input signal of amplitude proportional to the magnetic modulation was obtained from a five turn centre topped winding on the U core modulation output transformer. This output signal was taken to two balance type circuits, one using only R and the other using R and C. The outputs of these circuits were in quadrature and of controllable amplitude and on combination can be used to produce a signal of variable phase and amplitude. This signal was applied to the grid of V_7 via a suitable resistor network and the bucking controls were adjusted to produce zero phase detector output in the absence of signal at the input of the preamplifier.

The output load for the last valve V_9 was an RF transformer wound on a ferrite pot core with a tuned primary and a centre tapped secondary winding with twice the primary turns. A reference voltage was applied to terminals X and Y and the detected output appears across the 82K resistor. The signal passes through a variable time constant filter before being applied to the grid of V_{10}.

A 1mA recording meter of 1500Ω impedance was used as the final display. The magnetic sweep of the spectrometer was assumed to be linear with time making it possible to use a clock driven recording meter instead of an X-Y recorder to record absorption against field. The absorption curve has both positive and negative slopes making it necessary to bias the meter to mid scale in the

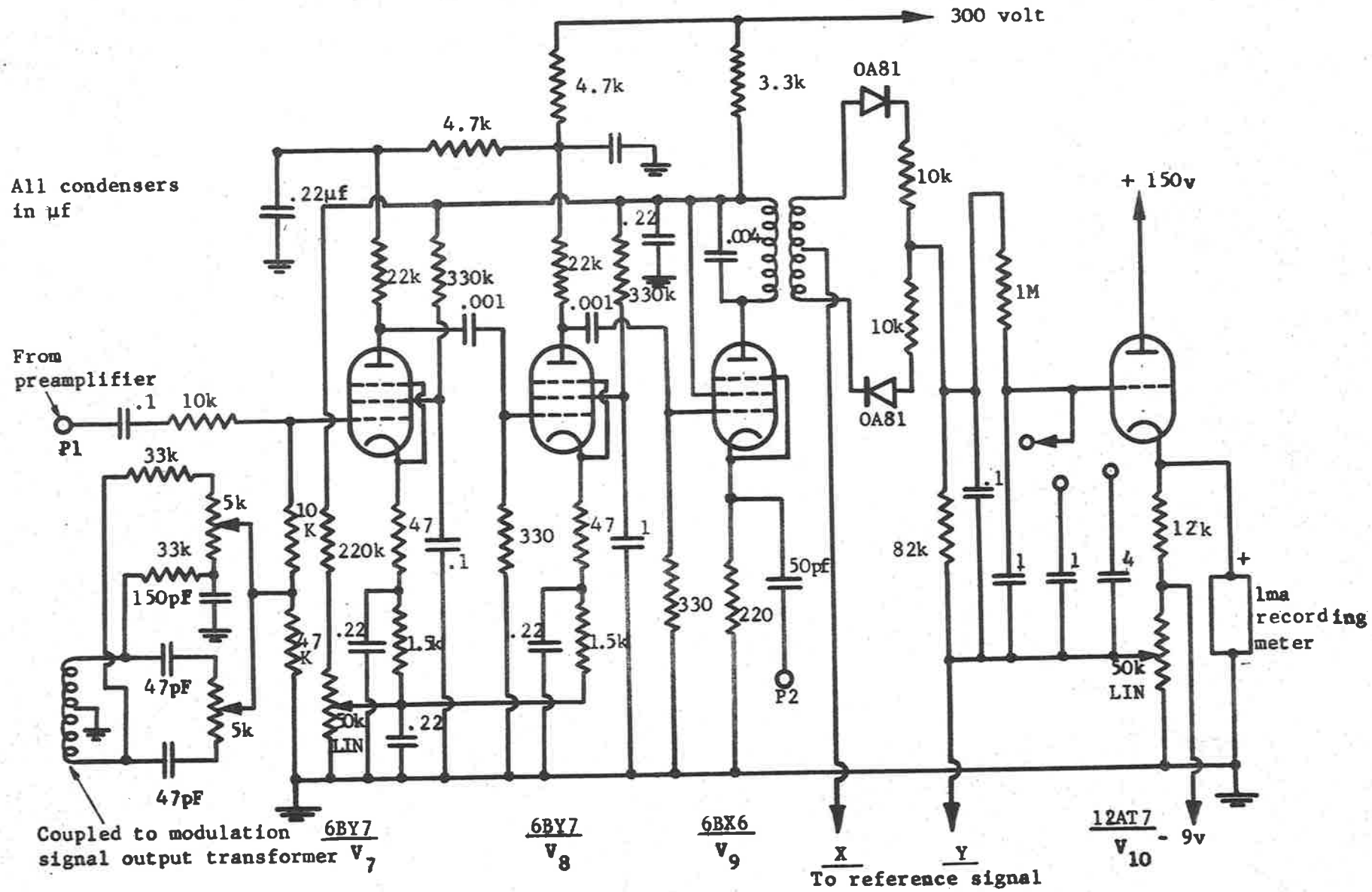

FIG.18
MAIN AMPLIFIER & PHASE DETECTOR

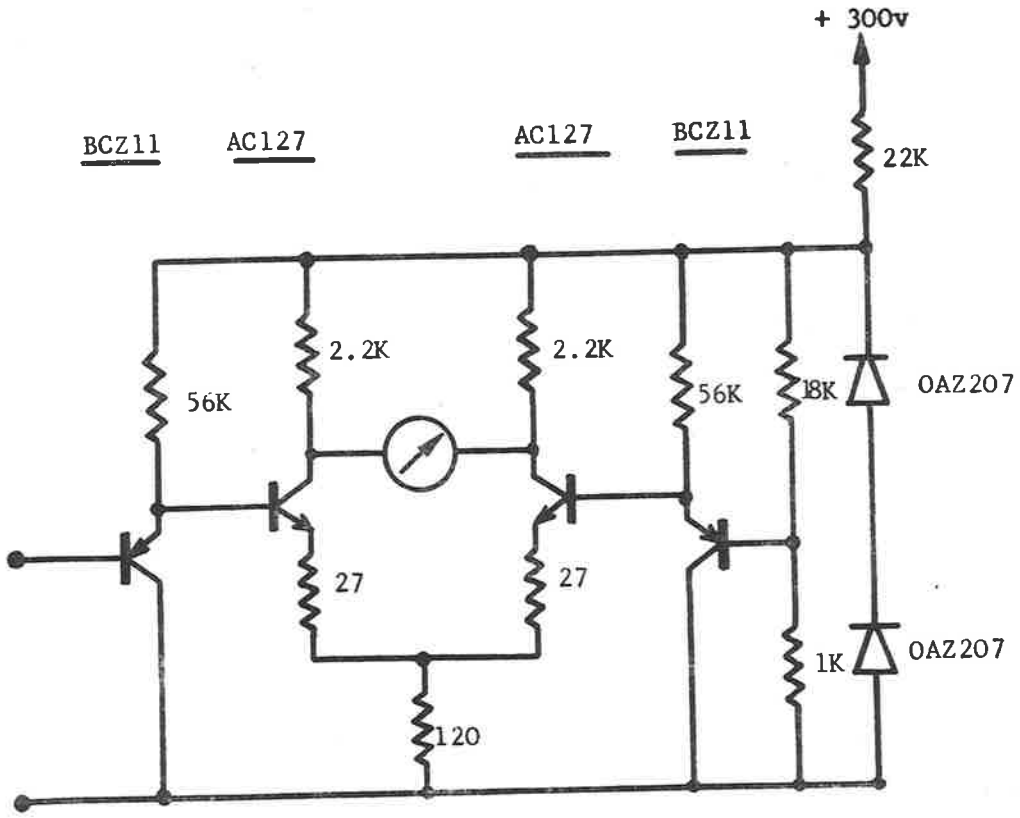

FIG.19

METER D.C. AMPLIFIER

absence of an input signal. For the particular meter used this required .75V and the meter voltage swing was required to be from 0 to 1.5V and so to preserve linearity a negative 9V line was used for the cathode return. The standing current through V_{10} was set by a potentiometer controlling the voltage at one end of the phase detector load resistance. The phase detector circuit was floating in the absence of this reference voltage.

When using the spectrometer it was found that a clearly detectable signal of 6mV at test point P2 produced only a small meter deflection and a small DC amplifier, shown in Fig.19, was constructed to precede the recording meter. This amplifier, which is mounted adjacent to the meter, derives its power from the main 300V HT line although the actual required potential rails are fixed at 18V by two Zener diodes. The amplifier uses two silicon transistors as emitter followers to drive a long tailed pair with the meter in the collector circuit. Silicon transistors were used for current stability and the measured amplifier gain was about 30.

The power supply for the previous circuits is shown in Fig.20.

5. MAGNET DESIGN

The magnetic field stability and uniformity required for electron spin resonance work is considerably less than that needed for nuclear magnetic resonance as, in general, the absorption lines are much broader. The magnetic field homogeneity required is determined by the width of the absorption line being studied and the volume of sample required to provide a good signal to noise ratio. The magnetic field uniformity is primarily determined by the ratio of the pole piece diameter to magnet gap although the quality of the pole piece material, the pole piece surface finish, the degree of alignment of the faces and the flux paths external to the magnet gap all influence the final field pattern. The magnetic field homogeneity can be improved by the use of Rose rings, Ref.11, which are rings placed over the pole to reduce the radial decrease in field towards the outside of gap.

FIG. 20

POWER SUPPLY FOR PHASE DETECTOR

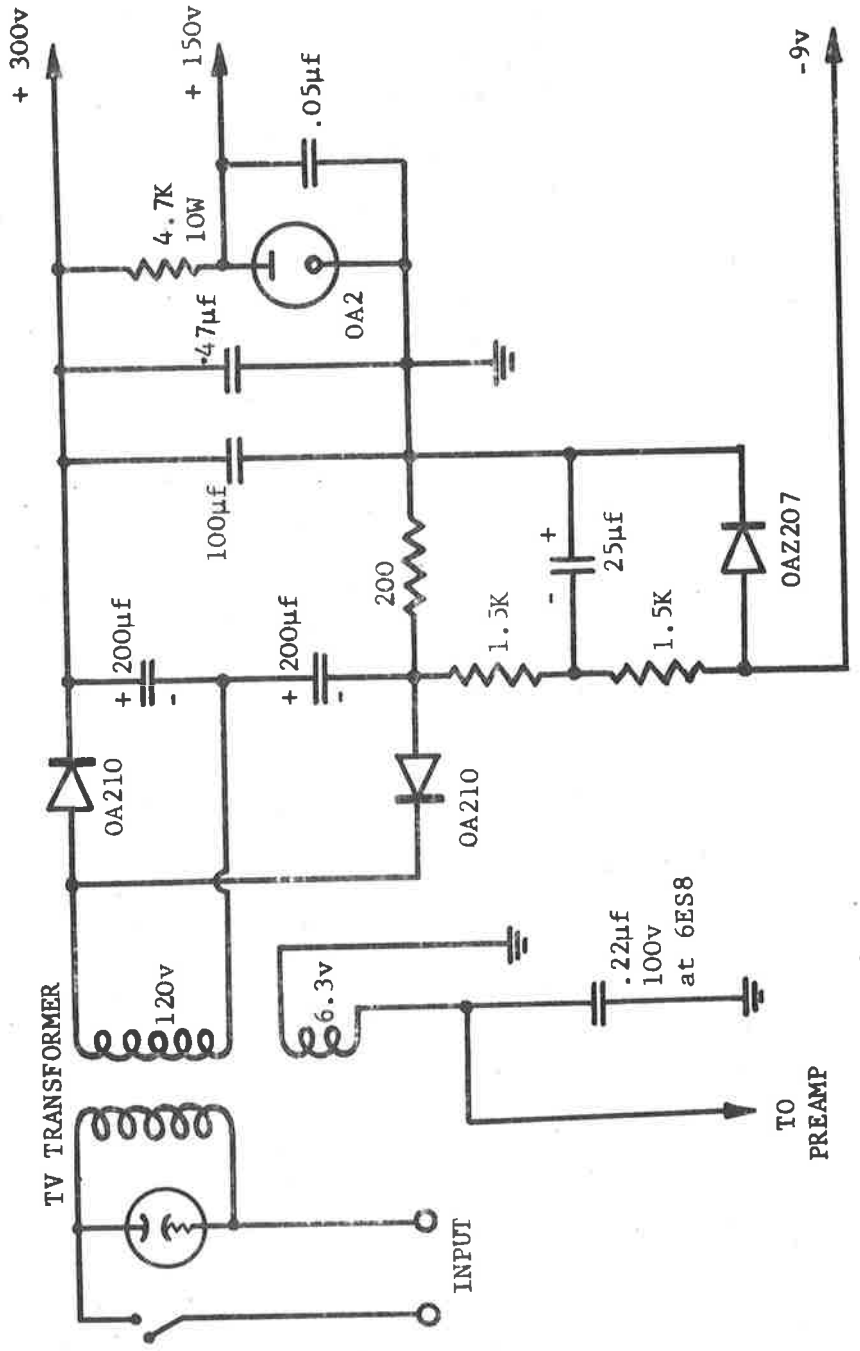

ESR spectrometers usually work at a fixed frequency and an electromagnet is commonly used to supply the large field variations required. A spectrometer working at 10,000 Mc requires a field of 3600 oe. to observe a material of g value 2. In a well designed electromagnet working at fields of this strength the upper limit of the field is set by the coil heating and not by pole piece saturation.

The magnet used in this spectrometer was constructed with a yoke made of 3" square section soft iron bars welded together to which were bolted two steel centered aluminium bobbins containing the current carrying coils. Three inch diameter detachable pole pieces, externally threaded for Rose rings, were made from high quality steel and surface ground to a fine finish before being attached to the yoke by a circular ring of small screws. The normal working gap was set to 1½ in., the minimum able to contain the sample cavity and field measuring probe. The diameter gap ratio of little greater than 2 resulted in poor field uniformity restricting the spectrometer to use on small samples of comparatively large linewidth. The field distribution with the Rose rings adjusted for maximum central homogeneity is shown in Fig.21.

6. MAGNET CURRENT SUPPLY CIRCUITS

Current for field stable electromagnets can be supplied from one of the following types of sources: electronically regulated supplies, storage batteries or special generators. The short term stability of the magnetic field is most important as the field should not fluctuate more than a few per cent of the line-width of the lines under study, which, for lines of a few gauss width require a current stability of about 1 part in 10^5. As this order of stability is required only during the magnetic sweep time, which is usually of the order of a minute, slow thermal drift errors are negligible after the initial warm-up period compared to other causes of current variation.

The DC power for the magnet was obtained by rectification from stabilised 240V mains. A transformer full wave rectifier combination using PL5544 thyrotrons was used which was capable of supplying 350V at the required current of 3A. With the magnet gap

FIG.21

RADIAL DECREASE IN FIELD TAKEN AT 3000 OE.

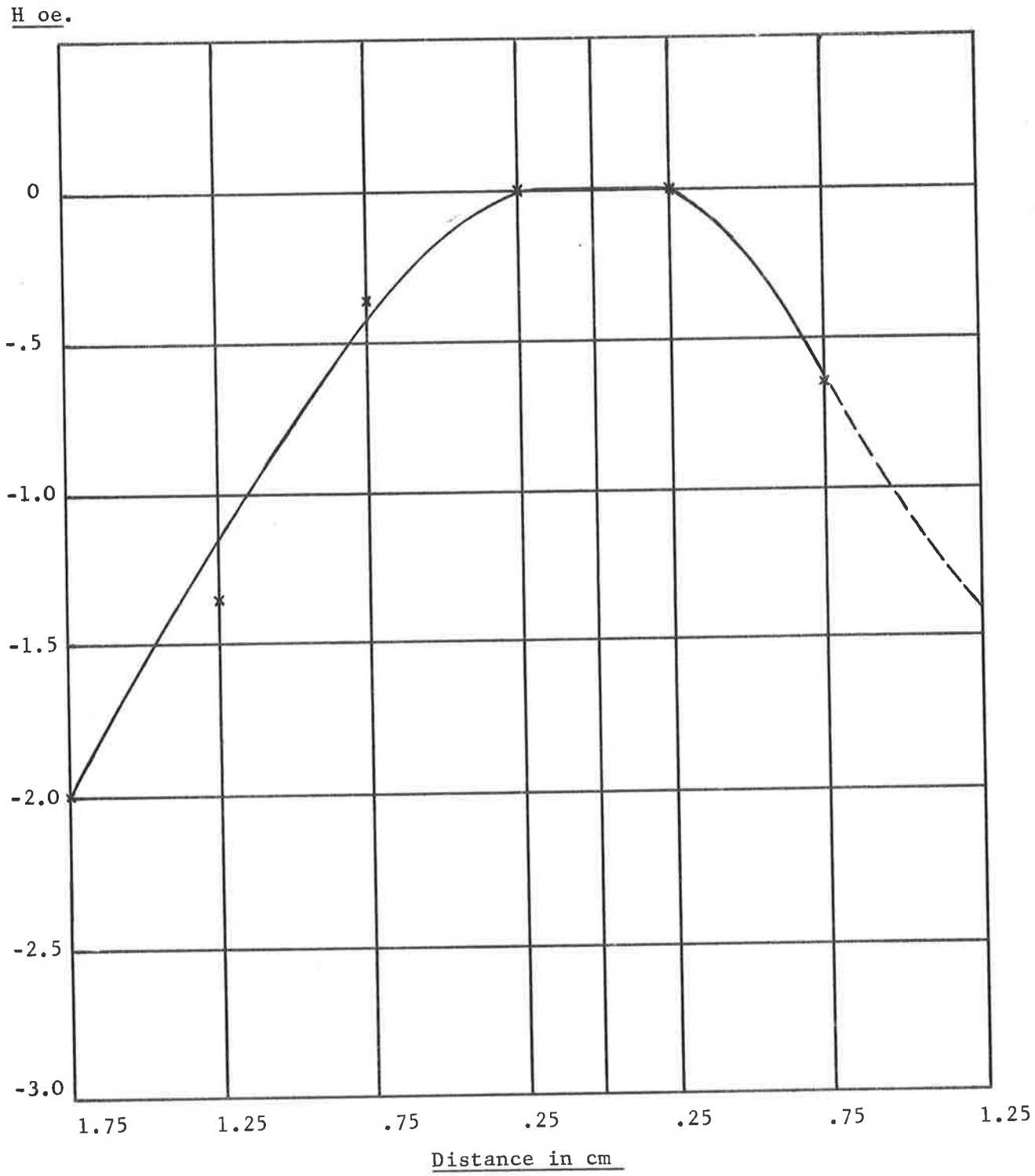

reduced by the special pole pieces only 100V was required to produce the normally required working fields. The output DC had 20V p to p of 100 cps ripple which was reduced to 0.1V at the magnet terminals by dropping the excess voltage in a baretter circuit and RC filter. The large value of magnet inductance had a reactance of about 20KΩ at the ripple frequency and so the resulting magnetic field variations should not be greater than 5×10^{-6}, a much smaller amount than the current variation.

The magnet current control circuit was required to perform both the functions of providing a constant easily set field and also a field sweep to scan spectra.

Magnetic field stabilising circuits require four basic components, a constant value reference, a unit to sense the magnetic field or a quantity proportional to the magnetic field, a unit to compare the reference standard with the controlled variable and to supply a correction voltage to the fourth unit, and a controlling element in series or shunt with the magnet. The circuit adopted is shown in Fig.22.

The reference voltage was obtained from an 83A1 cold cathode reference tube run at a constant current of about 5mA supplied from a stabilised 150V HT line via a high stability wire wound resistor chain. The voltage jumps for this valve are specified to be less than 1 part in 10^5 and the voltage temperature coefficient as $3 \times 10^{-5}/^{o}C$. The valve was located on the chassis away from any heat source and the short term stability was expected to be better than 1×10^5.

The measurement of the magnetic field to the accuracy required for stabilisation is very difficult to do. The usual methods of spinning coils or Hall effect probes have to be discarded in favour of a proton resonance magnetometer, described in section 8. It is possible to use this effect to maintain a constant field value, Ref.12, but only by the use of complex electronics. A simpler method of obtaining field stability was to use the proportionality existing in the magnet between field and current. Over the field range

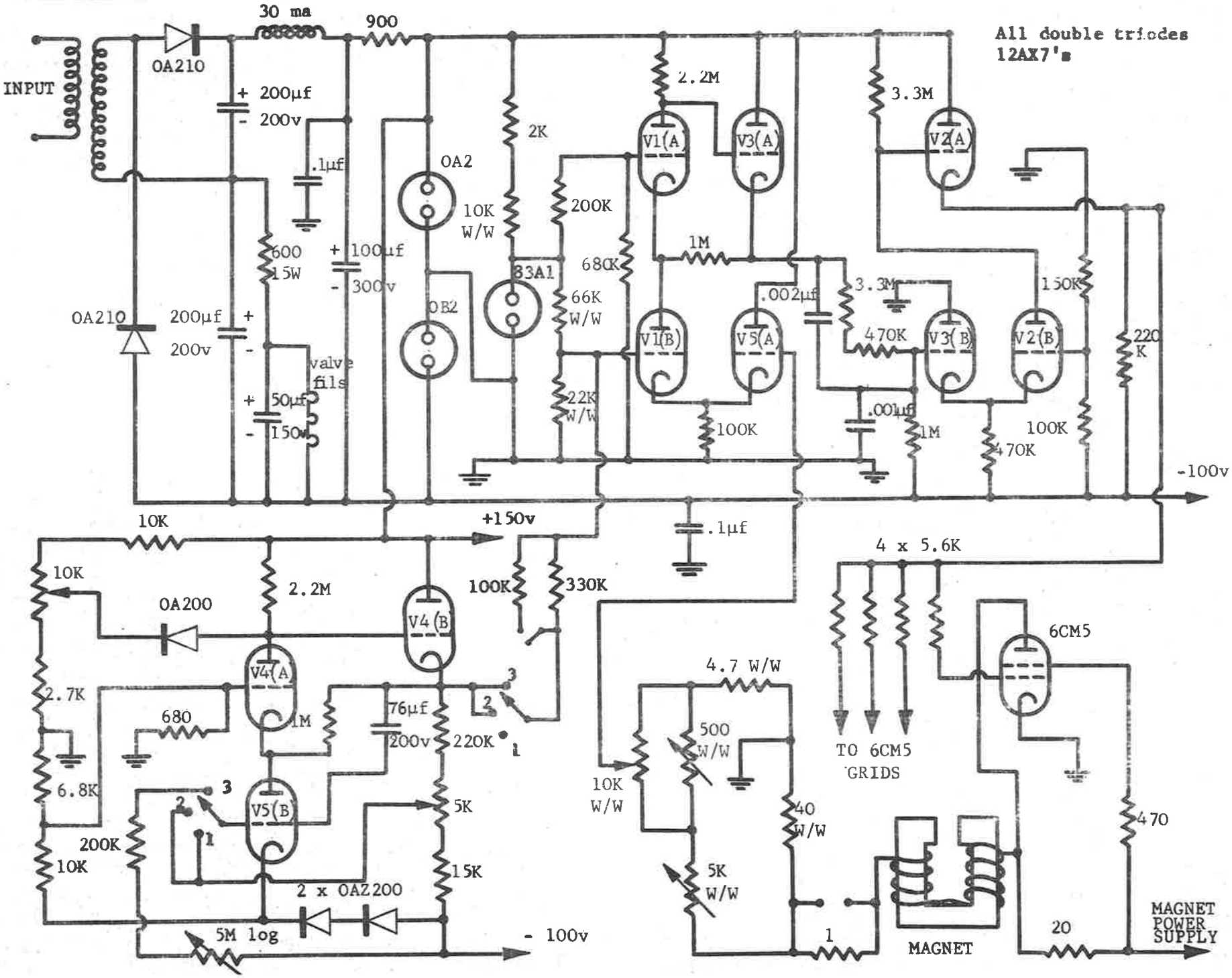

FIG.22
MAGNET CURRENT STABILISING CIRCUIT

considered, 2500-3600 oersteds, the effective magnet permeability was low and constant with a field current slope of approximately 3000 oersteds/A. See Fig.23.

The reference voltage for the control unit was derived from a high stability 40Ω four terminal resistor constructed by winding Eureka wire, temperature coefficient 4 parts in 10^5 /C, on a Tufnol former and immersing in a bath of transformer oil. Field variations of 1 part in 10^5 are produced by a current change of 3.3μA which will produce a change in resistor output voltage of 0.13mV. Variations in the absolute value of the magnetic field were produced by using a potentiometer chain to produce a constant output voltage from the varying voltage appearing across the control resistance. The potentiometer chain used three high quality wire wound potentiometers, one as a coarse control and two in the fine control circuit, one in series and one in shunt to control the range of the fine control. The output from this chain was compared with a voltage derived from the 83A1.

The control voltage for magnet current control circuit was obtained from a DC amplifier circuit consisting of four double triodes. In the actual circuit construction the valves were arranged to reduce interaction between the valve halves. The control circuit action is described below.

The reference voltage and the voltage from the 40Ω series resistor were compared in a long tailed pair formed by V1B and V5A, Fig.22. The out of balance voltage was amplified by the cascode section V1A and the output fed through the cathode follower V3A. The cathode resistor was returned to the anode of V1B to provide positive feedback to increase the section gain to about 1000. The DC voltage level at the output of this stage was about - 100V and this level was reduced before the next stage by a potential divider entailing a loss of signal by 5 to 1. The next stage, a long tailed pair of V3B and V2B feeds the cathode follower output valve V2A. With the attenuating network loss included the stage gain was about 5.

FIG.23

MAGNETIC FIELD PLOTTED AGAINST VOLTAGE ACROSS 1Ω SERIES RESISTOR

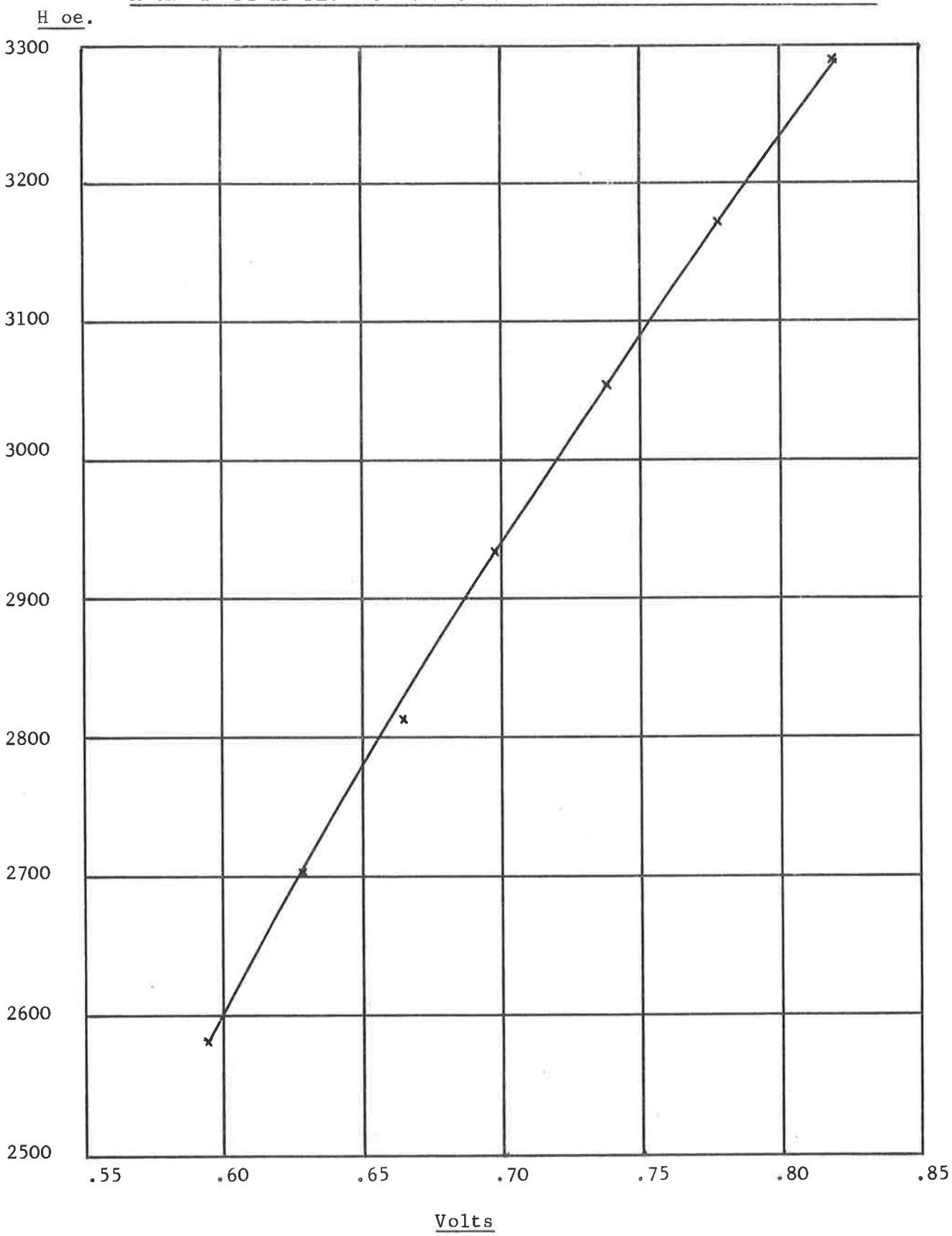

The magnet current was normally about 1A and it was required to vary this by about .3A to provide a suitable field range. A control element in shunt with the magnet was adopted as this did not require to carry the full magnet current but only the current variation. Four 6CM5 power pentode valves were placed in parallel across the magnet and the control voltage from the cathode follower V2A was applied to the first grids. The valve combination had a slope of about 80mA/V.

The magnet current and hence field were monitored by the measurement of the voltage developed across a 1Ω Eureka wound oil immersed resistor in series with the magnet. The voltage was measured on a Doran potentiometer capable of reading to 1μV. After the initial warm-up period the magnet stability was found to be 3 parts in 10^5 over about 5 minutes.

To trace out absorption lines a sawtooth waveform magnetic field was required. This was achieved by modifying the reference tube voltage applied to V1B with a sawtooth wave generated in a feedback integrator. A switch was inserted in this circuit to obtain two sweep ranges.

The feedback integrator circuit used was a Miller circuit with a cascode amplifier section feeding a cathode follower to drive the charged capacity. A three position rotary switch was used as a function switch in the following manner. In the first position the sawtooth circuit was disconnected from the main circuit. In the second position the circuit was connected but by suitable adjustment of the preset 5K potentiometer in V5B grid the reference voltage was unaltered. The third switch position applies - 100V to V5B grid via a slope controlling potentiometer. The sawtooth continues to run until the catch diode in the anode circuit of V4A stops the action. The diode voltage was set by a sawtooth amplitude potentiometer. A pair of contacts on the rotary switch are used to switch on the pen recorder motor at the start of the sawtooth.

Using the circuit components shown the magnet sawtooth has the following performance:

Range 1	Amplitude	0 → 780 oe.
	Slope	0 → 8.8 oe./sec.
Range 2	Amplitude	0 → 220 oe.
	Slope	0 → 2.5 oe./sec.

7. SAMPLE CAVITY CONSTRUCTION

The sample cavities used for ESR work are usually rectangular TE_{10} mode or right cylindrical TE_{011} mode types. The requirements are that the sample is located in a position of maximum RF magnetic field which is orthogonal to the applied DC magnetic field and it is also preferable that the sample is at an electric field node to minimise Q damping produced by dielectric loss. The cavity used with this spectrometer was a rectangular TE_{102} mode with the sample introduced through a hole in the centre of the narrow face in the E field nodal plane. The sample was contained in a small thin walled teflon test tube or, in the case of crystal samples, on the end of a thin perspex rod. The cavity was coupled to the main waveguide by a thin diaphragm of copper with a central hole. Although the spectrometer sensitivity changes slowly with coupling, a variety of diaphragms were made and the sensitivity optimised for small samples that produced a negligible Q change.

When using the high frequency magnetic modulation previously described, difficulty was experienced with external modulation coils and a metal cavity. The eddy currents induced in the cavity considerably reduced the field modulation seen by the sample and also the mechanical vibrations set up by the interaction of the eddy currents and the DC magnetic field produced a troublesome microwave modulation if the cavity was not on tune with the incoming signal. There are two ways of dispensing with external field modulation coils. The modulating loop, consisting of a half turn of stiff wire can be placed around the sample and, providing the sample is thin the coil will be close to the E field nodal plane and only slightly perturb the cavity resonance. The other method is to make

the whole cavity into a half turn loop by sawing a non radiating slot along the cavity axis and then applying the modulating RF to the whole cavity body, suitably insulated from the main waveguide run. This method is shown in Fig.24. Both of these methods suffer from the difficulty of requiring a very low output impedance transformer mounted close to the loop to minimise losses and the more fundamental disadvantage of producing a very nonuniform magnetic field. Neither of the above methods were used in the spectrometer but the alternative approach of reducing the eddy currents was adopted.

A plastic cavity with recessed external modulating coils was constructed and the inside thinly coated with a metal film to provide microwave conduction. The current is a maximum at the surface and decreases exponentially with depth in the conductor, the depth δ at which the current has fallen to e^{-1} of its surface value being known as the skin depth. From Ref.13,

$$\delta = \frac{1}{2\pi} \sqrt{\frac{\lambda \rho}{30\mu}} \qquad \ldots\ldots\ldots(41)$$

where

λ = free space wavelength in cm,

ρ = resistivity in ohm cm,

μ = permeability of conductor.

For silver $\rho = 1.63 \times 10^{-6}$ ohm cm at $20^{\circ}C$ giving a skin depth of 0.6 microns at 10,000 Mc and 200 microns at 100 kc. This considerable difference in skin depth can be used to provide a cavity with microwave conduction and yet present considerable resistance to eddy currents at 100 kc.

The sample cavity was designed to work in the TE_{012} mode at 9150 Mc, a frequency where the klystron signal output was high. The length was calculated from a knowledge of the guide wavelength obtained from the usual formula

$$\lambda_g = \frac{\lambda}{\left[1 - \left(\frac{\lambda}{\lambda_c}\right)^2\right]^{1/2}} \qquad \ldots\ldots\ldots(42)$$

FIG. 24

MAGNETIC FIELD MODULATION SYSTEM

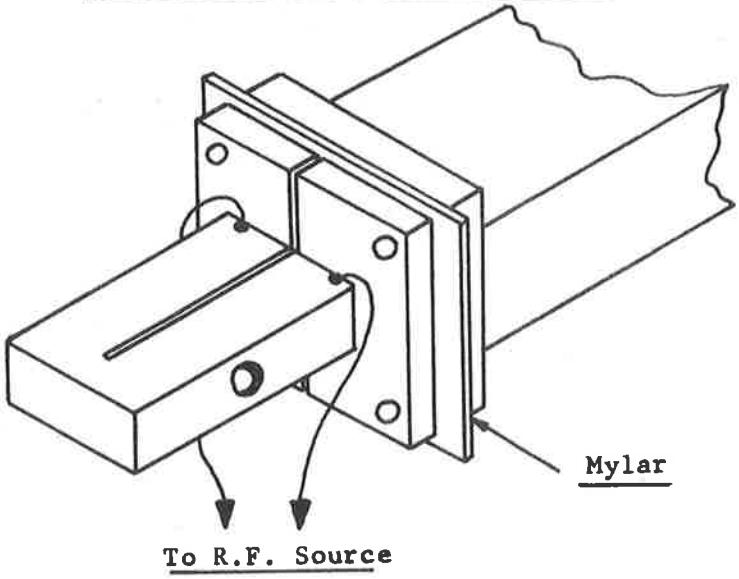

FIG. 25

MAGNETIC MODULATION FIELD UNIFORMITY

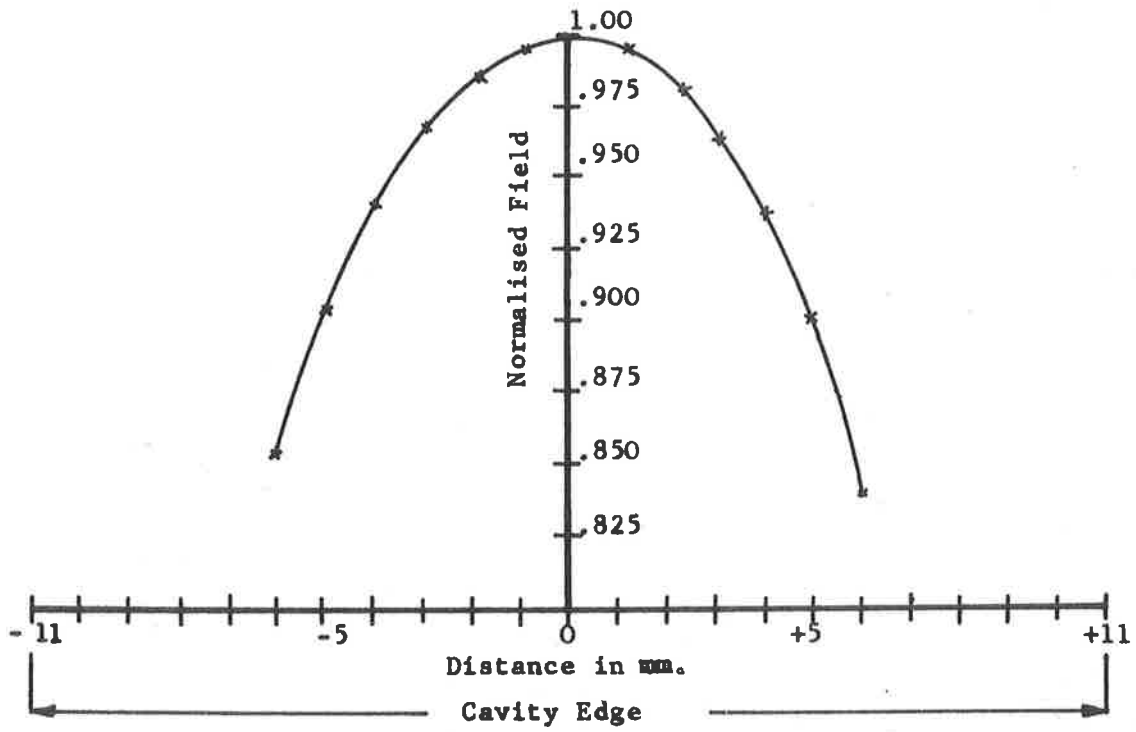

where

λ_g is the guide wavelength,

λ is the free space wavelength,

λ_c is the cutoff wavelength of the waveguide used.

The cavity was made by cementing 1/4" thick slabs of perspex with methylmethacrylate monomer and polymerising under UV radiation. After cleaning with 10% sodium hydroxide solution and sensitising with stannous chloride solution the conducting silver coating was applied by the usual chemical silvering process of reducing silver nitrate with sucrose solution. It was not found possible to produce the required thickness of 6 microns and additional silver was plated on. Only a very rough estimate of the film thickness was possible by weighing as the film had poor thickness uniformity. The main difficulty experienced was the deposition of silver into the corners and along the edges of the rectangular cavity.

The Q for a rectangular cavity in the TE_{012} mode is given in Ref.14

$$Q = \frac{\pi \zeta}{4R_s} \left\{ \frac{2b(a^2 + d^2)^{\frac{3}{2}}}{ad(a^2 + d^2) + 2b\,(a^3 + d^3)} \right\} \qquad \ldots\ldots\ldots(43)$$

where

$\zeta = \sqrt{\frac{\mu}{\epsilon}}$ = 377 ohms is the impedance of free space,

R_s = $2.52 \times 10^{-7}\sqrt{\nu}$ for silver,

a = broad face of waveguide in cm,

b = height of waveguide in cm,

d = cavity length in cm.

Using this formulae a theoretical Q of 6500 is obtainable and, measurement of the cavity produced a Q of about 4000, which was considered satisfactory.

The broad faces of the cavity were recessed for two bobbins 1.3/16" OD by 5/8" ID providing an approximate Helmholtz pair for the 95 kc magnetising field. The bobbins were each wound with 50 turns of copper wire and were resonant at 95 kc with .039 μf

in series. The shielding effect of the cavity was difficult to calculate and so both the modulation amplitude and the field uniformity were determined by means of a small search coil and oscilloscope. The field uniformity is shown in Fig.25 and it can be seen that over a 4 mm long test tube specimen the field variation is about $\pm$ 1%.

8. MEASUREMENT OF MAGNETIC FIELD STRENGTH

The most accurate method of magnetic field measurement uses the nuclear resonance of protons in the magnetic field. Nuclear magnetic resonance is similar to electron resonance except the radiation couples to the nuclear magnetic moment instead of the electron magnetic moment. The transition energy is considerably reduced due to the much smaller magnetic moment of the nucleus. The proton gyromagnetic ratio has been determined with great accuracy and the measurement of the magnetic field is replaced by the measurement of frequency which is easy to measure with great accuracy. The numerical relationship between field and frequency is

$$H \text{ oe.} = 2.3487 \times 10^{-4}. \text{ frequency in cps} \qquad \ldots\ldots\ldots(44)$$

Magnetic fields of 3000 gauss correspond to absorption at about 12.8 Mc. A proton resonance magnetometer consists of a tunable radio frequency oscillator with the main coil containing a hydrogen rich material situated in the DC magnetic field. Many substances are suitable as absorbers in the coil, such as a phial of glycerine, paraffin or an aqueous solution of manganese sulphate. To produce large changes in signal output with small energy absorption of the proton resonance, the oscillator has to work in a marginal manner. The circuit of the proton resonance magnetometer used is shown in Figs. 26 and 27.

Fig.26 shows the power supply which supplies a well filtered stabilised HT line and a regulated DC heater line. The proton resonance magnetometer, shown in Fig.27, incorporates a fine frequency control obtained by adding a variable capacity diode to the main oscillator circuit. Marginal oscillation was obtained by

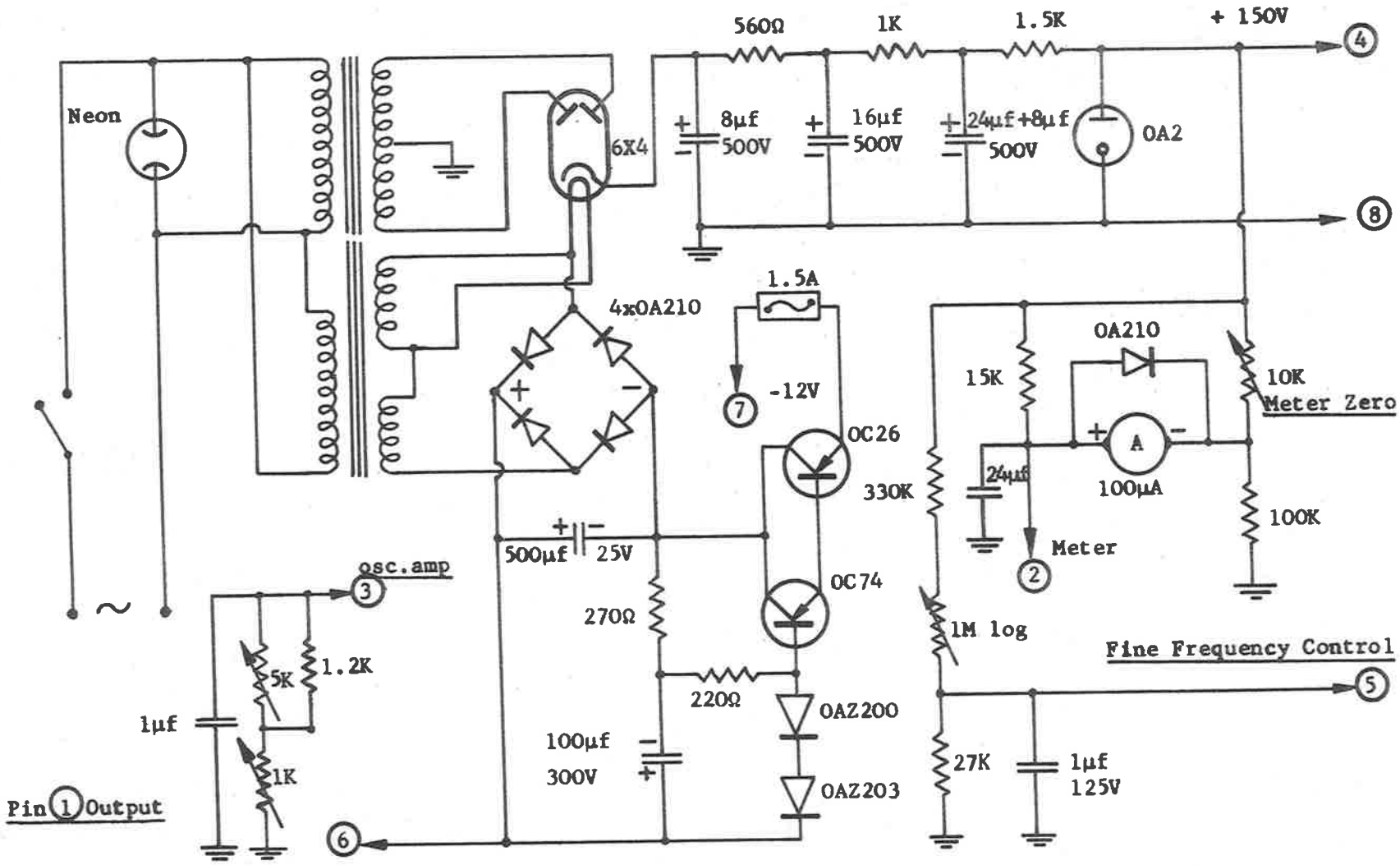

FIG.26
POWER SUPPLY

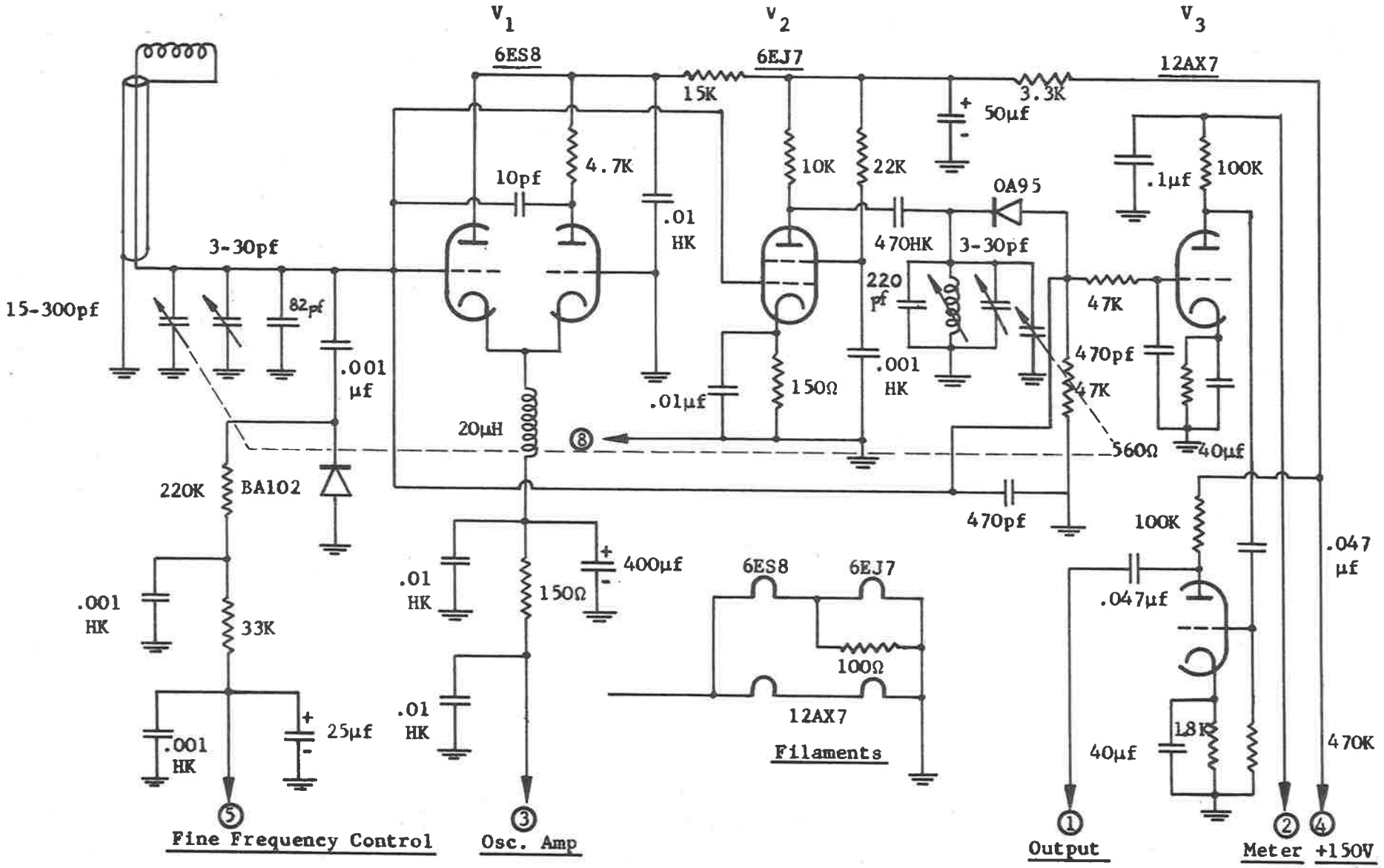

FIG. 27

PROTON RESONANCE MAGNETOMETER

incorporating a variable cathode resistor network in the oscillator valve. The magnetometer was used with the DC magnetic field modulated at 50 cps by additional coils wound on the magnet pole pieces. The 50 cps variations of the oscillator amplitude are amplified in V2, detected and further amplified in V3 before passing to the output to be displayed on an oscilloscope. The measurement of the magnetic field requires the measurement of the oscillator frequency which was done by comparison with a crystal controlled 10 kc harmonic spectrum. The frequency measurement accuracy was about 1 part in 10^5 determined by the measurement of the audio beat note between the oscillator and nearest 10 kc pip.

9. MEASUREMENTS OF SPECTROMETER SENSITIVITY

The determination of the absolute intensity of the electron resonance absorption can be done if the incident power to the cavity and the change in reflected power is known together with the cavity Q and filling factor. In practice it is very difficult to perform the required measurements and usually a known weight of a standard sample is employed to determine the spectrometer sensitivity. The stable free radical .1.1 diphenyl - 2 picrylhydrazyl (DPPH) is often used for a standard as each molecule possesses one unpaired spin. The molecular weight is 394 and each gram possesses 1.53×10^{21} unpaired spins enabling known weights of DPPH to be used for measuring the spectrometer sensitivity. There are several difficulties in the use of DPPH as a standard. The material is usually crystallised from chloroform and it is possible to have solvent inclusionswhich introduce an error when weighing the calibration samples. Spectrometers of high sensitivity require very small weights of DPPH since 1μgram contains 10^{15} spins. The radical is unstable in very small quantities making it unsuitable for use as a permanent standard. An alternative standard using charred dextrose has been suggested as being more stable and also easier to prepare with small spin concentration. Ref.15.

The sensitivity and correct functioning of the spectrometer have been confirmed by examining small quantities of DPPH. A small quantity, 1.5 mg, of DPPH was dissolved in 1 cc of chloroform and

FIG. 28

ESR SIGNAL DERIVATIVE TRACE

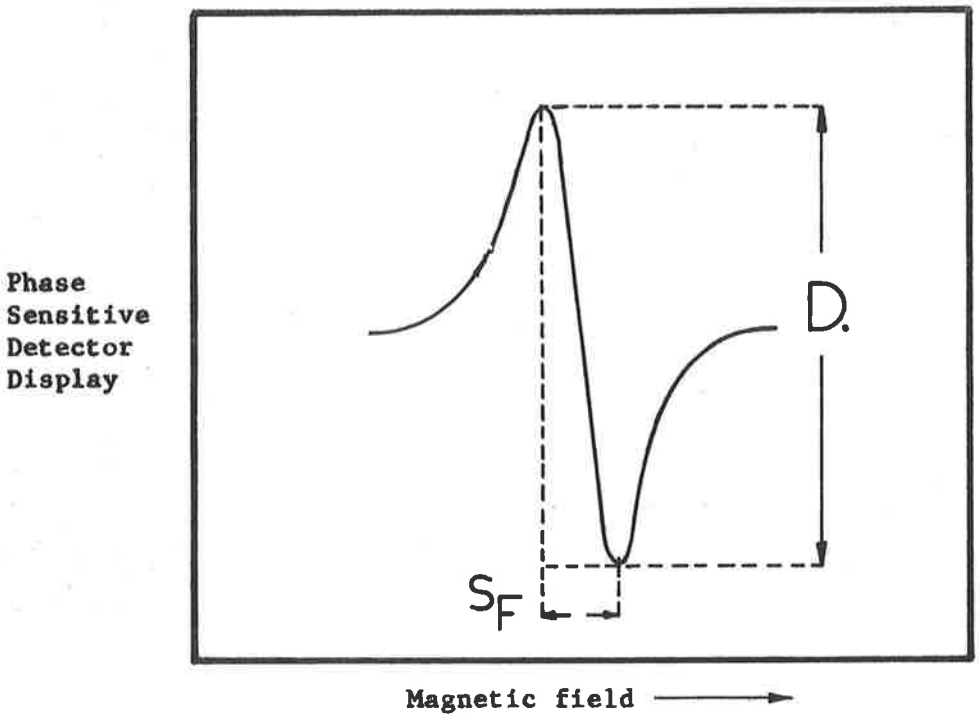

one drop, .02 cc, was evaporated on a filter paper in a small teflon test tube. The unpaired spin concentration of this sample was taken to be 5×10^{16} spins with an accuracy of perhaps $\pm$ 30%. Although the unpaired spin concentration is proportional to the area under the absorption curve it can be shown, Ref.16, that if the ESR curve is the first derivative of a Lorentzian curve the integrated absorption is proportional to $S_F^2 D$, see Fig.28, and can be directly compared with a Lorentz shaped curve for a standard sample. Using samples of DPPH S_F^2 is constant and the unpaired spin concentration is proportional to D. A range of 3 samples was made and calibrated against the above "standard".

Spectrometer performance curves showing DPPH unpaired spin concentration and magnetic field modulation amplitude are shown in Figs.29 to 32. From Fig.32 the ultimate detection sensitivity using slow magnetic sweep, magnetic modulation equal to the line-width and long final filter time constant is expected to be about 1×10^{14} unpaired spins of DPPH or about 3.5×10^{13} spin/oe.

10. CONCLUSIONS

A 3 cm electron spin resonance spectrometer has been constructed with a sensitivity of 3.5×10^{13} spin/oe. The sensitivity was limited by the noise generated by the 723A/B klystron and an improvement of about 5 could be expected if a special low noise klystron were used as a signal source. The small size of the magnet used limits the possible sample volume, unless only very broad lines are being studied, and it is usually not possible to obtain the optimum cavity filling factor which corresponds to the unloaded cavity Q being halved (Ref.17). With the present magnet the spectrometer is limited to studying lines greater than 1 oe. in width in samples having an unpaired spin concentration of at least 10^{15} spins cm^{-3}.

FIG. 29

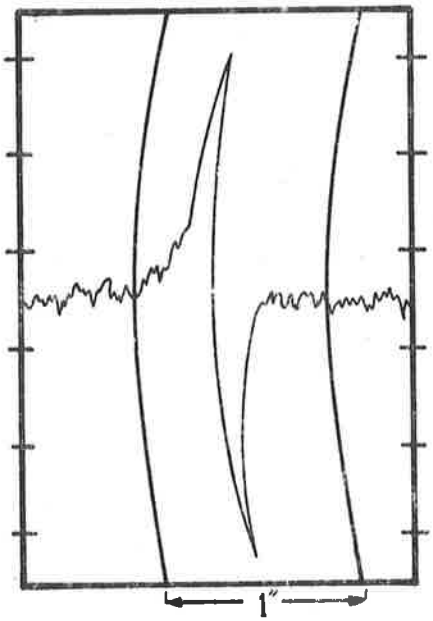

SPIN CONCENTRATION 3×10^{16}
MAGNETIC MODULATION .15 OE.
PEAK TO PEAK
FINAL FILTER TIME CONSTANT
2 SECONDS
CHART SPEED ½" PER MINUTE

FIG. 30

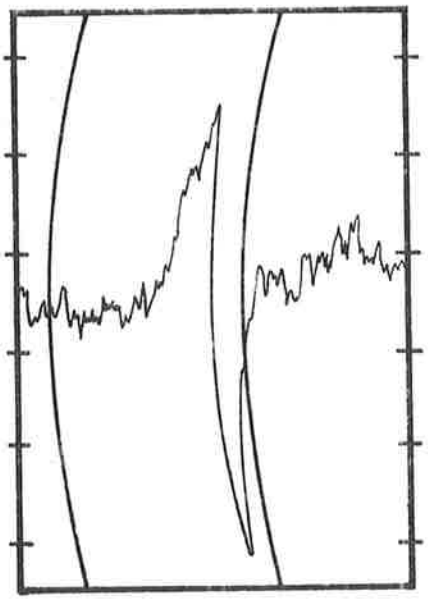

SPIN CONCENTRATION 6×10^{15}
MAGNETIC MODULATION .15 OE.
PEAK TO PEAK
FINAL FILTER TIME CONSTANT
2 SECONDS
CHART SPEED ½" PER MINUTE

FIG.31

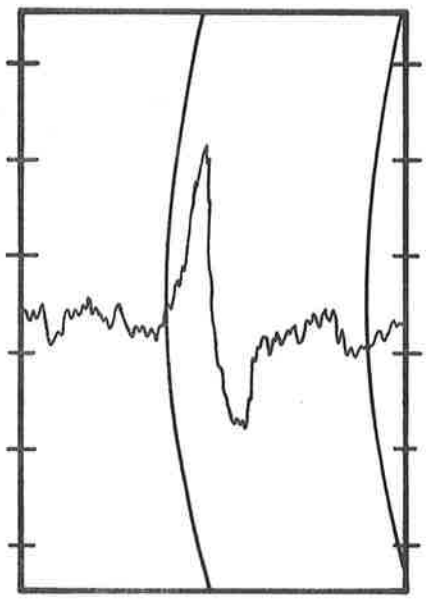

SPIN CONCENTRATION 8 x 10^{14}
MAGNETIC MODULATION 1 OE.
PEAK TO PEAK
FINAL FILTER TIME CONSTANT
5 SECONDS
CHART SPEED ½" PER MINUTE

FIG.32

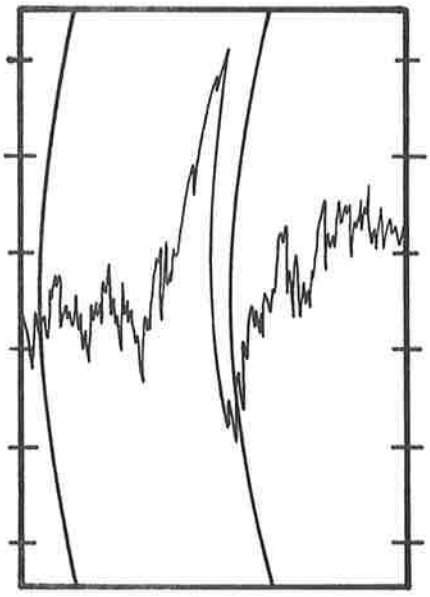

SPIN CONCENTRATION 8 x 10^{14}
MAGNETIC MODULATION .65 OE.
PEAK TO PEAK
FINAL FILTER TIME CONSTANT
2 SECONDS
CHART SPEED ½" PER MINUTE
HIGH AMPLIFIER GAIN

PART 2

1. INTRODUCTION

When in solution the complex cupric ion usually shows an ESR spectrum of four hyperfine lines produced by the interaction of the $3d^9$ electron with the nuclear spin I of $\frac{3}{2}$. At room temperature the nuclear levels are equally populated and so the $2I + 1$ lines are of equal intensity but McGarvey (Ref.17) has shown that the hyperfine lines differ in linewidth and also that the spectrum changes for different solvents. An explanation of the variation of the paramagnetic relaxation times with nuclear orientation has been suggested by McConnell (Ref.18) on the basis of a micro-crystalline unit in solution. The initial theory has recently been extended by Kivelson (Ref.19) and confirmed for the vanadyl ion in solution by Rogers and Pake (Ref.20).

2. THEORETICAL OUTLINE

2.1 The Spin Hamiltonian

The usual method of describing ESR spectral data is by use of the spin Hamiltonian, a brief description of which is given below.

The resonance spectrum of a transition group ion in a crystal is in general fairly complicated. The lowest energy levels in which microwave transitions are induced depend on the particular ion, the symmetry and strength of the crystal field, the spin orbit coupling and the hyperfine interaction between the electron and the nucleus. The experimentally obtained data can be conveniently represented by using a spin Hamiltonian. The lowest group of electronic states, which can be represented as a complicated mixture of spin and orbital wave functions, can also be represented by a single quantum number S' (Ref.21). S' is called the effective or fictitious spin of the system and is defined simply by equating $2S' + 1$ to the number of electronic levels in the lowest group. This use of the effective spin means that the paramagnetic ion is treated like a magnetic dipole which has $2S' + 1$ allowed orientations in an applied magnetic field and each energy level is associated with one orientation. The sum of all the interaction terms written

as a sum of energy operators to be applied to the effective spin states constitutes the spin Hamiltonian of the system. The actual energies are then the eigenvalues E_o which satisfy the operator equation

$$\mathcal{H}\psi = E_o\psi \qquad \ldots\ldots\ldots(45)$$

where ψ represents the wave function of the effective spin state.

The advantage of using the spin Hamiltonian is that the behaviour of the lowest energy levels of the paramagnetic ion in a magnetic field can be described in a simple way by specifying the effective spin together with a small number of parameters which measure the magnitude of the various terms in the Hamiltonian. The complete spin Hamiltonian is written

$$\begin{aligned}\mathcal{H} = {} & \beta(g_z H_z S_z + g_x H_x S_x + g_y H_y S_y) \\ & + D\left\{S_z^2 - \frac{1}{3}S(S+1)\right\} + E(S_x^2 - S_y^2) + A_z S_z I_z + A_x S_x I_x \\ & + A_y S_y I_y + P\left\{I_z^2 - \frac{1}{3}I(I+1)\right\} + P'(I_x^2 - I_y^2) - g_n\beta_n \underline{H}.\underline{I}\end{aligned} \qquad \ldots\ldots\ldots(46)$$

A description of the various component terms is given below.

In a resonance experiment the splitting between the effective spin levels by an applied magnetic field is $g\beta H$. The g value for an ion in a crystal is different to that for a free ion, as part of the magnetic moment arises from the orbital motion of the electron which is modified by the crystal electric field. Accordingly the magnitude of the orbital part of the magnetic moment shows an angular variation following the symmetry of the crystal field. The total g value, spin plus orbit, is anisotropic and in the spin Hamiltonian the splitting of the effective spin levels by H is represented by the energy operator

$$\mathcal{H} = \beta(g_z H_z S_z + g_x H_x S_x + g_y H_y S_y) \qquad \ldots\ldots\ldots(47)$$

where S is used to denote the effective spin rather than S'.

Very often there are initial splittings of the effective spin levels when H = 0 caused usually by the Stark effect arising from asymmetrical crystalline electric fields. For fields of axial symmetry these splittings may be represented in the Hamiltonian by the operator

$$D\left(S_z^2 - \frac{1}{3}\,S(S+1)\right)$$

where

$$S_x^2 + S_y^2 + S_z^2 = S(S+1)$$

and for fields of lower symmetry we add the term

$$E(S_x^2 - S_y^2)$$

The nucleus of the paramagnetic ion has a magnetic moment

$$\mu_n = I\, g_n\, \beta_n \qquad \text{.....(48)}$$

where

I is the nuclear spin,

g_n is the nuclear g value,

β_n is the nuclear magneton.

The interaction of the nuclear magnetic moment with the spin produces hyperfine spectral structure which may be anisotropic. This is represented in the spin Hamiltonian by the operator

$$A_z S_z I_z + A_x S_x I_x + A_y S_y I_y$$

where the hyperfine structure spacing is described by the three principal values of A.

The nucleus of a paramagnetic ion may have an electric quadrupole moment Q and if in an electric field gradient $\frac{\partial E}{\partial z}$ some orientations of the nucleus are energetically more favourable than others by an amount of order $\frac{eQ\,\partial E}{\partial z}$. This is represented in the spin Hamiltonian by operators such as

$$P\left(I_z^2 - \frac{1}{3}\,I(I+1)\right)$$

or if the electric field gradient has less than axial symmetry an additional term

$$P'\,(I_x^2 - I_y^2)$$

has to be added.

The nuclear magnetic moment μ_n interacts directly with the applied field H and is represented in the Hamiltonian by

$$-g_n \beta_n \underline{H}.\underline{I}.$$

This interaction usually produces only a very small or negligible effect of the observed spectrum.

2.2 The Spin Hamiltonian for a Tumbling Paramagnetic Complex

It is known that many transition group ions when in solution exhibit stable short range order between the ion and the nearest surrounding solvent neighbours and also if the transition ion is in an organometallic complex with large and specific ion-ligand interactions the average lifetime of the complex is long relative to the time taken for rotation produced by molecular tumbling. The McConnell model assumes a microcrystal with the same symmetry as the initial complex and subjected to a random tumbling as it is jostled by the molecular motions of the solvent liquid. To determine the effect of the motion on the ESR spectrum the Hamiltonian is transformed from a crystallographic to a laboratory coordinate system.

The Hamiltonian for the square planar copper salicylaldimine complex can be written as (Ref.18)

$$\mathcal{H} = \beta\left\{g_{//} H_r S_r + g_{\perp}(H_p S_p + H_q S_q)\right\} + A_{//} I_r S_r + A_{\perp}(I_p S_p + I_q S_q) \quad \ldots\ldots(49)$$

where

p,q and r are a set of orthogonal unit vectors fixed in the crystal with r parallel to the symmetry axis,

H is the magnetic field intensity due to the external applied field,

S is the electron spin vector in units of $\hbar$,

I is the nuclear spin vector in units of $\hbar$,

$g_{//}$ is the electronic g factor parallel to the r direction,

$g_{\perp}$ is the electronic g factor perpendicular to the r direction,

$A_{//}$ and $A_{\perp}$ are the hyperfine splitting constants.

This equation can be written in a laboratory coordinate system xyz with H along the z direction in the usual manner, i.e.

$$H_r = H_z \cos\theta,$$

$$S_r = S_z \cos\theta + S_x \sin\theta \cos\varphi + S_y \sin\theta \sin\varphi$$
$$= S_z \cos\theta + \tfrac{1}{2} (S_+ e^{-i\varphi} + S_- e^{i\varphi}) \sin\theta,$$

where

$$S_{\pm} = S_x \pm S_{iy}.$$

The transformed equation becomes (Ref.18)

$$\mathcal{H} = \mathcal{H}_o + \mathcal{H}_t \qquad \ldots\ldots(50)$$

where

$$\mathcal{H}_o = g\beta H S_z + a\, \underline{I}.\underline{S}, \qquad \ldots\ldots(51)$$

$$\mathcal{H}_t = (\Delta g\beta H + bI_z)(\cos^2\theta - \tfrac{1}{3})S_z$$
$$+ \tfrac{1}{2}(\Delta g\beta H + bI_z) \sin\theta \cos\theta (S_+ e^{-i\varphi} + S_- e^{+i\varphi})$$
$$- \frac{b}{4}(\cos^2\theta - \tfrac{1}{3})(S_+ I_- + S_- I_+)$$
$$+ \frac{b}{4}(\sin^2\theta)(I_+ S_+ e^{-2i\varphi} + I_- S_- e^{2i\varphi}) \qquad \ldots\ldots(52)$$
$$+ \tfrac{1}{2} b (\sin\theta \cos\theta)(I_+ e^{-i\varphi} + I_- e^{+i\varphi}) S_z,$$

and

$$g = \frac{1}{3}(g_{//} + 2 g_{\perp}), \quad \Delta g = g_{//} - g_{\perp},$$
$$a = \frac{1}{3}(A_{//} + 2A_{\perp}), \quad b = A_{//} - A_{\perp}.$$

Because of the Brownian motion θ and φ are functions of time and all the functions involving these are collected in $\mathcal{H}_t$. The centre of gravity of each of the hyperfine lines is obtained from the eigenvalues of $\mathcal{H}_o$. The time dependent perturbation $\mathcal{H}_t$ broadens the lines. The long time average of all the terms in $\mathcal{H}_t$ is zero but unless the microcrystal is rotating rapidly it does not sample all orientations during the relaxation time and the value of $\mathcal{H}_t$ is not zero, producing line broadening dependent upon nuclear orientation.

The amount the spectral lines are broadened depends on the ratio of the correlation time τ_c which is a measure of the length of time over which some correlation persists, to the relaxation time of the line.

When the correlation time is much less than the relaxation time the line broadening is small, increasing with increasing correlation time. For a simple spherical model in a viscous liquid

$$\tau_c = \frac{4\pi\eta a^3}{3kT}, \qquad \text{.....(53)}$$

where

η is the viscosity

a is the sphere radius.

For copper salicylaldimine dissolved in ether a rough estimate of the correlation time can be found using the following values

η = .002 poise

a = 10Å

$$\tau_c = \frac{4\pi .2 \times 10^{-3} \cdot 10^{-21}}{3.1{\cdot}38 \times 10^{-16} .3 \times 10^{2}} \simeq 2 \times 10^{-10} \text{ sec.}$$

The linewidth of the hyperfine lines of copper salicylaldimine is about 30 oe giving a relaxation time of 1.2×10^{-8} sec which is comparable to the correlation time. This crude calculation would lead one to expect some line broadening even when copper salicylaldimine is dissolved in the least viscous solvent used.

3. EXPERIMENTAL SECTION

3.1 Experimental Objective

When a metal ion combines with an electron donor the resulting substance is said to be a complex or coordination compound. If the substance that combines with the metal contains two or more donor groups so that one or more rings are formed the resulting structure is said to be a chelate (Ref.22).

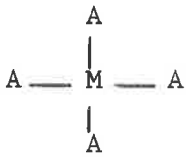

Metal Complex

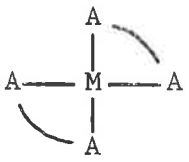

Metal Chelate

M is the metal ion

A the complexing agent.

Recently ESR studies have been made on a variety of copper chelates to determine the type of bonding of the copper ion and also the correct values of the constants in the spin Hamiltonian (Refs. 23, 24, 25).

The present study on copper salicylaldimine has been made in order to determine the effect on the hyperfine spectrum when a straight chain hydrocarbon group is added to the basic chelate. The aliphatic chain was expected to act as a "paddle wheel" increasing the effective radius of the microcrystal and, by increasing the correlation time, producing a hyperfine line broadening. Chelates were used with aliphatic chains of 3, 8 and 14 members. Bis (N-propylsalicylaldimine) copper II has a 3 membered aliphatic chain added to copper salicylaldimine and can be written as

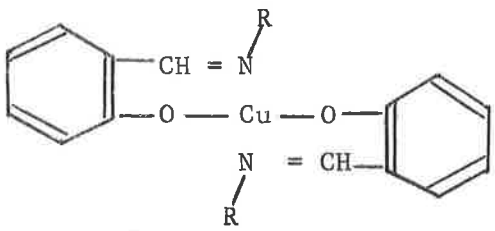

where

$R = CH_3\ CH_2\ CH_2$

Experiments were performed using N propyl R = 3, N octyl R = 8 and N tetradecyl R = 14, each dissolved in three nonpolar solvents, ether, benzene and carbon tetrachloride whose viscosities at room temperature are respectively .222, .608 and .906 centipoise.

3.2 Experimental Procedure

The copper chelates were prepared according to Charles (Ref.26) by methods involving the condensation of salicylaldehyde with the appropriate amine (RNH_2) followed by reaction with copper acetate. The complexes were twice recrystalled from ethanol before use and were in the form of a microcrystalline powder that dissolved readily in the three solvents used. The solvents were chosen to cover a viscosity range of 4:1 and also to have a low dielectric loss at 10,000 Mc/s in order not to damp the sample cavity Q.

McGarvey (Ref.17) found that the hyperfine line shapes of the copper chelates were independent of concentration for dilute solutions in the range .001 mol to .01 mol and so a solution strength of .01 mol was used to produce a good signal to noise ratio. Nine solutions of .01 mol concentration were made using the three compounds and the three solvents carbon tetrachloride, benzene and ether. The molecular weights of the three compounds are given below:

Bis (N propyl.....) copper II 388
Bis (N octyl .....) copper II 528
Bis (N tetradecyl .....) copper II 696

The solutions were used to fill $\frac{1}{8}$ in ID teflon test tubes to a depth of about $\frac{1}{4}$ in and these were then placed in the sample cavity.

The expected lines were about 30 oe wide and so the magnetic field modulation was set to 0.5 oe, a value that would eliminate any appreciable magnetic modulation line broadening (page 10). The field sweep amplitude was set using the proton resonance magnetometer. The starting field was 2865 oe corresponding to a frequency of 12.2 Mc/s and the final field was set to 3500 oe or 14.5 Mc/s. These frequencies could be accurately set by beating with the harmonics of a 100 kc crystal oscillator. The sweep slope was set at 2 oe/sec.

Although the cavity frequency could be measured with an absorption wavemeter two runs were made with each specimen, the second run being made with a small amount of DPPH powder in the cavity to provide a g marker at g = 2.0036.

In order to provide a larger graph for the later curve fitting, the results of the nine spectral scans were transferred from the 2½ in recorder chart to a 5 in chart by means of a 2:1 pantograph. These scans are shown as continuous lines in Fig.33 to 41. It will be noticed that a few have considerable base line drift which is to be expected when high amplifier gains are used together with a scan length of about 5 minutes. Two sources of drift exist in the equipment that are added in addition to the basic drift of the DC amplifier:

1. Vibration in the cavity walls produced by the interaction of the wall eddy currents and the applied magnetic field. These vibrations produce a signal when the klystron is not quite locked to the cavity frequency. The amplitude of these vibrations is proportional to the strength of the DC magnetic field but small random variations of the klystron about the cavity frequency produced a nonreproducible recorder drift that could not be calibrated and subtracted from the measurements.

2. Noise generated and radiated by the thyratrons in the magnet power supply. The noise output from this source increases with increasing current and produces a recorder drift.

4. MEASUREMENT OF LINEWIDTHS

The hyperfine spectral lines overlap considerably making the true value of the component lines differ considerably from the apparent width. It is possible to obtain the true linewidths by curve fitting a curve produced from the sum of the four component lines of Lorentzian shape (Ref.17) which, because of the equal

FIG.33

ESR SPECTRA OF BIS (N-TETRADECYLSALICYLALDIMINE) Cu II IN CARBON TETRACHLORIDE

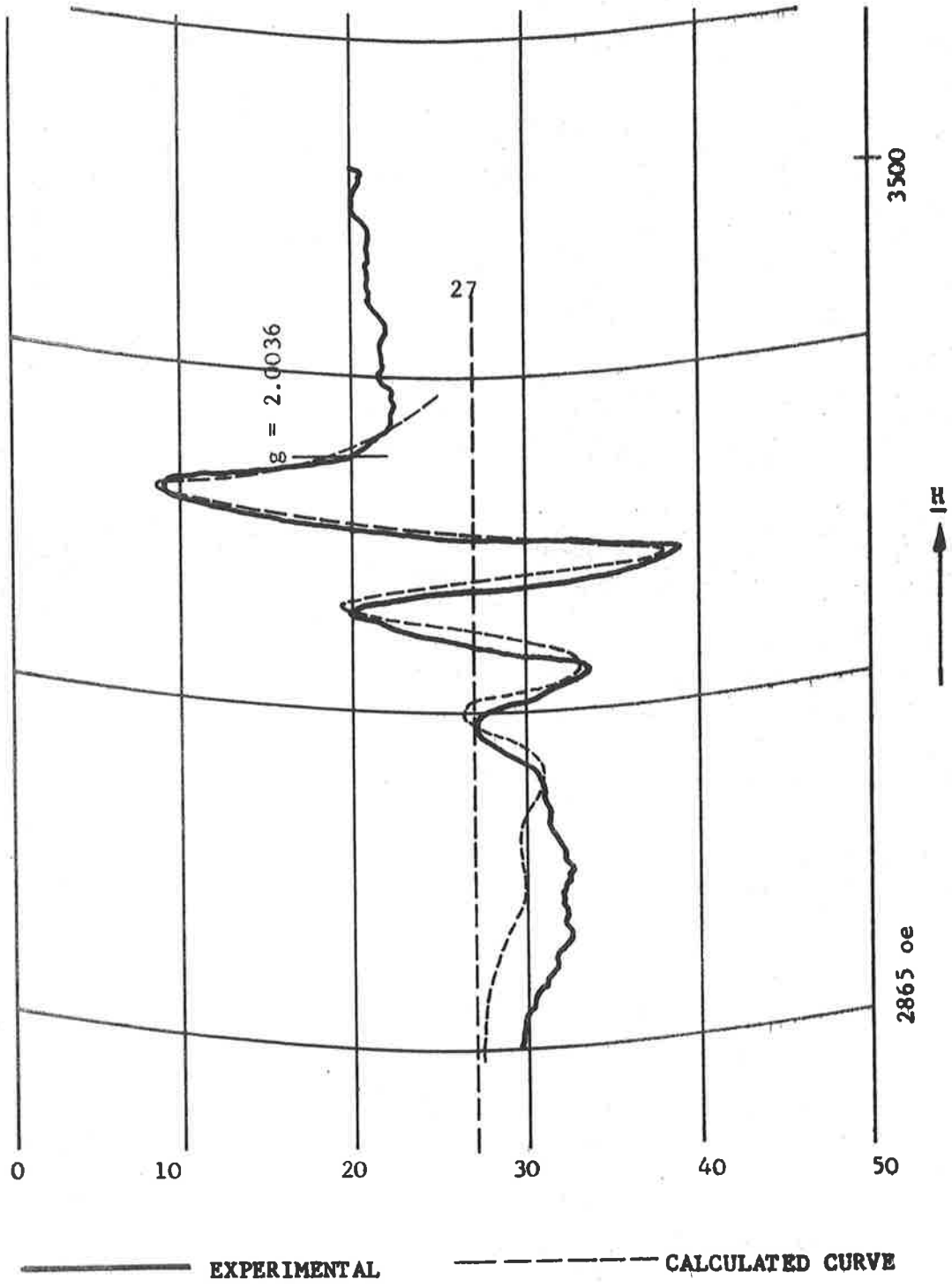

FIG.34

ESR SPECTRA OF BIS (N-TETRADECYLSALICYLALDIMINE) Cu II IN BENZENE

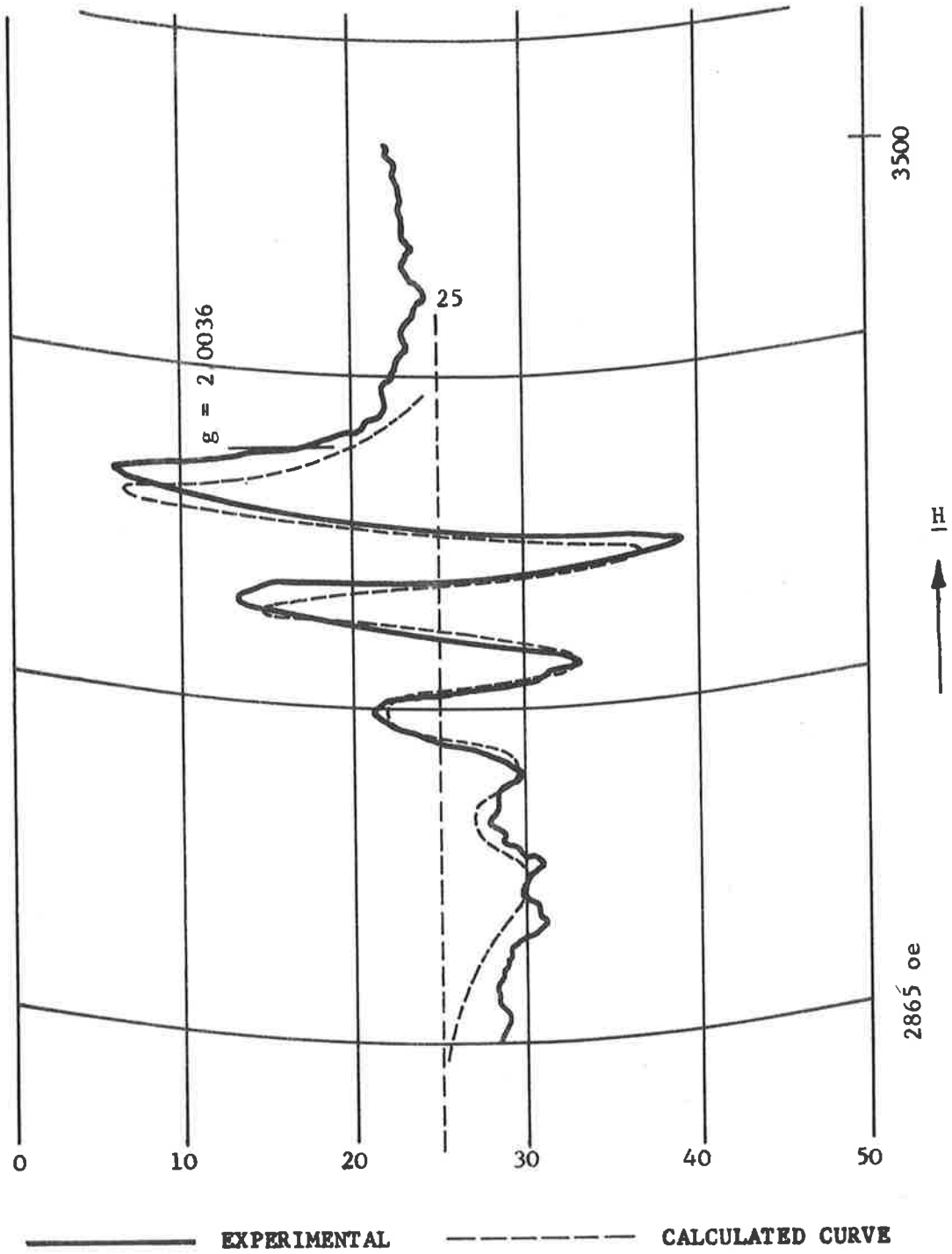

FIG.35

ESR SPECTRA OF BIS (N-TETRADECYLSALICYLALDIMINE) Cu II IN ETHER

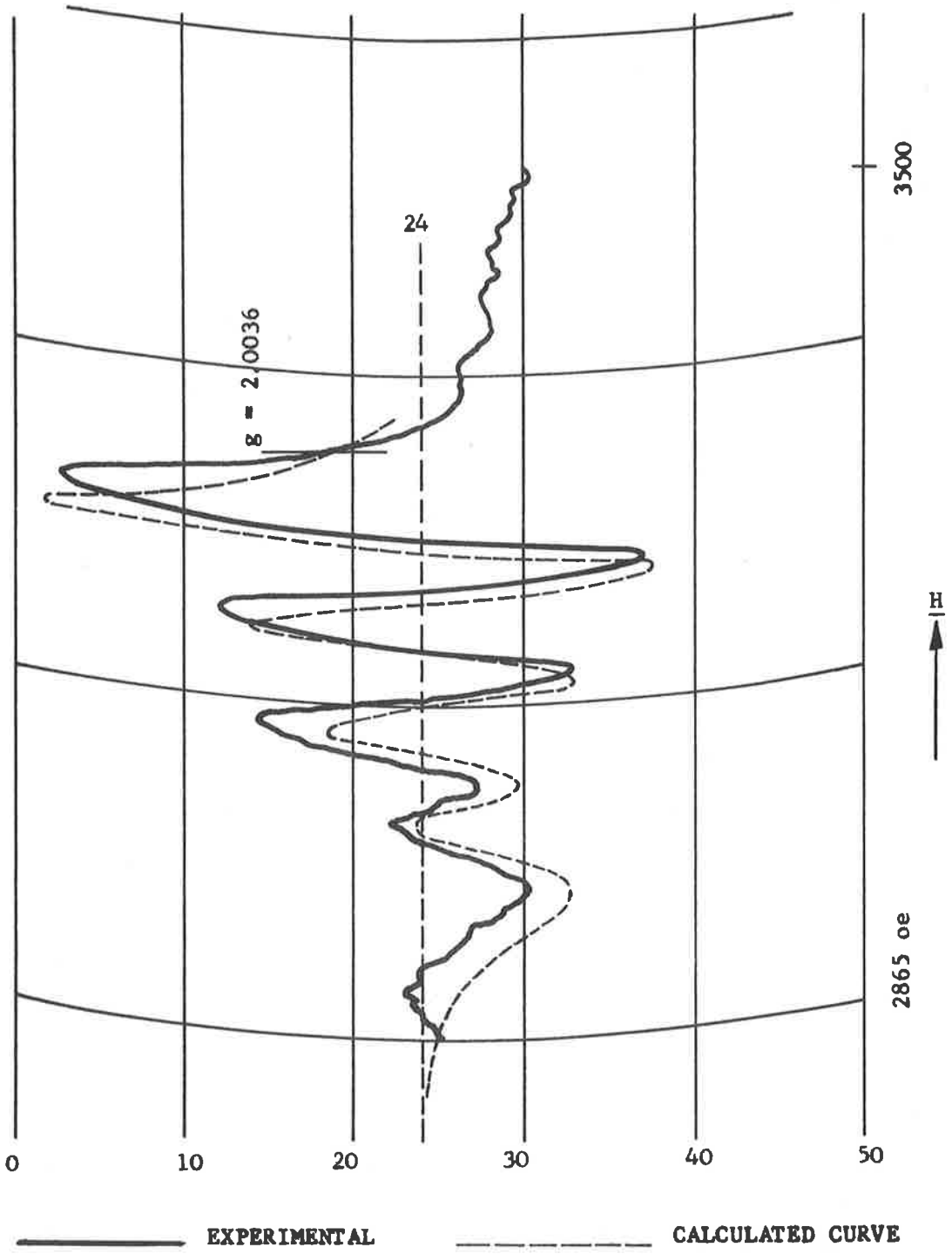

FIG.36

ESR SPECTRA OF BIS (N-OCTYLSALICYLALDIMINE) Cu II IN CARBON TETRACHLORIDE

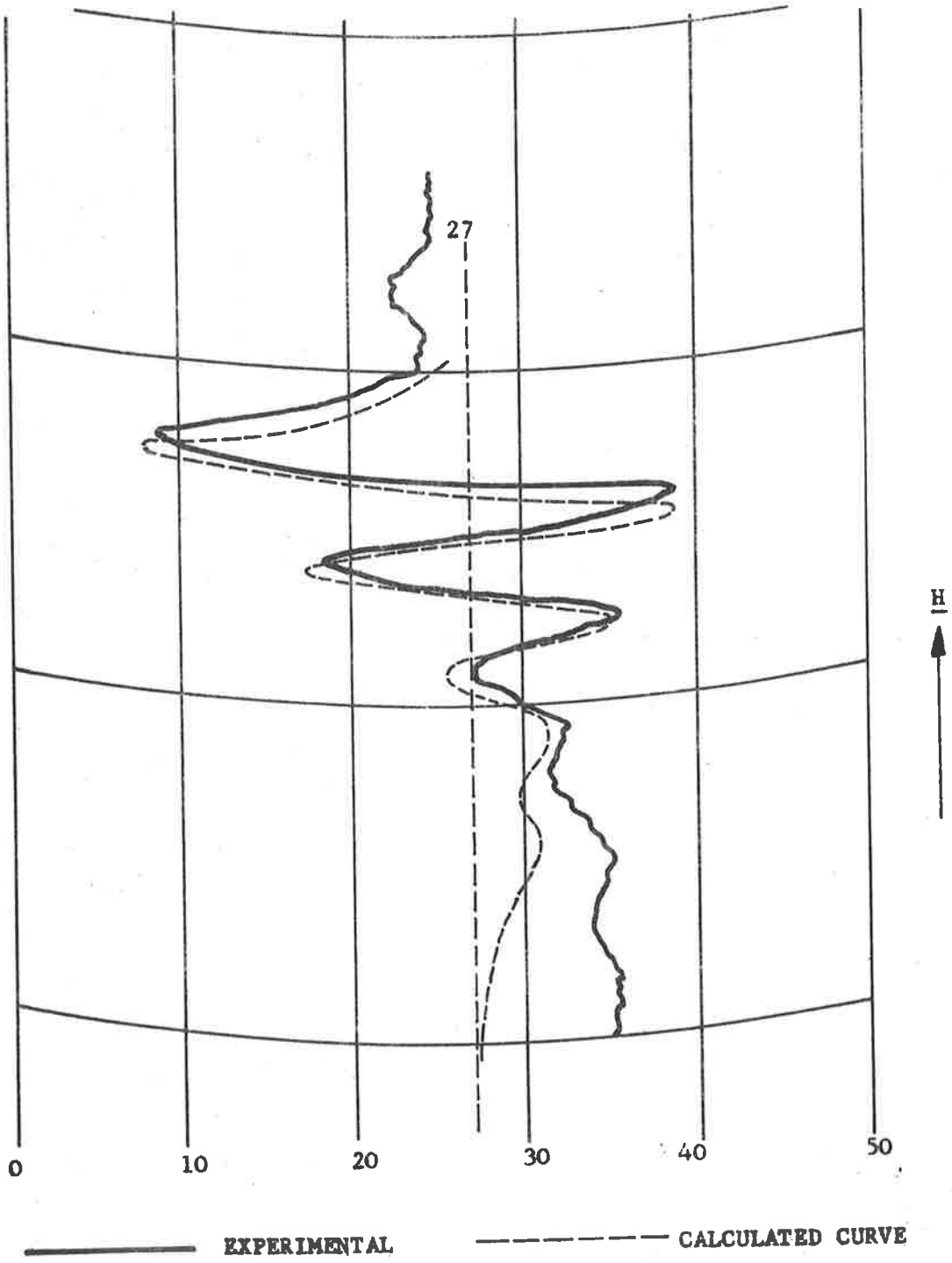

FIG.37

ESR SPECTRA OF BIS (N-OCTYLSALICYLALDIMINE) Cu II IN BENZENE

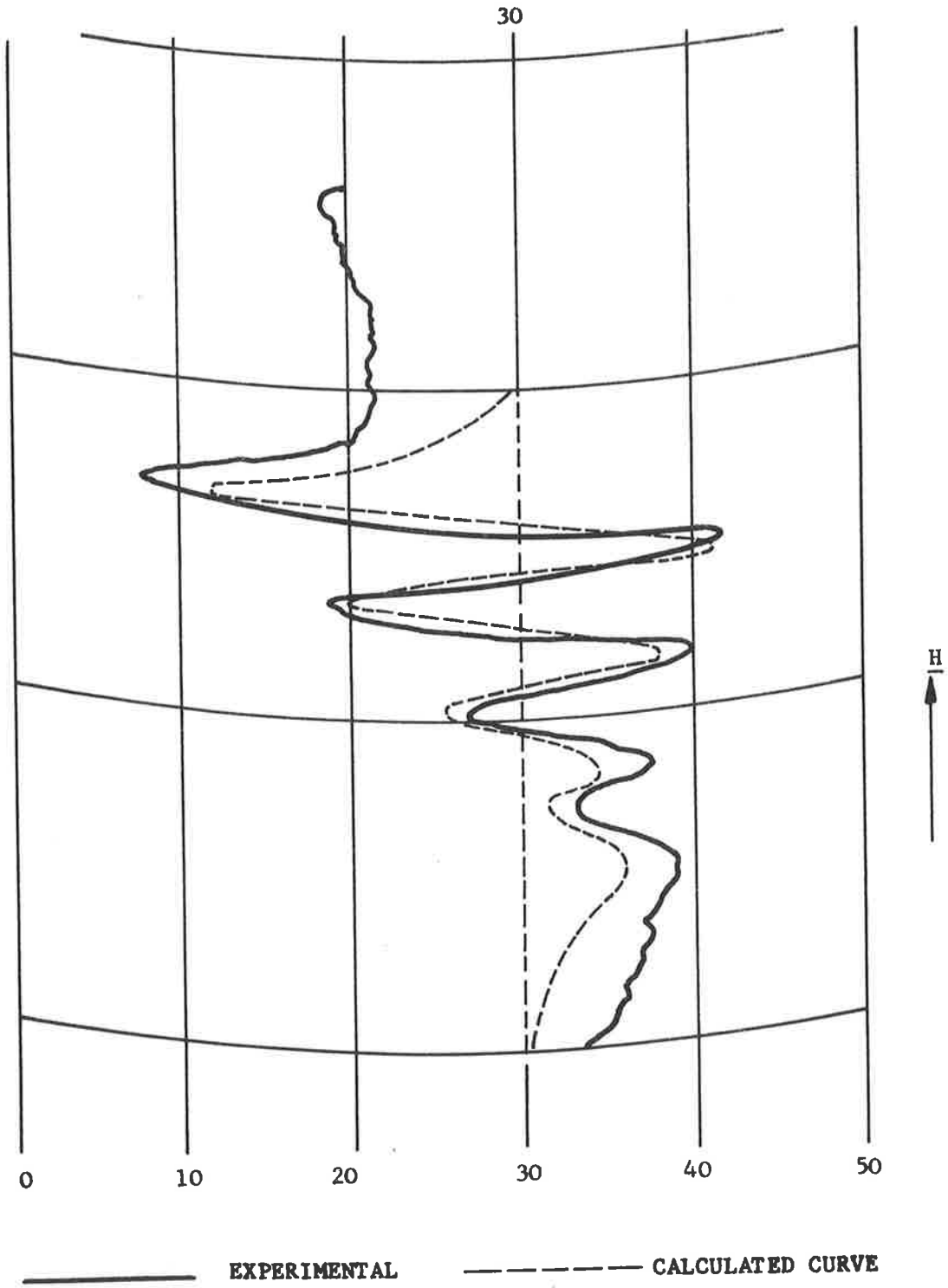

FIG. 38

ESR SPECTRA OF BIS (N-OCTYLSALICYLALDIMINE) Cu II IN ETHER

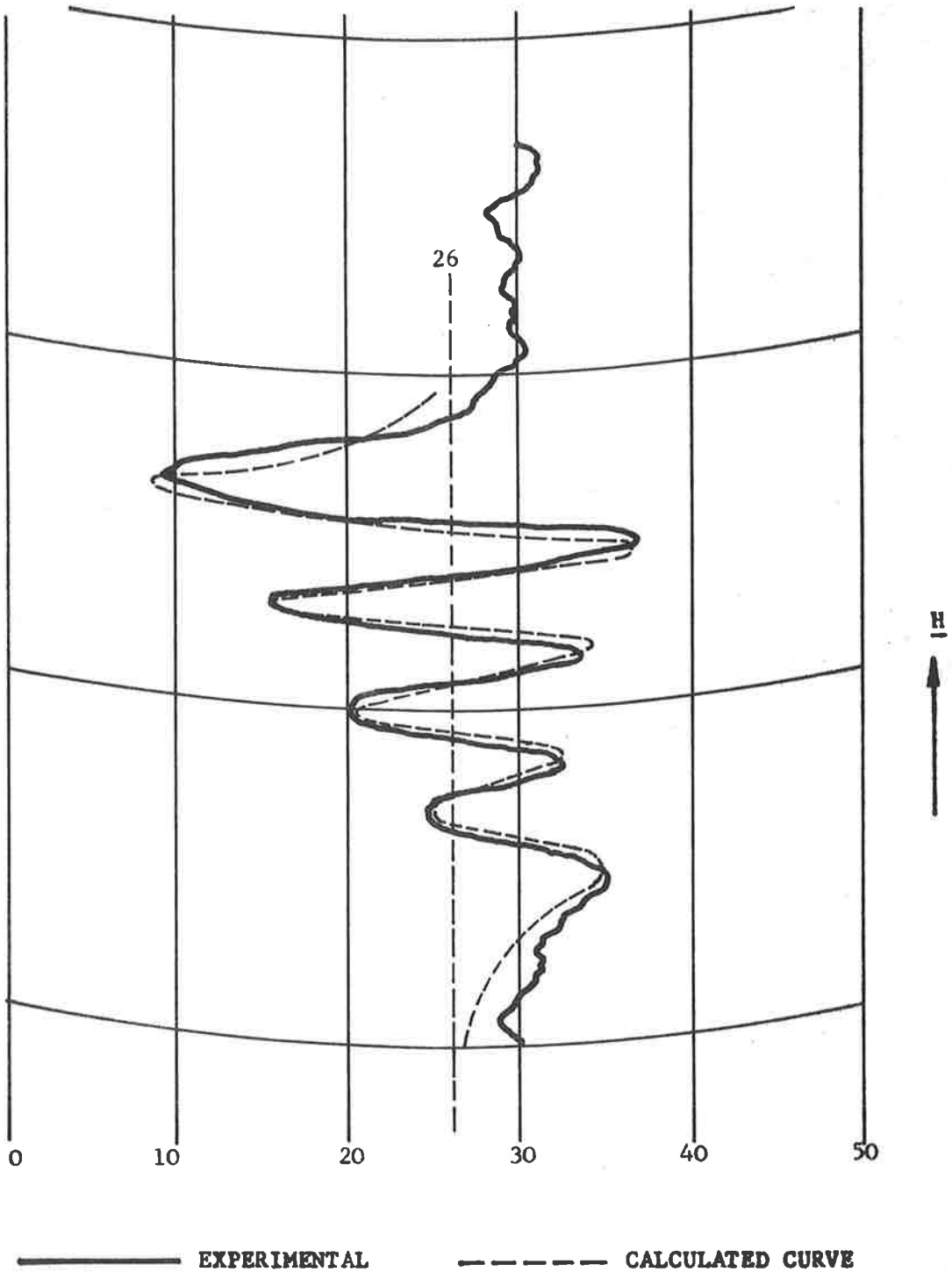

FIG.39

ESR SPECTRA OF BIS (N-PROPYLSALICYLALDIMINE) Cu II IN CARBON TETRACHLORIDE

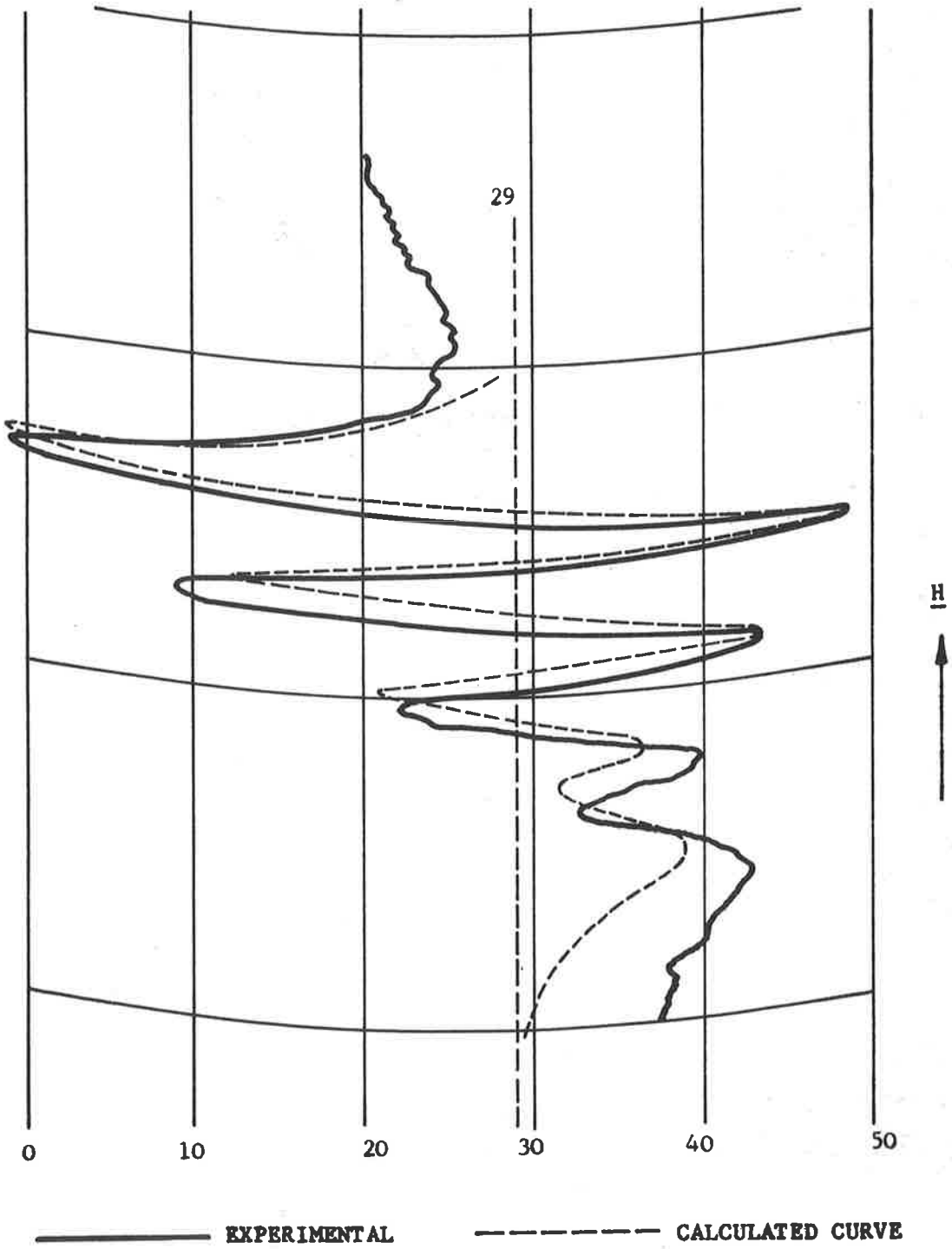

FIG.40

ESR SPECTRA OF BIS (N-PROPYLSALICYLALDIMINE) Cu II IN BENZENE

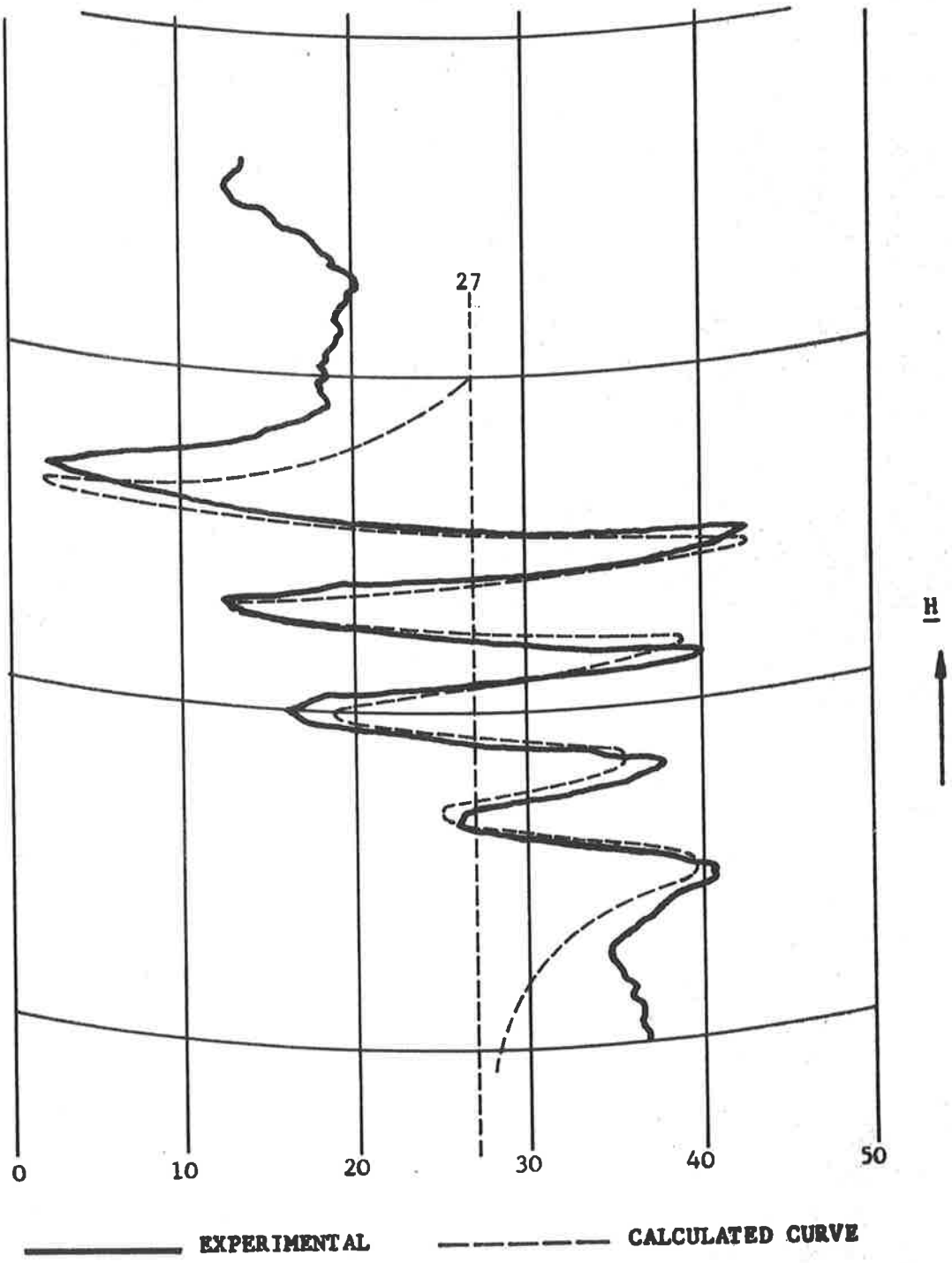

FIG.41

ESR SPECTRA OF BIS (N- PROPYLSALICYLALDIMINE) Cu II IN ETHER

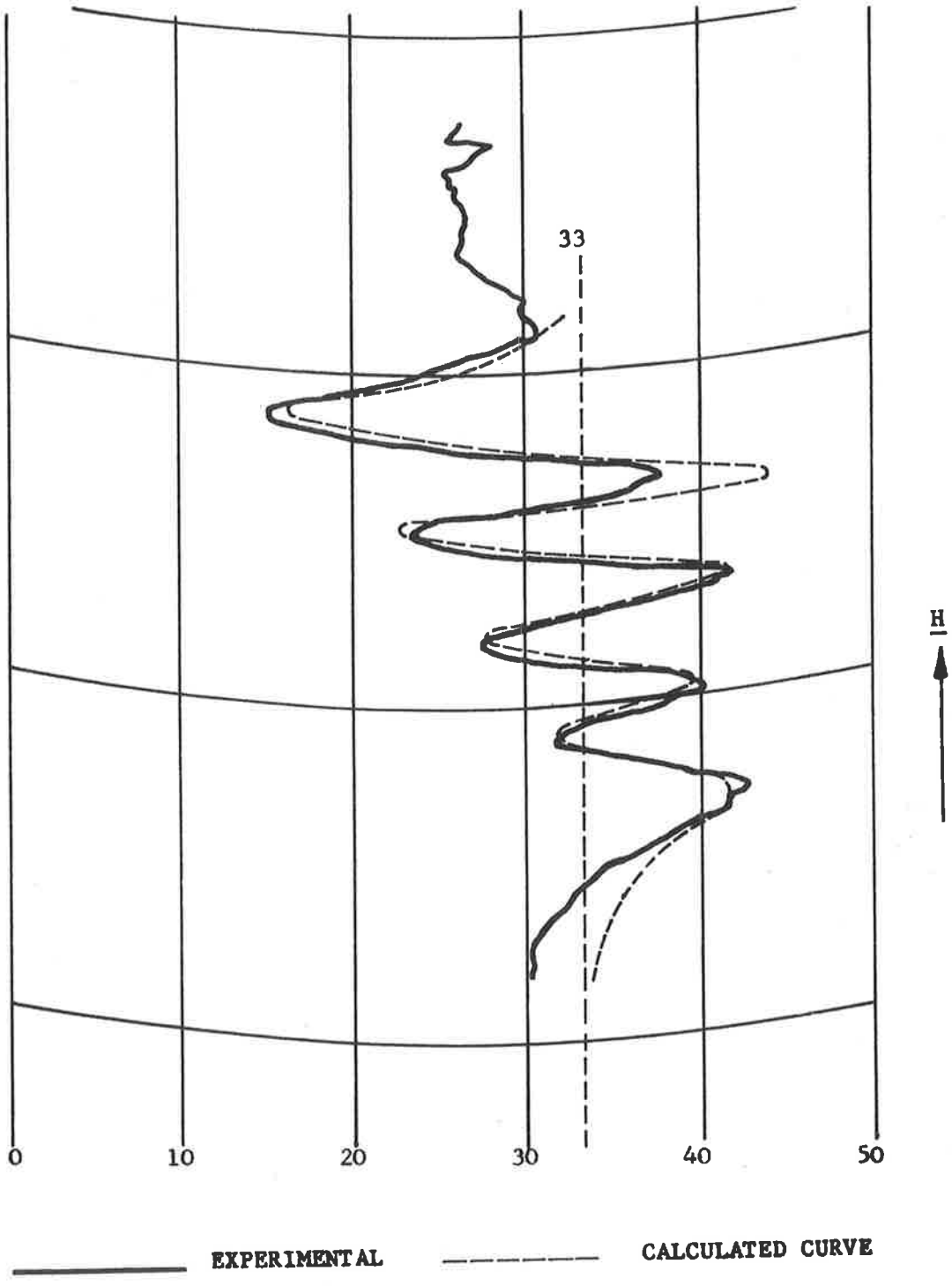

probability of all nuclear orientations, should all be of equal intensity but should differ in linewidth. Fig.42 shows four curves that are the derivative of four Lorentzian curves summed to produce a composite curve.

The Lorentzian curve has the equation (Ref.2)

$$g\ (\omega - \omega_o) = \frac{B}{\pi T_2} \quad \frac{1}{\left(\frac{1}{T_2}\right)^2 + (\omega - \omega_o)^2} \qquad \ldots\ldots(54)$$

where the total half-height width is $\frac{2}{T_2}$ and B is a scaling factor. The total width at the points of maximum slope is $\frac{2}{T_2}\sqrt{3}$. Approximate values for the linewidths were obtained by derivative curve fitting using the series

$$B' \sum_{n=1}^{4} W_n \quad \frac{x - x_n}{\left(3W_n^2 + (x - x_n)^2\right)^2} \qquad \ldots\ldots(55)$$

where W_n is the linewidth from the curve centre, x_n, to the point of maximum slope.

It will be seen that there are two parameters for each curve, the width and the position of the line centre which of course determines the separation between the lines and a scaling factor B'. It will be remembered that the time independent part of the Hamiltonian was

$$\mathcal{H}_o = g\beta H S_z + a\ \underline{I}.\underline{S}$$

giving lines spaced by the splitting factor a.

Initial attempts at curve fitting were made for bis (N octylsalicylaldimine) copper II in ether, Fig.38, as for this solution the correlation time was fairly short and the line broadening terms were small. In this figure the DC drift appeared to be small allowing a better curve fit. Equal line separations were assumed and various curves were constructed using successive approximations of linewidth, separation and scaling factor to produce a good fit. The curve fit was inspected by plotting on transparent paper and overlaying. Using this method a splitting factor of 72.5 oe was estimated.

FIG.42

SUM CURVE OF 4 EQUALLY SPACED LORENTZIAN DERIVATIVE CURVES

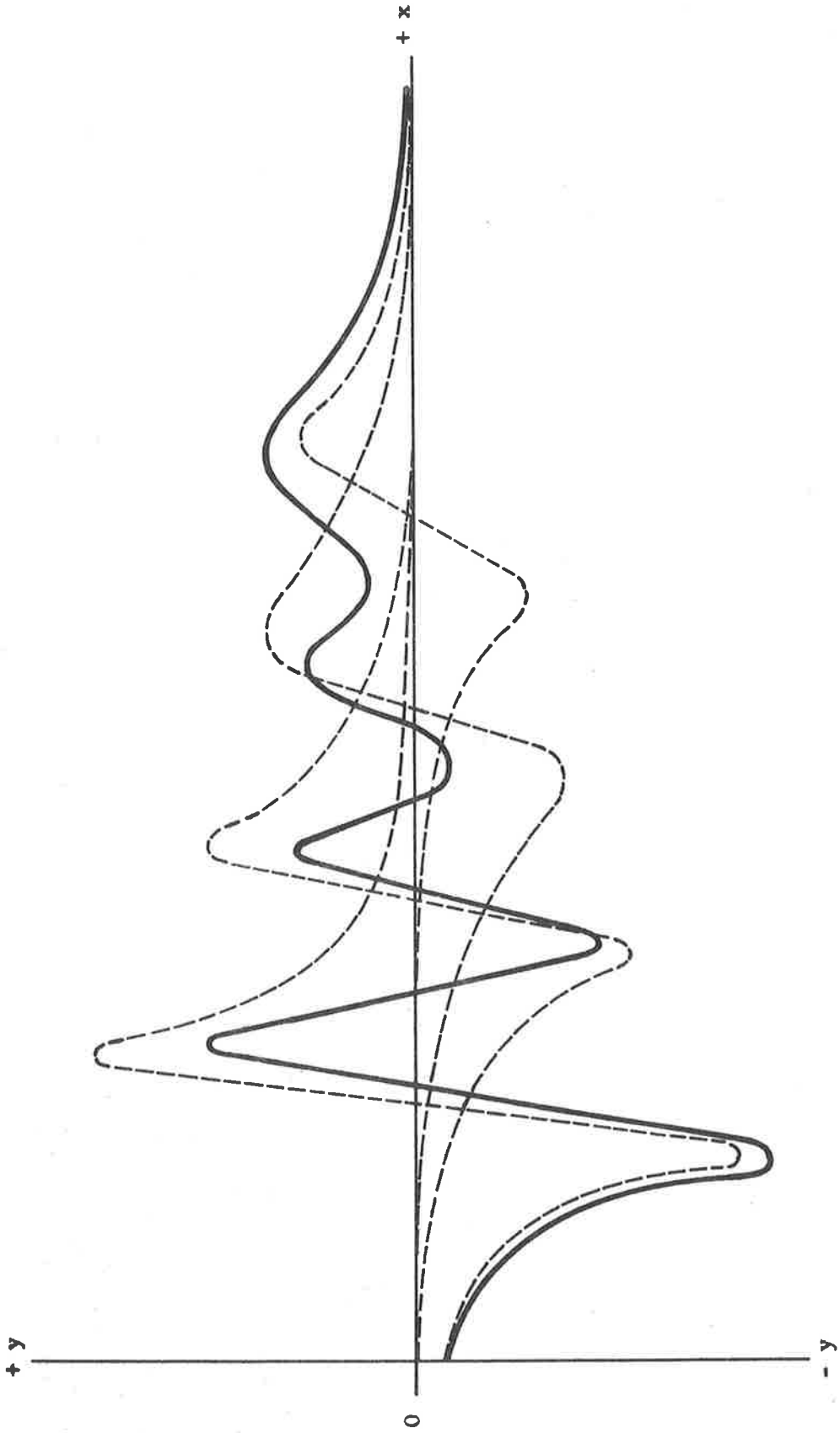

The values of g and a for Cu^{++} bissalicylaldimine (Ref.25) are

$$g_{//} = 2.14$$
$$g_{\perp} = 2.08$$
$$A_{//} \times 10^4 = 168 \text{ cm}^{-1}$$
$$A_{\perp} \times 10^4 = 16 \text{ cm}^{-1}$$
$$g = \frac{1}{3}(g_{//} + 2g_{\perp}) = 2.1$$
$$a = \frac{1}{3}(A_{//} + 2A_{\perp}) = 66.6 \times 10^{-4} \text{ cm}^{-1} = 71.5 \text{ oe}.$$

The result for the splitting constant is in good agreement with that found from curve fitting. The eigenvalues of the time independent Hamiltonian to second order are (Ref.20)

$$\hbar\omega = g\beta H + am_I + \frac{a^2}{2g\beta H}\left\{ I(I+1) - m_I^2 \right\} \quad \ldots\ldots\ldots\ldots(56)$$

where m_I is the nuclear quantum number.

Using figures from (Ref.25) the line separations for the magnetic field value corresponding to g = 2.1 must be 72.5 oe between $m_I = -\frac{3}{2}$ and $-\frac{1}{2}$, 71.5 between $-\frac{1}{2}$ and $+\frac{1}{2}$ and 70.5 between $+\frac{1}{2}$ and $+\frac{3}{2}$. These line separations were used for all subsequent curve plotting with variations of the linewidth to obtain a good curve fit.

Using Fig.35 the central g value was found to be 2.09 compared to the figure of 2.1 from Ref.25 .

Using the synthesising technique described above, the hyperfine linewidths were found for all the curves and plotted as dotted lines in Figs.33 to 41.

The above method of obtaining the linewidths suffered from two main errors:

1. DC drift in the recorded spectrum that was comparable to the recorded line amplitude.
2. Excessive labour required to calculate and sum the four curves and the difficulty of assessing the best fit.

Both of these errors were reduced as follows:
A large part of the DC drift was produced by noise originating in the thyratrons used for the magnet power supply. These thyratrons were removed and replaced by high current silicon diodes Type BYZ10 and all the experiments were repeated. Direct tracings of the nine curves are shown in Figs. 43, 44 and 45. It will be noticed that although the curves are improved there is still considerable drift.

The manual curve fitting was replaced by an iterative least squares method described in Appendix 1. Eight parameters were used in a function to fit the experimental derivative curves. The function used was

$$y = p_1 + p_2 x + p_3 \left\{ \frac{-2P_4(x-p_8)}{\left(p_4^2 + (x-p_8)^2\right)^2} - \frac{2p_5\,(x-p_8-k_1)}{\left(p_5^2+(x-p_8-k_1)^2\right)^2} \right.$$

$$\left. - \frac{2p_6(x-p_8-k_2)}{\left(p_6^2 + (x-p_8-k_2)^2\right)^2} - \frac{2p_7\,(x-p_8-k_3)}{\left(p_7^2 + (x-p_8-k_3)^2\right)^2} \right\}$$

where

p_1 and p_2 represent linear drift terms,
p_3 is a scaling factor,
p_4, p_5, p_6 and p_7 are the half linewidths at the half power points,
p_8 is the first curve centre,
k_1, k_2 and k_3 are the line separations which were fixed.

Using this function the fitting curve could be displaced along the ordinate by p_1 and the abscissa by p_8, tilted by p_2 and scaled by p_3. The actual iterative calculation was done on an IBM 1620 computer using about 40 points on each curve. The FORTRAN program for this curve fitting is shown in Appendix 2.

FIG.43

ESR SPECTRA OF COPPER SALICYLALDIMINE IN ETHER

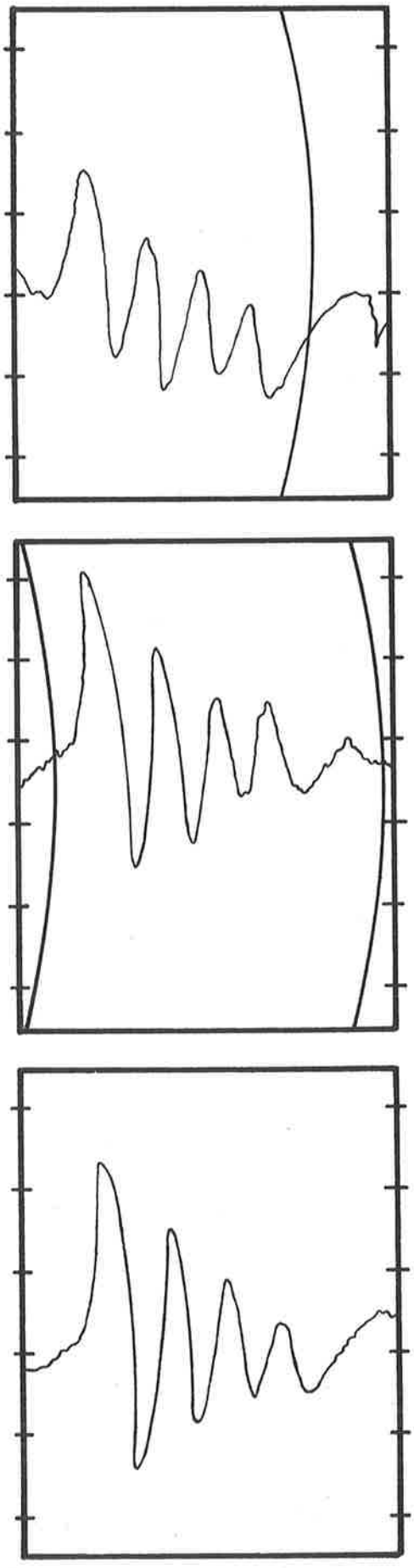

FIG.44

ESR SPECTRA OF COPPER SALICYLALDIMINE IN BENZENE

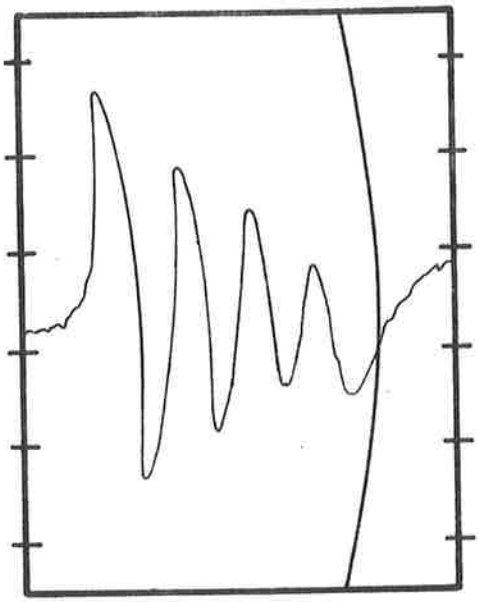

PROPYL

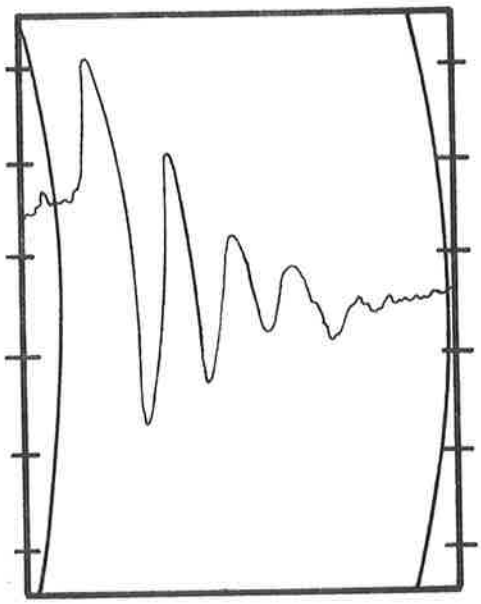

OCTYL

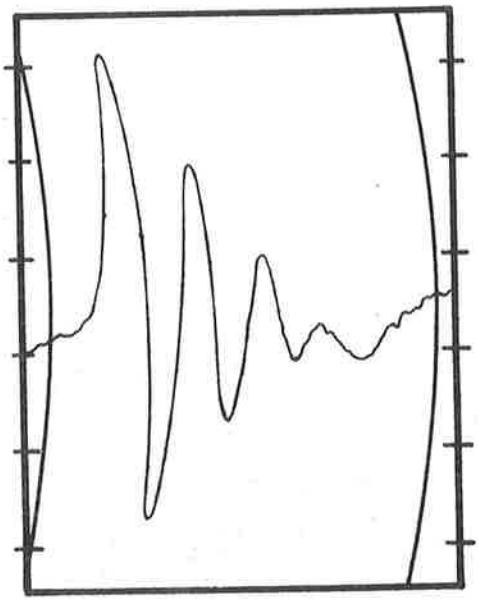

TETRADECYL

FIG.45

ESR SPECTRA OF COPPER SALICYLALDIMINE IN CARBON TETRACHLORIDE

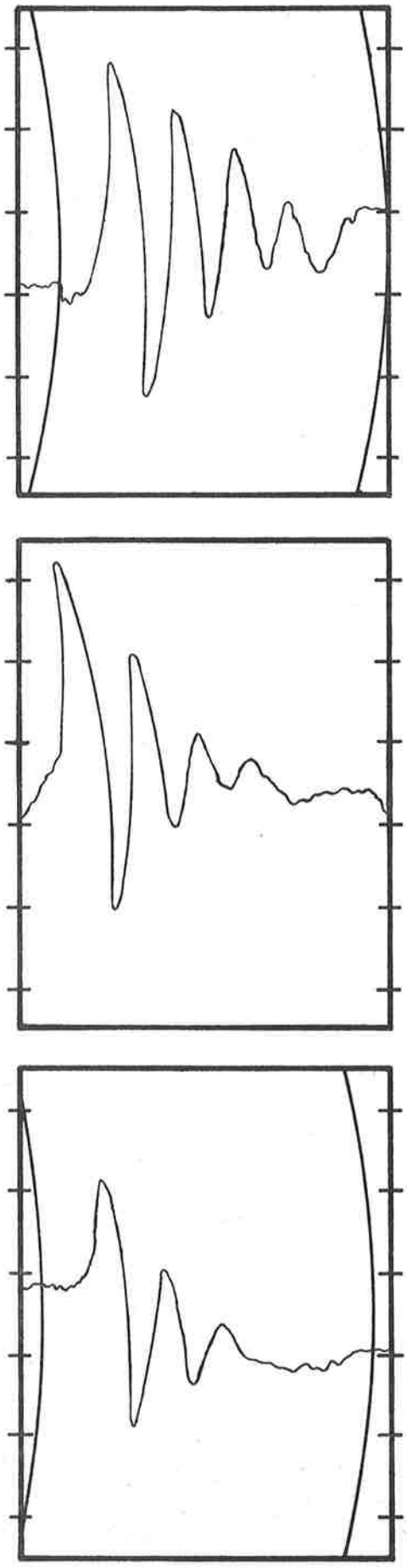

Using the above technique the values of the half linewidths at the half power points are shown below together with the values found by the graphical method. Appendix 3 lists the initial values of all the parameters together with the successive errors found during the iterative calculations. It will be seen that, although most of the parameters converge rapidly, the value of p_2, which determines the linear slope, tends to oscillate. It should be possible to improve the convergence of this term by curve fitting to experimental data in which the magnetic field sweep extends considerably beyond either side of the four hyperfine lines. Although the large variations in the interim values of p_2 in the iterative calculation do not appear to effect the convergence of the other terms an experiment was performed to confirm this.

The computer program was rewritten so that a fixed value of p_2 was used during the calculation and the experimental data from N tetradecyl dissolved in benzene, chosen because of the previous large variation in the interim values of p_2, was re-run using a fixed value of p_2 determined from the end points of the experimental curve. It was found that each of the successive error terms for p_1, p_3, p_4, ... p_8 were repeated and also the final values obtained for these parameters were unchanged. It was concluded that although p_2 could not be determined accurately without extending the experimental curves this did not affect the values obtained for the wanted parameters p_4, p_5, p_6 and p_7.

Solvent Carbon Tetrachloride

m_I =	$-\frac{3}{2}$	$-\frac{1}{2}$	$+\frac{1}{2}$	$+\frac{3}{2}$
		Graphical		
N tetradecyl	28.3	36.6	53.6	83.5
N octyl	28.3	33.6	48.2	72.3
N propyl	28.3	33.1	43.0	53.7
		Computer		
N tetradecyl	30.5	42.6	65.0	78.9
N octyl	27.8	37.6	56.4	67.7
N propyl	31.56	33.43	44.9	54.5

Solvent Benzene

m_I =	$-\frac{3}{2}$	$-\frac{1}{2}$	$+\frac{1}{2}$	$+\frac{3}{2}$
		Graphical		
N tetradecyl	28.3	36.8	44.9	61.0
N octyl	28.3	33.0	43.2	53.5
N propyl	28.8	33.1	38.9	43.0
		Computer		
N tetradecyl	29.8	38.8	59.6	68.9
N octyl	31.6	36.9	48.8	59.9
N propyl	32.0	37.7	49.3	60.4

Solvent Ether

m_I =	$-\frac{3}{2}$	$-\frac{1}{2}$	$+\frac{1}{2}$	$+\frac{3}{2}$
		Graphical		
N tetradecyl	28.3	35.3	42.2	48.2
N octyl	28.7	33.1	38.9	43.0
N propyl	28.7	33.1	38.9	43.0
		Computer		
N tetradecyl	32.5	36.88	56.4	68.9
N octyl	31.9	37.1	53.6	64.1
N propyl	41.9	40.8	49.8	57.2

If copper salicylaldimine were dissolved in a solvent of zero viscosity each of the hyperfine lines would have the same linewidth. The amount a particular line is broadened in a real solvent depends on $\mathcal{H}_t$ which is a function of the correlation time or viscosity of the solvent as well as the nuclear quantum number. If the values of the linewidth obtained above are plotted against the nuclear quantum the slope of the line through the points can be used as a measure of the correlation time. In Figs.46, 47 and 48 the values of the linewidths have been plotted against nuclear quantum number for the three solvents and a least squares line $y = mx + c$ has been drawn through these points using the

FIG.46

HYPERFINE LINEWIDTH AGAINST NUCLEAR ORIENTATION FOR CARBON TETRACHLORIDE SOLUTION

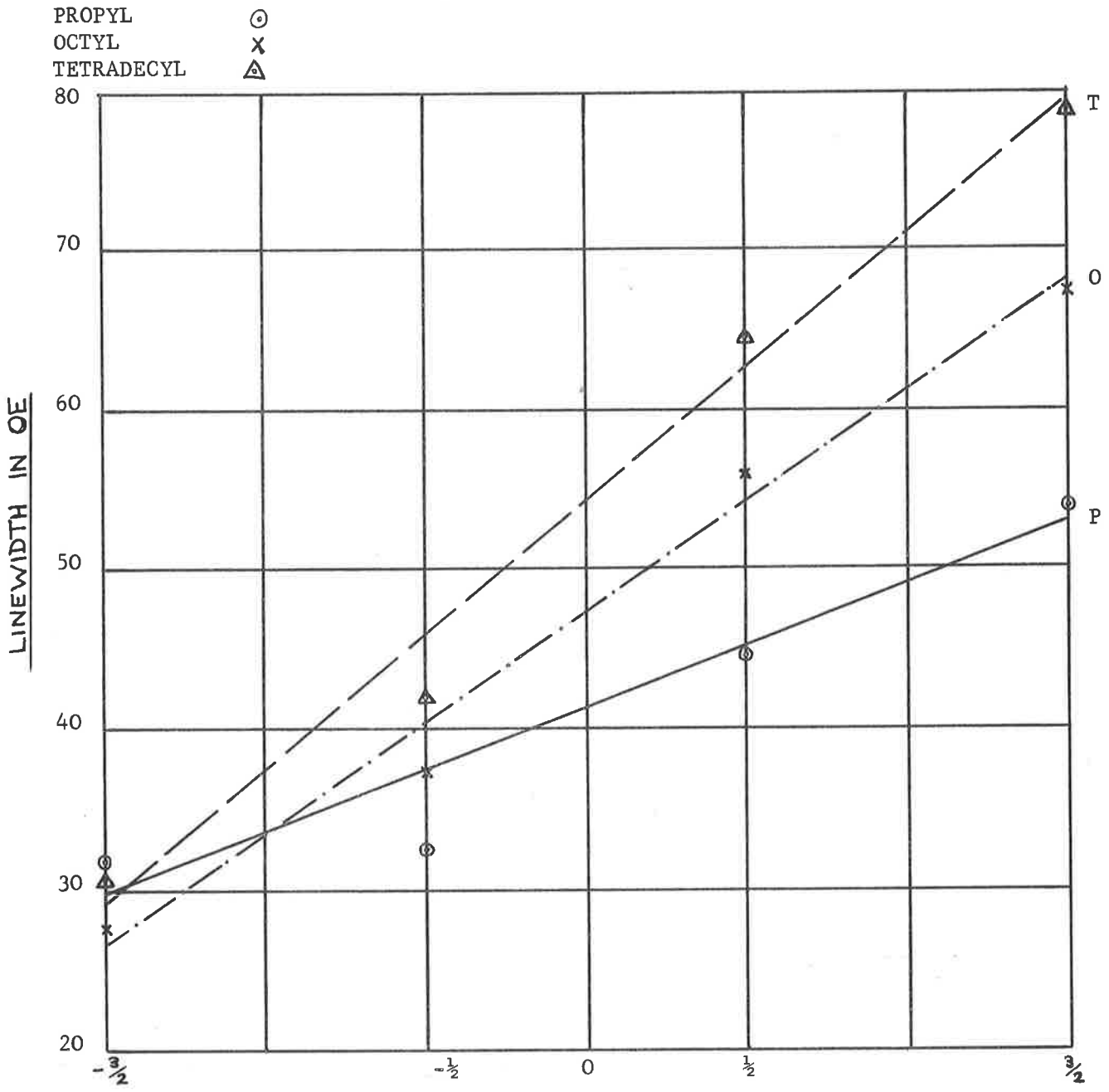

FIG.47

HYPERFINE LINEWIDTH AGAINST NUCLEAR ORIENTATION FOR BENZENE SOLUTION

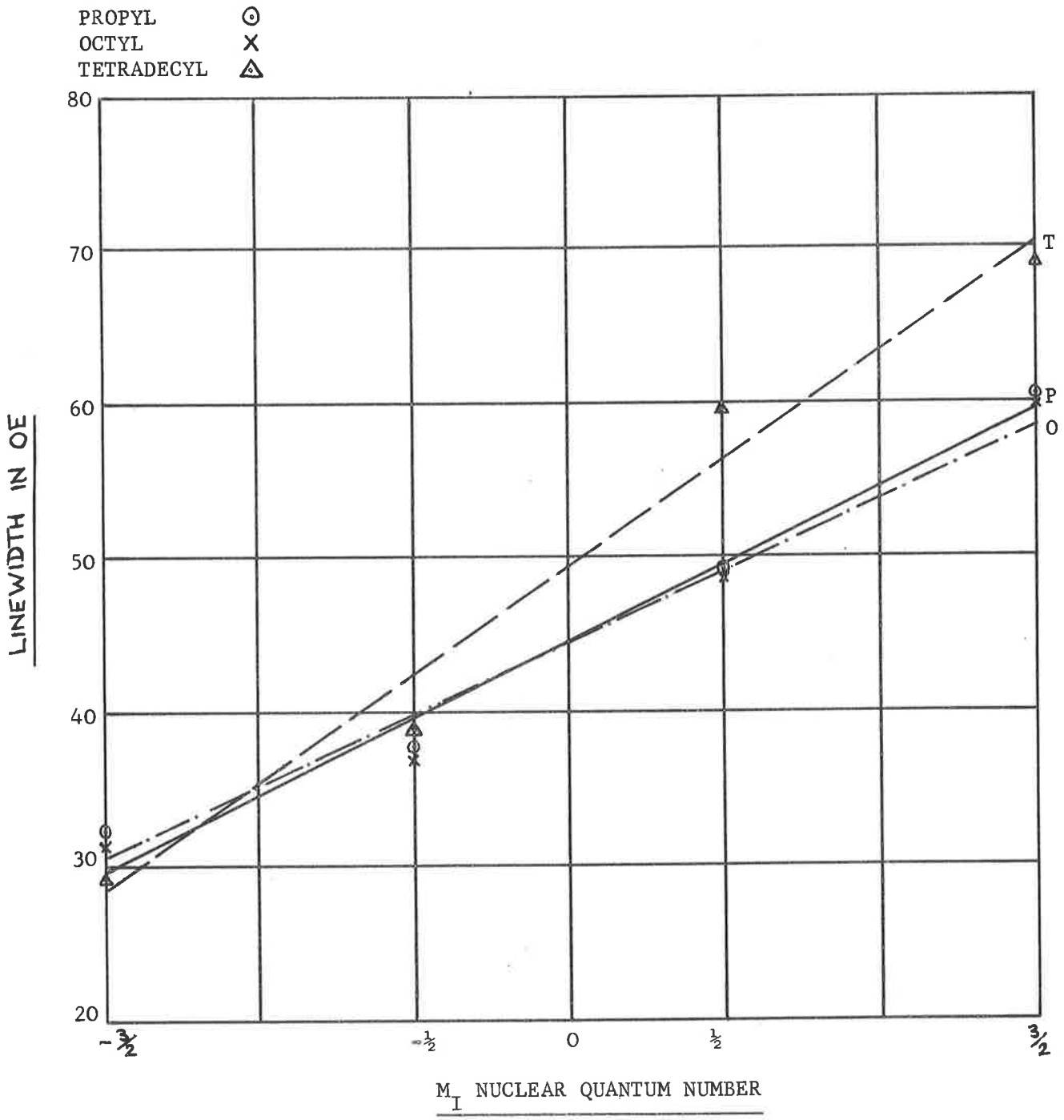

FIG.48

HYPERFINE LINEWIDTH AGAINST NUCLEAR ORIENTATION FOR ETHER SOLUTION

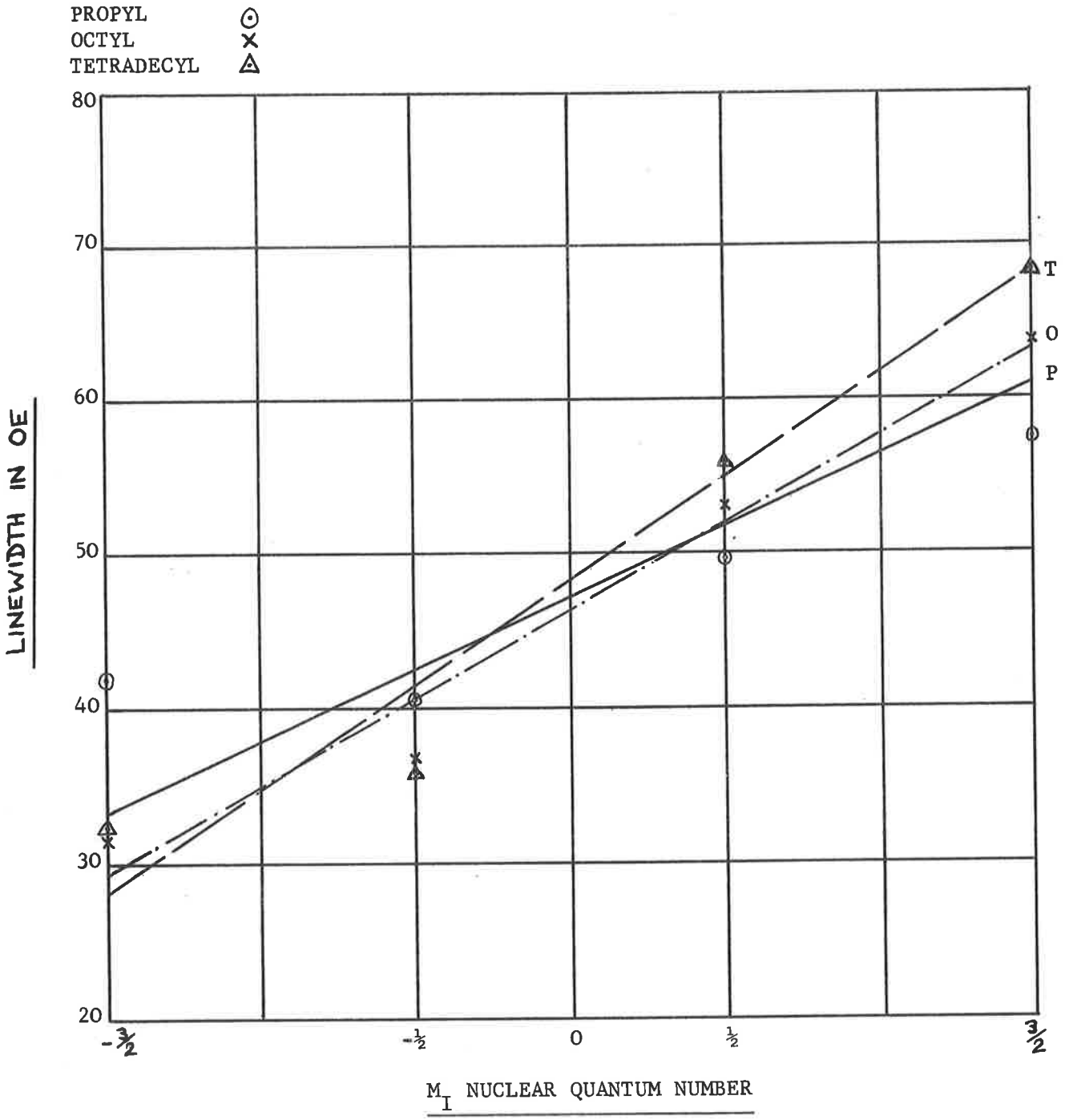

conventional formulae

$$\text{Slope } m = \frac{N\sum XY - X\sum Y}{N\sum X^2 - (\sum X)^2} \qquad \ldots\ldots(58)$$

$$c = \frac{\sum Y - m\sum X}{N} \qquad \ldots\ldots(59)$$

The values of the slopes are

	Carbon Tetrachloride	Benzene	Ether
m_{propyl}	= 8.05	9.67	9.48
m_{octyl}	= 13.86	9.71	11.32
$m_{tetradecyl}$	= 16.77	13.84	12.88

5. DISCUSSION

The previous work was intended to determine the linewidths of the hyperfine lines of copper salicylaldimine in solution. It was expected that these lines could be broadened by reducing the effective rotational speed of the microcrystal, produced by Brownian motion, and two methods of speed reduction were used. It had been shown by other workers that the rotational speed is determined by the viscosity of the solvent and by the effective radius of the microcrystal. Linewidth studies have been made of copper salicylaldimine in solution of varying viscosities and with the effective microcrystal radius altered by the addition of aliphatic chains of various length to the basic chelate.

The expected increase in the linewidth has been experimentally observed and a measure of the linebroadening produced in each experiment has been obtained from the slope, m, of the line obtained by plotting the hyperfine linewidth against the nuclear quantum number. The copper salicylaldimine crystal is planar and increasing the aliphatic chain length should increase the planar area but not the thickness. Using this hypothesis the linebroadening should be proportional to ηL^2, L being the aliphatic chain length, and Fig.49 shows the increase of the linebroadenings produced by ηL^2. Comparing the increase in line slope m produced by a known

FIG.49

HYPERFINE LINEWIDTH SLOPE AGAINST ηL^2

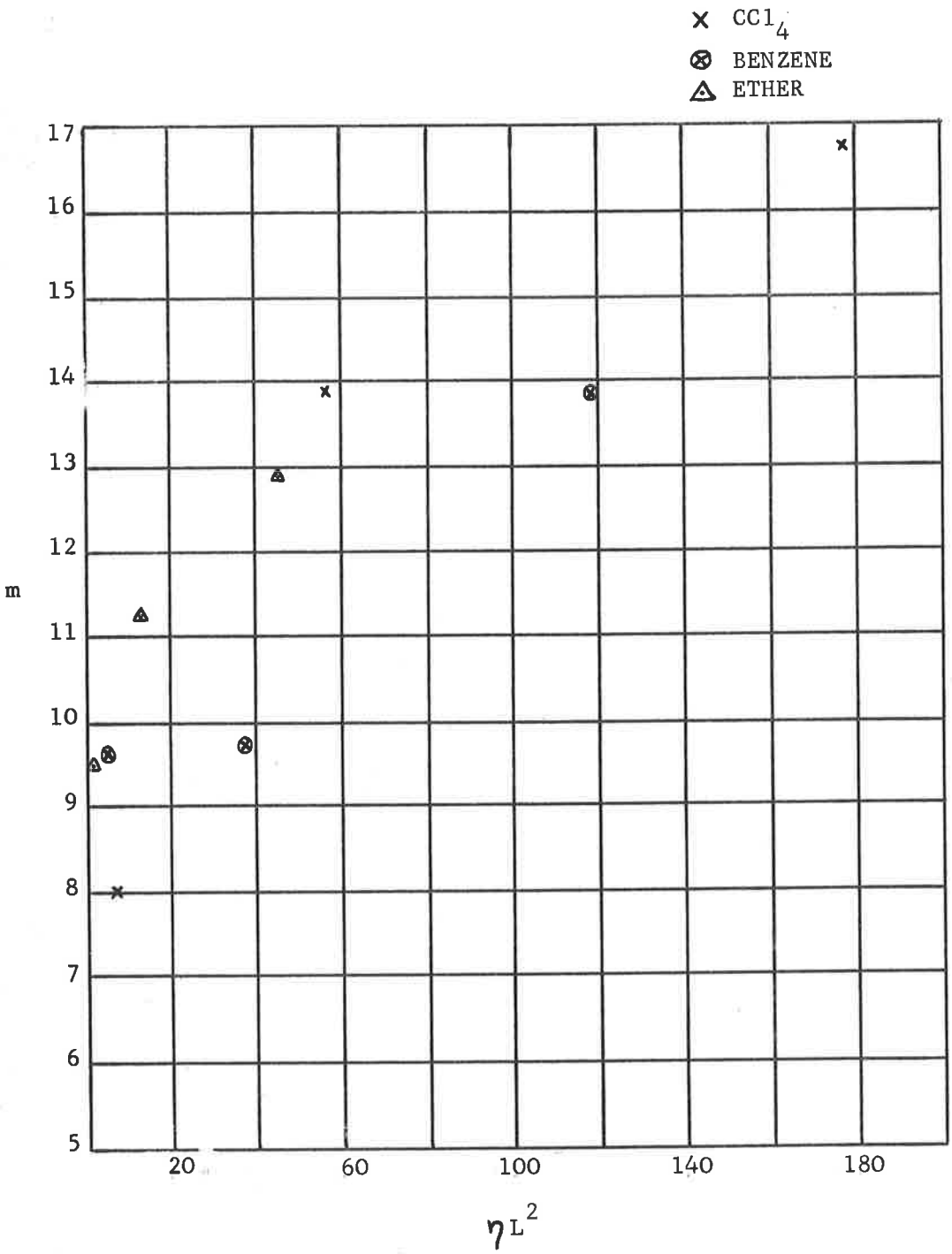

solvent viscosity change and by increasing the aliphatic chain length it was hoped to determine the relative increase in the radius of the microcrystal produced by adding the aliphatic chain. The experimental results, however, appear to be too inaccurate to do this satisfactorily. Examination of Appendix 3 shows that in general the final iterative errors are small and so the major errors are deduced to be in the experimental curve data. One limitation of the present equipment is a final chart recorder with only a 2½ inch chart making accurate reading difficult. The experimental accuracy could possibly be improved by the use of a larger instrument together with repeated runs to eliminate the random drift terms with zero mean.

6. REFERENCES

1. A. Weissberger, Physical Methods of Organic Chemistry, Part 4, Interscience Publishers, 1960.
2. D. Ingram, Free Radicals, Butterworth, 1958.
3. Methods of Experimental Physics, Vol.3, Academic Press, 1962.
4. D. Ingram, Spectroscopy at Radio and Microwave Frequencies, Butterworth.
5. C. Montgomery, Technique of Microwave Measurements, McGraw-Hill, 1947.
6. N. Bloembergen, E.M. Purcell and R.V. Pound, Phys. Rev. 73, 679, 1948.
7. G. Feher, B.S.T.J., 36, 449, 1957.
8. R. Karplus, Phys. Rev., 73, 1027, 1948.
9. R. Beringer and J. Castle, Phys. Rev., 78, 581, 1950.
10. G. Wilson, J. Appl. Phys. 34, 3276, 1963.
11. M. Rose, Phys. Rev., 53, 715, 1938.
12. R. Eades, G. Jenks and A. Bradbury, J. Sci. Inst. (GB) 38, 210, 1961.
13. T. Morento, Microwave Transmission Design Data, Dover, 1958.
14. American Institute of Physics Handbook, 5, 65, McGraw-Hill, 1957.
15. R. Hoskins and R. Pastor, J. Appl. Phys. 31, 1507.
16. L. Singer and J. Kommandeur, J. Chem. Phys. 34, 133, 1961.
17. B.R. McGarvey, J. Phys. Chem. 60, 71, 1956.
18. H.M. McConnell, J. Chem. Phys. 25, 709, 1956.
19. D. Kivelson, J. Chem. Phys. 33, 1094, 1960.
20. R.N. Rogers and G.E. Pake, J. Chem. Phys. 33, 1107.
21. K.D. Bowers and J. Owen, Reports on Progress in Physics, 28, 1955.
22. A. Martell and M. Calvin, Chemistry of the Metal Chelate Compounds, Prentice-Hall.
23. D. Kivelson and R. Neiman, J. Chem. Phys. 35, 149, 1961.
24. D. Kivelson and R. Neiman, J. Chem. Phys. 35, 156, 1961.
25. H.R. Gessmann and J.D. Swalen, J. Chem. Phys. 36,3221, 1962.
26. R. Charles, J. Org. Chem. 22, 677, 1957.
27. P. McWilliams, W.S. Hall and H.E. Wegner, Rev. Sci. Inst., 33, 70, 1962.
28. D.R. Tilley, Mullard Research Laboratories Technical Note No.602, 1963.

APPENDIX I

Curve Fitting by Gauss' Iterative Least Squares Method

The following method from Ref.27 has been used to fit four equal area Lorentzian curves to the ESR derivative traces.

Let the unknown curve be represented by the function

$$y = f(x, p_1, p_2, p_i \ldots\ldots\ldots p_m) \qquad \ldots\ldots(60)$$

where

x is an independent variable,

$p_1, p_2, p_i \ldots\ldots p_m$ are parameters to be determined.

If p_{io} is an initial estimate of the i^{th} parameter, the function may be expanded in a Taylor series about the point $(\ldots p_{io} \ldots)$:

$$y = f(x, p_{10}, p_{20} \cdots p_{io} \cdots p_{mo}) + \frac{\partial f}{\partial p_1}(\Delta p_1) + \frac{\partial f}{\partial p_2}(\Delta p_2) + \frac{\partial f}{\partial p_m}(\Delta p_m) + \text{higher-order terms}, \qquad \ldots\ldots(61)$$

where

$$\Delta p_i = p_i - p_{io} \qquad \ldots\ldots(62)$$

In the iterative procedure to be followed it is possible and convenient to ignore the higher order terms.

In classical least squares calculations the sum of the squares of the differences between the input y values (y_i) and the corresponding value of the fitted curve is minimised. The sum of the differences is

$$Q = \sum_i (y_i - y)^2 \qquad \ldots\ldots(63)$$

$$= \sum_i \left\{ y_i - \left[f(x, p_{10} \cdots p_{io} \cdots p_{mo}) + \left(\frac{\partial f}{\partial p_1}\right)\Delta p_1 + \left(\frac{\partial f}{\partial p_2}\right)\Delta p_2 \cdots \left(\frac{\partial f}{\partial p_m}\right)\Delta p_m \right] \right\}^2 \qquad \ldots\ldots(64)$$

Minimising Q with respect to each Δp_i gives the equations

$$0 = \frac{\partial Q}{\partial (\Delta p_1)} = \sum_i 2\,(y_i - y) \cdot - \frac{\partial y}{\partial (\Delta p_1)} \qquad \ldots\ldots(65)$$

$$0 = \frac{\partial Q}{\partial(\Delta p_2)} = \sum_i 2\,(y_i - y).\ -\frac{\partial y}{\partial(\Delta p_2)} \qquad \ldots\ldots(66)$$

$$0 = \frac{\partial Q}{\partial(\Delta p_m)} = \sum_i 2\,(y_i - y).\ -\frac{\partial y}{\partial(\Delta p_m)} \qquad \ldots\ldots\ldots(67)$$

Using equation (61) these can be rewritten

$$0 = \sum_i \left[\left\{ f(x_i, p_{10}, p_{20} \cdots p_{io} \cdots p_{mo}) - y_i \right\} \left(\frac{\partial f}{\partial p_1}\right)_i + \left(\frac{\partial f}{\partial p_1}\right)_i \left(\frac{\partial f}{\partial p_1}\right)_i \Delta p_1 \right. \qquad \ldots\ldots\ldots(68)$$

$$\left. + \left(\frac{\partial f}{\partial p_1}\right)_i \left(\frac{\partial f}{\partial p_2}\right)_i \Delta p_2 + \quad + \left(\frac{\partial f}{\partial p_1}\right)_i \left(\frac{\partial f}{\partial p_m}\right)_i \Delta p_m \right]$$

and so on. This set of equations can be solved for the error terms Δp which can then provide new values of the curve fitting parameters. With reasonably good initial estimates of the original parameters only about four iterations are needed to produce small values of Δp.

Four equal-area Lorentz curves of fixed separation plus drift terms can be represented by a function with nine parameters:

$$y = p_o + p_1 x + \tfrac{1}{2} p_2 x^2 + p_3 \left\{ \frac{p_4^{-1}}{1+(x-p_8)^2 (p_4)^{-2}} + \frac{p_5^{-1}}{1+(x-k_1-p_8)^2 (p_5)^{-2}} \right.$$

$$\left. + \frac{p_6^{-1}}{1+(x-k_2-p_8)^2 (p_6)^{-2}} + \frac{p_7^{-1}}{1+(x-k_3-p_8)^2 (p_7)^{-2}} \right\} \qquad \ldots\ldots(69)$$

where

p_o, p_1 and p_2 are zero mean and drift terms,
p_3 is a scaling constant,
p_4, p_5, p_6 and p_7 are the half linewidths at the half power points,
p_8 is the first curve centre,
k_1, k_2 and k_3 are line separations.

The experimental curve is the derivative of the true absorption curve. The derivative of equation 69 is

$$\frac{dy}{dx} = y' = p_1 + p_2 x + p_3 \left\{ -\frac{2p_4(x-p_8)}{\left\{p_4^2+(x-p_8)^2\right\}^2} \quad \text{-------} \right\} \qquad \text{.....(70)}$$

The partial derivatives of this equation w.r.t. the eight parameters are as follows

$$\frac{\partial y'}{\partial p_1} = 1 \qquad \text{.....(71)}$$

$$\frac{\partial y'}{\partial p_2} = x \qquad \text{.....(72)}$$

$$\frac{\partial y'}{\partial p_3} = -\frac{2p_4(x-p_8)}{\left\{p_4^2+(x-p_8)^2\right\}^2} - \frac{2p_5(x-k_1-p_8)}{\left\{p_5^2+(x-k_1-p_8)^2\right\}^2}$$

$$- \frac{2p_6(x-k_2-p_8)}{\left\{p_6^2+(x-k_2-p_8)^2\right\}^2} - \frac{2p_7(x-k_3-p_8)}{\left\{p_7^2+(x-k_3-p_8)^2\right\}^2} \qquad \text{.....(73)}$$

$$\frac{\partial y'}{\partial p_4} = \frac{2p_3(x-p_8)\left\{3p_4^2-(x-p_8)^2\right\}}{\left\{p_4^2+(x-p_8)^2\right\}^3} \qquad \text{.....(74)}$$

$$\frac{\partial y'}{\partial p_5} = \frac{2p_3(x-k_1-p_8)\left\{3p_5^2-(x-k_1-p_8)^2\right\}}{\left\{p_5^2+(x-k_1-p_8)^2\right\}^3} \qquad \text{.....(75)}$$

$$\frac{\partial y'}{\partial p_6} = \frac{2p_3(x-k_2-p_8)\left\{3p_6^2-(x-k_2-p_8)^2\right\}}{\left\{p_6^2+(x-k_2-p_8)^2\right\}^3} \qquad \text{.....(76)}$$

$$\frac{\partial y'}{\partial p_7} = \frac{2p_3(x-k_3-p_8)\left\{3p_7^2-(x-k_3-p_8)^2\right\}}{\left\{p_7^2+(x-k_3-p_8)^2\right\}^3} \qquad \text{.....(77)}$$

$$\frac{\partial y'}{\partial p_8} = \frac{2p_3\ p_4\left\{p_4^{\,2}-3(x-p_8)^2\right\}}{\left\{p_4^{\,2}+(x-p_8)^2\right\}^3} + \frac{2p_3\ p_5\left\{p_5^{\,2}-3(x-k_1-p_8)^2\right\}}{\left\{p_5^{\,2}+(x-k_1-p_8)^2\right\}^3}$$

$$+ \frac{2p_3\ p_6\left\{p_6^{\,2}-3(x-k_2-p_8)^2\right\}}{\left\{p_6^{\,2}+(x-k_2-p_8)^2\right\}^3} + \frac{2p_3\ p_7\left\{p_7^{\,2}-3(x-k_3-p_8)^2\right\}}{\left\{p_7^{\,2}+(x-k_3-p_8)^2\right\}^3} \quad \ldots\ldots\ldots(78)$$

Using the above equations it is possible to calculate the coefficients of the ΔP's in the eight linear equations and so solve for each ΔP. To produce an accurate figure for the linewidth as many points as possible should be used (Ref.28). In the present experiments forty points were taken from each experimental curve and used for curve fitting. This required an impracticable length of calculating time on a desk calculator and so the calculation was performed on a digital computer. A program was written in FORTRAN for use on an IBM 1620 (Appendix 2). Using this computer each iteration took about ten minutes with three or four iterations being required to reduce the errors to a suitable small amount.

APPENDIX 2

Fortran program for four equal area Lorentzian curves

Each curve fitting was performed by taking a set of ordinate values from the experimental curves with equal field separation between each point. Provision was made in the program to accept 50 fitting points although usually only about 40 were used. The experimental points were called YM ( ) the number of points NDATA and the field separation between each point FACTR. In addition it was necessary to know the initial values of the eight parameters and also the separation between the curve centres. The input data was punched on cards in the following order:

Number of experimental points (Fixed point number).
Field separation between the points.
Predicted values of the eight parameters.
Values of the curve separations.
Experimental points.

In order to simplify the writing of the computer program the following substitutions were used

$x-p_8 = X(1)$ .....(79) $\qquad x-k_1-p_8 = X(2)$ .....(80)

$x-k_2-p_8 = X(3)$ ....(81) $\qquad x-k_3-p_8 = X(4)$ .....(82)

$(p_4^2+X(1)^2)^2 = CUR(1)$ ..... (83)

$(p_5^2+X(2)^2)^2 = CUR(2)$ ..... (84)

$(p_6^2+X(3)^2)^2 = CUR(3)$ ..... (85)

$(p_7^2+X(4)^2)^2 = CUR(4)$ ..... (86)

$DIV(1) = \frac{X(1)}{CUR(1)}$ ..... (87)

Equations 70 to 78 of Appendix 1 can be rewritten as

$$y' = p_1+p_2x+p_3\left\{\frac{-2p_4X(1)}{CUR(1)} - \frac{2p_5X(2)}{CUR(2)} - \frac{2p_6X(3)}{CUR(3)} - \frac{2p_7X(4)}{CUR(4)}\right\} \qquad .....(88)$$

$$= p_1+p_2x-2p_3 \sum_{I=1}^{4} P(I+3).DIV(I)$$

$$\frac{dy'}{dp_1} = 1 \qquad \ldots\ldots(89)$$

$$\frac{dy'}{dp_2} = x \qquad \ldots\ldots(90)$$

$$\frac{dy'}{dp_3} = \frac{-2p_4X(1)}{CUR(1)} - \frac{2p_5X(2)}{CUR(2)} - \frac{2p_6X(3)}{CUR(3)} - \frac{2p_7X(4)}{CUR(4)} \qquad \ldots\ldots(91)$$

$$= -2 \sum_{I=1}^{4} P(I+3).DIV(I)$$

$$\frac{dy'}{dp_4} = \frac{2p_3X(1)\left\{3p_4^2 - X(1)^2\right\}}{CUR(1)^{\frac{3}{2}}} \qquad \ldots\ldots(92)$$

$$\frac{dy'}{dp_5} = \frac{2p_3X(2)\left\{3p_5^2 - X(2)^2\right\}}{CUR(2)^{\frac{3}{2}}} \qquad \ldots\ldots(93)$$

$$\frac{dy'}{dp_6} = \frac{2p_3X(3)\left\{3p_6^2 - X(3)^2\right\}}{CUR(3)^{\frac{3}{2}}} \qquad \ldots\ldots(94)$$

$$\frac{dy'}{dp_7} = \frac{2p_3X(4)\left\{3p_7^2 - X(4)^2\right\}}{CUR(4)^{\frac{3}{2}}} \qquad \ldots\ldots(95)$$

$$\frac{dy'}{dp_8} = \frac{2p_3p_4(p_4^2 - 3X(1)^2)}{CUR(1)^{\frac{3}{2}}} + \frac{2p_3p_5(p_5^2 - 3X(2)^2)}{CUR(2)^{\frac{3}{2}}} \qquad \ldots\ldots(96)$$

$$+ \frac{2p_3p_6(p_6^2 - 3X(3)^2)}{CUR(3)^{\frac{3}{2}}} + \frac{2p_3p_7(p_7^2 - 3X(4)^2)}{CUR(4)^{\frac{3}{2}}}$$

FIG.50

FLOW DIAGRAM

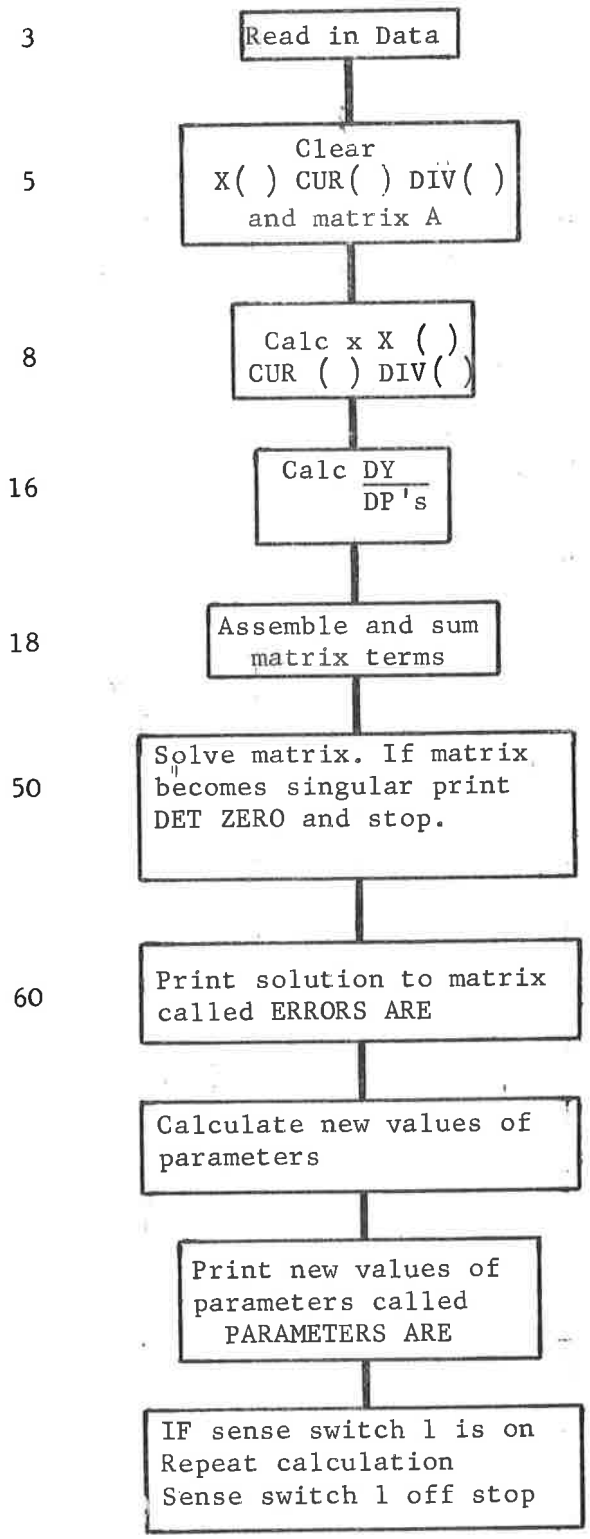

The program follows the flow diagram shown in Fig.50

FORTRAN PROGRAM

```
C       ESR RESULTS CURVE FITTING PRØGRAM
        DIMENSIØNDYDP(8),P(8),C(3),YM(50),X(4),CUR(4),DIV(4),A(8,9)
        READ,NDATA,FACTR
        DØ1I=1,8
    1   READ,P(I)
        DØ2I=1,3
    2   READ,C(I)
        DØ3K=1,NDATA
    3   READ,YM(K)
   64   DØ4I=1,4
        X(I)=0
        CUR(I)=0
    4   DIV(I)=0
        DØ5I=1,8
        DØ5J=1,9
    5   A(I,J)=0
        DØ2ØK=1,NDATA
        XØ=K-1
        XØ=XØ*FACTR
        X(1)=XØ-P(8)
        DØ7I=1,3
    7   X(I+1)=X(I)-C(I)
        DØ8I=1,4
        CUR(I)=((P(I+3))*(P(I+3))+X(I)*X(I))**2
    8   DIV(I)=X(I)/CUR(I)
        SUMA=0
        DØ1ØI=1,4
   10   SUMA=SUMA+P(I+3)*DIV(I)
        Y=P(1)+P(2)*XØ-2.*P(3)*SUMA
        CØ=YM(K)-Y
        DYDP(1)=1
        DYDP(2)=XØ
```

```
      DYDP(3)=-2.*SUMA
      SUMB=0
      DØ16I=1,4
      DYDP(I+3)=2.*P(3)*X(I)*(3.*P(I+3)*P(I+3)-X(I)*X(I))/CUR(I)**1.5
   16 SUMB=SUMB+P(I+3)*(P(I+3)*P(I+3)-3.*X(I)*X(I))/CUR(I)**1.5
      DYDP(8)=2.*P(3)*SUMB
      DØ18I=1,8
      DØ17J=1,8
   17 A(I,J)=A(I,J)+DYDP(I)*DYDP(J)
   18 A(I,9)=A(I,9)+CØ*DYDP(I)
   20 CØNTINUE
      N=8
      NI=N+1
      ND=N-1
      DØ26J=1,ND
      JR=J
      SL=A(J,J)
      K=J+1
      DØ22I=K,N
      IF(ABSF(SL)-ABSF(A(I,J)))23,22,22
   23 SL=A(I,J)
      JR=I
   22 CØNTINUE
      IF(SL)35,30,35
   30 PRINT34
   34 FORMAT(9HbDETbZERØ)
      GØTØ65
   35 IF(JR-J)27,27,28
   28 DO25L=J,NI
      TEMP=A(J,L)
      A(J,L)=A(JR,L)
   25 A(JR,L)=TEMP
   27 DØ26I=K,N
      AM=A(I,J)/A(J,J)
      DØ26L=J,NI
   26 A(I,L)=A(I,L)-AM*A(J,L)
```

```
      IF(A(N,N))29,30,29
29    A(N,NI)=A(N,NI)/A(N,N)
      DO5OK=2,N
      S=O
      I=N-K+1
      L=I+1
      DØ51M=L,N
51    S=S+A(I,M)*A(M,NI)
50    A(I,NI)=(A(I,NI)-S)/A(I,I)
      DØ62I=1,N,2
      PRINT6O,A(I,NI),A(I+1,NI)
60    FØRMAT(1OHERRORSbARE2E14.8)
      P(I)=P(I)+A(I,NI)
      P(I+1)=P(I+1)+A(I+1,NI)
62    PRINT63,P(I),P(I+1)
63    FØRMAT(14HPARAMETERSbARE2E14.8)
      IF(SENSESWITCH1)64,65
65    STØP
      END
```

APPENDIX 3

The following figures show the initial estimates of the eight parameters used, the successive calculated error terms and the final values of the parameters.

SOLVENT CARBON TETRACHLORIDE

	P_1	Errors	P_2	Errors	P_3	Errors	P_8	Errors
				Propyl				
INITIAL	0.01	-8.42	0.001	.041	33,000	2,333.4	120.0	3.54
	-8.41	.459	0.042	-.043	35,233.4	-3,263.0	123.54	.793
	-7.95	-.561	-.0097	.045	31,970.4	2,958.6	124.34	.880
	-8.51	.142	.0445	-.046	34,929.1	-944.5	125.21	.027
FINAL	-8.37		-.0015		33,984.6		125.24	
				Octyl				
INITIAL	0.01	-2.44	0.001	.0075	35,000	-6,609.5	122.0	1.367
	-2.43	-.195	.0085	-.0067	28,390.5	1,183.0	123.36	.216
	-2.63	.0608	.0018	.0064	29,573.5	-371.0	123.58	-.0403
FINAL	-2.56		.0082		29,202.5		123.54	
				Tetra				
INITIAL	0.01	-.296	0.001	.0063	-28,000	4,907.8	120	-.138
	-.286		.0073		-23,092.1		119.8	
		-.142		-.0057		507.7		-.409
	-.428		.0016		-22,584.4		119.4	
		.0028		.0057		-42.34		-.225
FINAL	-.426		.0073		-22,626.8		119.2	

	P_4	Errors	P_5	Errors	P_6	Errors	P_7	Errors
				Propyl				
INITIAL	28.3	2.88	33.1	4.42	43.0	8.46	53.7	7.87
	31.18	-.938	37.52	-4.38	51.46	-7.31	61.57	-8.96
	30.25	1.44	33.14	1.22	44.14	2.93	52.61	5.08
	31.69	-.126	34.36	-.923	47.08	-2.08	57.70	-3.16
FINAL	31.56		33.43		44.99		54.53	
				Octyl				
INITIAL	28.3	-.77	33.6	3.01	48.2	5.69	72.3	-5.71
	27.52	.491	36.61	1.28	53.89	2.99	67.48	1.19
	28.01	-.199	37.89	-.221	56.88	-.449	68.67	-.940
FINAL	27.81		37.67		56.43		67.74	
				Tetra				
INITIAL	28.3	1.93	36.6	3.79	53.6	7.18	83.5	-5.16
	30.23	.272	40.39	1.74	60.78	3.831	78.33	.751
	30.50	.008	42.14	.448	64.61	.396	79.08	- .151
FINAL	30.51		42.59		65.01		78.93	

SOLVENT BENZENE

	P_1	Errors	P_2	Errors	P_3	Errors	P_8	Errors
				Propyl				
INITIAL	0.01	-3.73	0.001	.0116	25,000	8,292.4	110.0	8.707
	-3.72	.206	.0126	-.012	33,292.4	-1,920.1	118.70	5.582
	-3.52	-1.27	-.00018	.018	31,372.2	4,824.9	124.29	-.366
FINAL	-4.79		.0179		36,197.3		123.92	
				Octyl				
INITIAL	0.01	-3.37	0.001	-.0025	-28,000	-4,230.9	92.3	.310
	-3.36	-.598	-.0015	.0053	-32,230.9	2,292.0	92.61	-.226
	-3.96	.353	.0038	-.0070	-29,938.8	-1,598.4	92.38	.035
FINAL	-3.61		-.0032		-31,537.3		92.42	
				Tetra				
INITIAL	0.01	-5.18	0.001	.017	35,000	3,626.3	125.0	-2.00
	-5.17	.610	.018	-.020	38,626.3	-2,765.4	122.9	-.603
	-4.56	-.217	-.0015	.021	35,860.9	1,269.2	122.3	-.333
FINAL	-4.77		.019		37,130.1		122.0	

	P_4	Errors	P_5	Errors	P_6	Errors	P_7	Errors
				Propyl				
INITIAL	28.8	7.09	33.1	20.35	38.9	32.35	43.0	29.47
	35.9	-7.29	53.45	-10.05	71.25	-.652	72.47	-3.49
	28.6	3.42	43.40	- 5.64	70.6	-21.28	68.98	-8.55
FINAL	32.03		37.76		49.31		60.42	
				Octyl				
INITIAL	28.3	3.71	33.0	3.80	43.2	4.57	53.5	5.31
	32.01	-1.25	36.8	-.49	47.77	.376	58.81	.458
	30.75	.818	36.31	.628	48.15	.626	59.26	.708
FINAL	31.57		36.93		48.78		59.97	
				Tetra				
INITIAL	28.3	2.67	36.8	.878	44.9	10.47	61.0	7.87
	30.97	-1.69	37.67	.285	55.37	3.05	68.87	-.737
	29.28	.486	37.96	.885	58.42	1.24	68.14	.820
FINAL	29.77		38.85		59.66		68.96	

SOLVENT ETHER

	P_1	Errors	P_2	Errors	P_3	Errors	P_8	Errors
				Propyl				
INITIAL	0.01	4.13	0.001	-.012	-30,000	-6,251.9	120.0	.982
	4.14	.303	-.011	.010	-36,251.9	-2,738.6	120.98	.972
	4.44	-.216	-.00027	-.0096	-38,990.5	1,289.7	121.95	.325
FINAL	4.23		-.0098		-37,700.7		122.28	
				Octyl				
INITIAL	0.01	-4.37	0.001	.015	33,000	-790.2	138.0	3.147
	-4.36	.044	.0160	-.015	32,209.8	397.0	141.14	1.015
	-4.32	.010	.00074	.015	32,606.9	-144.2	142.16	-.092
FINAL	-4.31		.0160		32,462.6		142.07	
				Tetra				
INITIAL	0.01	-2.42	0.001	.0058	35,000	-4,615.1	78.0	-.385
	-2.41	.0283	.0069	-.0059	30,384.8	837.3	77.61	-.549
	-2.38	.122	.00091	.0054	31,222.1	-566.6	77.06	-.357
FINAL	-2.26		.0063		30,655.6		76.71	

	P_4	Errors	P_5	Errors	P_6	Errors	P_7	Errors
				Propyl				
INITIAL	28.70	9.840	33.10	6.45	38.9	9.357	43.0	12.64
	38.54	3.783	39.55	2.007	48.26	2.721	55.64	3.24
	42.32	-.392	41.56	-.694	50.98	-1.137	58.88	-1.65
FINAL	41.93		40.86		49.84		57.23	
				Octyl				
INITIAL	28.7	2.70	33.1	4.79	38.9	10.25	43.0	13.83
	31.40	.453	37.89	-.294	49.15	4.59	56.83	7.39
	31.85	- .049	37.59	-.446	53.75	-.147	64.23	-.011
FINAL	31.90		37.15		53.59		64.15	
				Tetra				
INITIAL	28.3	3.05	35.3	.573	42.2	8.05	48.2	12.62
	31.35	1.46	35.87	1.05	50.25	5.85	60.82	9.11
	32.81	- .299	36.92	-.0457	56.11	.281	69.93	-1.07
FINAL	32.51		36.88		56.39		68.86	